

# Process intensification for the production of MVA and influenza A virus in high density suspension cultures of AGE1.CR.pIX cells

## **Dissertation**

zur Erlangung des akademischen Grades

## **Doktoringenieur**

**(Dr.-Ing.)**

von: Daniel Vázquez Ramírez, M.Sc.

geboren am: 11. März 1983 in Mexiko Stadt, Mexiko

genehmigt durch die Fakultät für Verfahrens- und Systemtechnik  
der Otto-von-Guericke-Universität Magdeburg

Promotionskommission:

Prof. Dr.-Ing. Andreas Seidel-Morgenstern	(Vorsitz)
Prof. Dr.-Ing. Udo Reichl	(Gutachter)
Dr. Véronique Chotteau	(Gutachter)
Prof. Dr.-Ing. Ralf Pörtner	(Gutachter)

eingereicht am: 25. Februar 2021

Promotionskolloquium am: 8. Juli 2021



## Abstract

Industrial cell culture-based processes have reached a maturity level, thanks to economies of scale, an ever-growing industrial competition and the development of innovative process technologies. In this regard, process intensification has become an imperative area of study during the past years, especially in monoclonal antibody production. For example, process intensification approaches using high seeding concentrations are used to increase the manufacturing capacity and the overall productivity. These applications have become every time more accessible due to the appearance of new and robust cell expansion systems that enable very high cell densities.

While technology and know-how have seen great advances in the monoclonal antibody field, process intensification for viral vaccine production has attracted more interest only recently. The present work aimed at developing an intensified high cell density processes for the production of two viruses with high relevance as viral vaccines: modified vaccinia Ankara (MVA) virus and influenza A virus (IAV). MVA is a highly attenuated virus derived from the vaccinia virus, which was used as vaccine to eradicate smallpox. Besides its potential application as next-generation smallpox vaccine, MVA is currently tested as viral vector against infectious diseases and cancer. In this work, the strain MVA-CR19 (kindly provided by ProBioGen AG) was used due to its capacity to propagate efficiently in suspension cell cultures. In addition, the IAV strain A/PR/8/34 (H1N1), used for the production of seasonal influenza vaccines, was applied as a model for influenza virus production.

The avian suspension cell line AGE1.CR.pIX<sup>®</sup> (kindly provided by ProBioGen AG) was used as production platform to study the propagation of the MVA-CR19 and A/PR/8/34 (H1N1) at high cell densities. AGE1.CR.pIX<sup>®</sup> cells (here abbreviated as CR.pIX) are permissive for MVA-CR19 virus and for A/PR/8/34 (H1N1), yielding titers in the order of  $10^8$  plaque forming units (pfu) per mL and around  $2.4 \log_{10}$  HA units (HAU) per 100  $\mu$ L, respectively, in conventional batch processes. For the intensification of the typical production process for MVA and IAV via high cell density cultures, two key aspects were addressed. On the one hand, the optimal cell expansion to high cell concentrations in the seeding step using a perfusion system. On the other hand, the definition of strategies for optimal virus propagation at high cell densities to higher titers maintaining or even improving specific and volumetric productivity.

For the cell expansion to high cell densities, a perfusion process was established in shake flasks (semi-perfusion) and a 1 L bench-top bioreactor. Here, the medium consumption was reduced to the minimum possible based on the glucose uptake rate, i.e. applying a constant specific perfusion rate of 0.06 nL/(cell $\times$ d). Under these conditions, cells grew exponentially at a mean specific cell growth rate of 0.026 1/h and achieved viable cell concentrations  $> 80 \times 10^6$  cells/mL in around 8 d. This was a key

aspect to define, since this medium saving had a strong impact on the volumetric productivity at the end of the virus propagation phase.

In a next step, several strategies for optimal MVA-CR19 virus propagation at cell densities between 40 and  $60 \times 10^6$  cells/mL were analyzed in multiple shake flask cultivations. A simple fed-batch process using a medium with 10-times concentrated glucose and glutamine did not improve virus titers. In contrast, strategies with medium exchange and a fed-batch process using basal medium increased virus titers even above a factor of 10 compared to the standard batch process at low cell densities, maintaining comparable cell-specific yields.

A hybrid strategy comprising a fed-batch process followed by a medium exchange regime provided the highest yields in shake flasks. This strategy was later scaled-up to a controlled 1 L bench-top bioreactor and adapted as a hybrid fed-batch/perfusion strategy. Under these conditions, MVA-CR19 virus titers up to  $1 \times 10^{10}$  pfu/mL were obtained, which represented a 10- to 100-fold increase (compared to typical reported titers for MVA), with cell-specific yields comparable to other production platforms (such as chicken embryo fibroblasts) and volumetric productivities 10 times higher than for reported conventional batch processes.

The hybrid fed-batch/perfusion strategy was also evaluated for the propagation of IAV. Compared to the reference process at conventional cell densities, virus titers increased 10-fold from 2.23 to 3.27  $\log_{10}$  (HAU/100  $\mu$ L), which corresponded well to the same increase in cell concentration. This way, cell-specific yield and volumetric productivity were maintained constant, and the cell-density effect known for perfusion processes at high cell density was circumvented.

Concerning process monitoring and control, this study explored the implementation of three applications. First, an alternative pH-based perfusion control, based on the lactate accumulation and medium acidification, was applied to propagate cells up to  $25 \times 10^6$  cells/mL with cell growth rates comparable to the strategy based on a fixed specific perfusion rate. Second, an accurate on-line capacitance-based monitoring of viable cell concentrations was possible up to late stage of MVA-CR19 virus and IAV infection. And third, an insight in the dynamics of virus propagation was possible by identifying regular changes in dielectric properties (measured on-line) of the infected cells. Overall, these strategies showed a very high potential for development and implementation as Process analytical technology (PAT) tools for high cell density vaccine production processes.

In summary, this work identifies the intrinsic constraints of virus production in batch mode and applies solutions to circumvent their negative effects for virus propagation at high cell densities. It can also serve as a starting point to develop and establish fully or semi-continuous and highly productive production processes at high cell densities using appropriate retention systems. In addition, with the use of on-line monitoring systems, these complex processes can be simplified and support vaccine manufacturing in an industrial scale.

# Kurzfassung

Industrielle zellkulturbasierte Prozesse haben aufgrund von Skaleneffekten, einem immer stärker werdenden industriellen Wettbewerb und der Entwicklung innovativer Prozesstechnologien einen hohen Reifegrad erreicht. In diesem Zusammenhang ist die Prozessintensivierung in den letzten Jahren zu einem wichtigen Thema geworden, insbesondere bei der Produktion monoklonaler Antikörper. So werden beispielsweise Prozessintensivierungsansätze mit hohen Seeding-Konzentrationen eingesetzt, um die Herstellungskapazität und die Gesamtproduktivität zu erhöhen. Diese Anwendungen sind durch das Aufkommen neuer und robuster Zellexpansionssysteme, die sehr hohe Zelldichten ermöglichen, immer zugänglicher geworden.

Während die Technologie und das Wissen im Bereich der monoklonalen Antikörper große Fortschritte gemacht haben, ist die Prozessintensivierung für die Produktion viraler Impfstoffe erst seit Kurzem in den Fokus des Interesses gerückt. Die vorliegende Arbeit zielte auf die Entwicklung eines intensivierten Hochzelldichteprozesses für die Produktion zweier Viren mit hoher Relevanz als virale Impfstoffe: das Modified-Vaccinia-Ankara-Virus (MVA) und das Influenza-A-Virus (IAV). MVA ist ein hoch abgeschwächtes Virus, das vom Vaccinia-Virus abgeleitet ist, welches als Impfstoff zur Ausrottung der Pocken verwendet wurde. Neben seiner potenziellen Anwendung als Pockenimpfstoff der nächsten Generation wird MVA derzeit als viraler Vektor gegen Infektionskrankheiten und Krebs getestet. In dieser Arbeit wurde der Stamm MVA-CR19 (freundlicherweise von der ProBioGen AG zur Verfügung gestellt) verwendet, da er sich in Suspensionszellkulturen effizient vermehren kann. Zusätzlich wurde der IAV-Stamm A/PR/8/34 (H1N1), der für die Produktion von saisonalen Grippeimpfstoffen verwendet wird, als Modell für die Influenzavirusproduktion eingesetzt.

Die aviäre Suspensionszelllinie AGE1.CR.pIX<sup>®</sup> (freundlicherweise von der ProBioGen AG zur Verfügung gestellt) wurde als Produktionsplattform verwendet, um die Vermehrung von MVA-CR19 und A/PR/8/34 (H1N1) bei hohen Zelldichten zu untersuchen. AGE1.CR.pIX<sup>®</sup>-Zellen (hier abgekürzt als CR.pIX) sind permissiv für das MVA-CR19-Virus und für A/PR/8/34 (H1N1) und liefern in konventionellen Batch-Prozessen Titer in der Größenordnung von  $10^8$  plaquebildenden Einheiten (pfu) pro mL bzw. etwa  $2,4 \log^{10}$  HA-Einheiten (HAU) pro 100  $\mu$ L. Für die Intensivierung des typischen Produktionsprozesses für MVA und IAV über Hochzelldichtekulturen wurden zwei Schlüsselaspekte adressiert. Dies betraf einerseits die optimale Zellexpansion auf hohe Zellkonzentrationen im Seeding-Schritt unter Verwendung eines Perfusionssystems und andererseits die Definition von Strategien für eine optimale Virusvermehrung bei hohen Zelldichten zu höheren Titern unter Beibehaltung oder sogar Verbesserung der spezifischen und volumetrischen Produktivität.

Für die Zellexpansion zu hohen Zelldichten wurde ein Perfusionsverfahren in Schüttelkolben (Semi-Perfusion) und einem 1-Liter-Tischbioreaktor etabliert. Dabei wurde der Verbrauch des Mediums,

welches an die Aufnahmerate von Glukose angepasst wurde, auf das mögliche Minimum reduziert, d. h. es wurde eine konstante spezifische Perfusionsrate von  $0,06 \text{ nL}/(\text{Zelle} \times \text{d})$  angewendet. Unter diesen Bedingungen wuchsen die Zellen exponentiell mit einer mittleren spezifischen Zellwachstumsrate von  $0,026 \text{ 1/h}$  und erreichten lebensfähige Zellkonzentrationen  $> 80 \times 10^6 \text{ Zellen/mL}$  in ca. acht Tagen. Dies war ein zentraler Aspekt, den es zu definieren galt, da diese Medieneinsparung einen starken Einfluss auf die volumetrische Produktivität am Ende der Virusvermehrung hatte.

In einem nächsten Schritt wurden verschiedene Strategien zur optimalen MVA-CR19-Virusvermehrung bei Zelldichten zwischen  $40$  und  $60 \times 10^6 \text{ Zellen/mL}$  in mehreren Kultivierungen in Schüttelkolben analysiert. Ein einfacher Fed-Batch-Prozess unter Verwendung eines Mediums mit 10-fach konzentrierter Glukose und Glutamin führte zu keiner Verbesserung der Virustiter. Im Gegensatz dazu erhöhten Strategien mit einem Wechsel des Mediums und ein Fed-Batch-Prozess unter Verwendung von einem Basalmedium die Virustiter sogar mit einem Faktor größer als 10 im Vergleich zum Standard-Batch-Prozess bei niedrigen Zelldichten, wobei vergleichbare zellspezifische Ausbeute erhalten blieben.

Eine hybride Strategie, bestehend aus einem Fed-Batch-Prozess gefolgt von einem System zum Austausch des Mediums, lieferte die höchsten Ausbeute in Schüttelkolben. Diese Strategie wurde später auf einen kontrollierten 1-Liter-Tisch-Bioreaktor hochskaliert und als hybride Fed-Batch/Perfusionsstrategie angepasst. Unter diesen Bedingungen wurden MVA-CR19-Virustiter bis zu  $1 \times 10^{10} \text{ pfu/mL}$  erzielt, was einer 10- bis 100-fachen Steigerung (im Vergleich zu typischen berichteten Titern für MVA) entspricht, mit zellspezifischen Ausbeuten, die mit anderen Produktionsplattformen (wie z. B. Hühnerembryo-Fibroblasten) vergleichbar sind, und volumetrischen Produktivitäten, die 10-mal höher sind als bei berichteten herkömmlichen Batch-Prozessen.

Die hybride Fed-Batch/Perfusionsstrategie wurde auch für die Vermehrung von IAV evaluiert. Im Vergleich zum Referenzprozess bei konventionellen Zelldichten stiegen die Virustiter um das 10-fache von  $2,23$  auf  $3,27 \text{ log}_{10} (\text{HAU}/100 \text{ } \mu\text{L})$ , was gut mit der gleichen Erhöhung der Zellkonzentration korrespondierte. Auf diese Weise wurden die zellspezifische Ausbeute und die volumetrische Produktivität konstant gehalten, und der für Perfusionsprozesse bekannte Zelldichte-Effekt bei hoher Zelldichte umgangen.

In Bezug auf die Prozessüberwachung und -steuerung wurde in dieser Studie die Implementierung von drei Anwendungen untersucht. Erstens wurde eine alternative pH-basierte Perfusionskontrolle, die auf der Laktatakkumulation und der Versauerung des Mediums basiert, angewandt, um Zellen bis zu  $25 \times 10^6 \text{ Zellen/mL}$  mit Zellwachstumsraten zu vermehren, die mit der Strategie vergleichbar sind, die auf einer festen spezifischen Perfusionsrate basiert. Zweitens war eine genaue kapazitätsbasierte Online-Überwachung der Konzentrationen lebensfähiger Zellen bis zum späten Stadium der MVA-CR19-Virus- und IAV-Infektion möglich. Und drittens war ein Einblick in die Dynamik der Virusvermehrung möglich, indem regelmäßige Änderungen der dielektrischen Eigenschaften (online

gemessen) der infizierten Zellen identifiziert werden konnten. Insgesamt zeigten diese Strategien ein sehr hohes Potenzial für die Entwicklung und Implementierung als Werkzeuge der Prozessanalytischen Technologie (PAT) für Produktionsprozesse von Impfstoffen mit hoher Zelldichte.

Zusammenfassend identifiziert diese Arbeit die intrinsischen Beschränkungen der Virusproduktion im Batch-Modus und wendet Lösungen an, um deren negative Auswirkungen für die Virusvermehrung bei hohen Zelldichten zu umgehen. Sie kann auch als Ausgangspunkt dienen, um voll- oder halbkontinuierliche und hochproduktive Produktionsprozesse bei hohen Zelldichten unter Verwendung geeigneter Rückhaltesysteme zu entwickeln und zu etablieren. Darüber hinaus können diese komplexen Prozesse durch den Einsatz von Online-Überwachungssystemen vereinfacht werden und die Impfstoffherstellung im industriellen Maßstab unterstützen.





# Content

<b>Abstract</b> .....	<b>III</b>
<b>Kurzfassung</b> .....	<b>V</b>
<b>List of abbreviations</b> .....	<b>XII</b>
<b>List of symbols</b> .....	<b>XIV</b>
<b>1 Introduction</b> .....	<b>1</b>
<b>2 Background</b> .....	<b>4</b>
2.1 The beginnings of vaccination .....	4
2.2 Current platforms for viral vaccine production .....	6
2.2.1 Embryonated chicken eggs.....	6
2.2.2 Primary cell cultures.....	8
2.2.3 Continuous cell lines .....	10
2.2.4 Designer cell lines .....	12
2.3 Influenza virus vaccine .....	13
2.3.1 Influenza virus structure and replication cycle.....	13
2.3.2 Cell culture-based influenza vaccine production .....	17
2.4 MVA virus for vaccine production.....	20
2.4.1 Vaccinia virus structure and replication cycle.....	20
2.4.2 MVA virus as vector vaccine .....	24
2.4.3 MVA virus production .....	24
2.5 High cell density approaches in animal cell culture processes.....	27
2.5.1 Cultivation options for the production of recombinant proteins at high cell densities.....	27
2.5.2 Current high cell density approaches for the production of viral vaccines .....	31
2.6 On-line monitoring and control for cell culture-based vaccine production processes .....	40
<b>3 Materials and Methods</b> .....	<b>43</b>
3.1 Cells and medium .....	43
3.2 Cultivations in shake flasks .....	43
3.3 Cultivations in bioreactors.....	45
3.3.1 Characterization of the bioreactor .....	45
3.3.2 Standard process parameters .....	46
3.3.3 Operational set-up of the perfusion bioreactor with an ATF2 system .....	46
3.4 Virus handling.....	49
3.4.1 MVA-CR19 virus .....	49

3.4.2	Influenza A virus .....	50
3.5	Analytics .....	50
3.5.1	Cell concentration and viability.....	50
3.5.2	Extracellular metabolites .....	51
3.5.3	MVA-CR19 virus titration .....	52
3.5.4	Influenza A virus titration .....	52
3.5.5	Virus productivity estimations .....	53
3.5.6	Determination of infection rates using flow cytometry.....	55
<b>4</b>	<b>Results and Discussion .....</b>	<b>56</b>
4.1	Characterization of the benchtop bioreactor BIOSTAT®B plus.....	57
4.1.1	Estimation of the volumetric oxygen transfer coefficient .....	57
4.1.2	Maximum cell concentration supported by the bioreactor .....	60
4.2	Definition of the semi-perfusion and perfusion processes for the cultivation of CR.pIX cells at high cell density .....	62
4.2.1	Definition of the perfusion process in bioreactor .....	63
4.2.2	Definition of the semi-perfusion process in shake flasks.....	65
4.3	Propagation of MVA-CR19 virus in batch cultures .....	67
4.4	Propagation of MVA-CR19 virus in high cell density cultures.....	68
4.4.1	MVA-CR19 virus propagation applying perfusion.....	68
4.4.2	MVA-CR19 virus propagation applying alternative feeding strategies .....	73
4.4.3	MVA-CR19 virus propagation applying a hybrid fed-batch/perfusion strategy.....	82
4.5	Propagation of influenza A virus in high cell density cultures.....	88
4.5.1	Influenza A virus propagation applying perfusion.....	89
4.5.2	Influenza A virus propagation applying the hybrid fed-batch/perfusion strategy.....	91
4.6	Implementation of on-line tools for perfusion process control and virus production monitoring at high cell density .....	94
4.6.1	On-line pH-based perfusion control .....	94
4.6.2	On-line capacitance-based monitoring of cell concentration .....	96
4.6.3	On-line monitoring of cellular dielectric properties during virus propagation .....	97
<b>5</b>	<b>Conclusions .....</b>	<b>99</b>
5.1	Cultivation of CR.pIX cells at high cell density in perfusion.....	99
5.2	Propagation of MVA-CR19 virus at high cell density .....	100
5.3	Propagation of influenza A virus at high cell density.....	102
5.4	Using on-line tools for perfusion process control and virus production monitoring at high cell density .....	103

5.5 Final remarks .....	104
<b>List of figures.....</b>	<b>105</b>
<b>List of tables .....</b>	<b>108</b>
<b>References.....</b>	<b>110</b>
<b>List of contributions .....</b>	<b>132</b>
<b>Appendices.....</b>	<b>134</b>
Appendix 1. List of hollow fiber modules .....	134
Appendix 2. Calibration curve of the capacitance probe .....	134

## List of abbreviations

<b>Abbreviation</b>	<b>Description</b>
$\beta$ -PL	$\beta$ -propiolactone
Ad5	Human adenovirus 5
AIDS	Acquired immune deficiency syndrome
A/PR/8/34	A/Puerto Rico/8/1934
ALV	Avian leucosis viruses
ATF	Alternating tangential flow filtration
BEI	Binary ethyleneimine
BHK	Baby hamster kidney cells
BK	Bovine kidney cells
bp	Base pairs
CAP	CEVEC's amniocyte production cells
CCD	Conventional cell density
CDC	Centers for disease control and prevention
CEF	Chicken embryo fibroblasts
CEK	Chick embryo kidney cells
CEV	Cell-associated enveloped virus
CHO	Chinese hamster ovary cells
COG	Cost of goods
CR	Cairina retina
CVA	Chorioallantois vaccinia Ankara virus
DNA	Deoxyribonucleic acid
DS	Dielectric spectroscopy
EEV	Extracellular enveloped virus
EMA	European Medicines Agency
FB	Fed-batch
FCS	Fetal calf serum
FDA	Food and Drug Administration
GAG	Glycosaminoglycan
GISN	Global Influenza Surveillance Network
HA	Hemagglutinin
HCD	High cell density
HDC	Human diploid cells
HDCS	Human diploid cell strain
HEK293	Human embryonic kidney 293 cells
Hela	Henrietta Lacks cells
HFBR	Hollow fiber bioreactor
IAV	Influenza A virus
IEV	Intracellular enveloped virus
IMV	Intracellular mature virus
IPV	Inactivated poliovirus vaccine
IV	Immature virus
JE	Japanese encephalitis virus
kb	Kilobase
LAIV	Live attenuated influenza viruses
LMH	Leghorn male hepatoma cells

<b>Abbreviation</b>	<b>Description</b>
mAb	Monoclonal antibody
MDCK	Madyn-Darbin canine kidney cells
MEV	Mink enteritis virus
MHC	Major histocompatibility complex
MNNG	N-methyl-N'-nitro-N-nitrosoguanidine
NIRS	Near infrared spectroscopy
M-M-R	Measles, mumps, rubella vaccine
MRC	Medical Research Council
MVA	Modified vaccinia Ankara virus
MVA-CR19	MVA virus strain passage 19 in CR cells
NA	Neuraminidase
NEP	Nuclear export protein
NP	Nucleoprotein
NS	Non-structural protein
PA	Polymerase acidic
PAT	Process analytical technology
PB	Polymerase basic
PBS	Phosphate buffer saline
PMKC	Primary monkey kidney cells
QbD	Quality by design
QT35	Quail tumor 35
RNA	Ribonucleic acid
RNP	Ribonucleoprotein
RSD	Relative standard deviation
RSV	Respiratory syncytial virus
RTR	Real-time release
SARS	Severe acute respiratory syndrome
SPF	Specific-pathogen-free
STR	Stirred tank bioreactor
SV40	Simian virus 40
TFF	Tangential flow filtration
TOI	Time of infection
VACV	Vaccinia virus
Vero	Verda reno (green kidney)
VP	Virus particle
VCV	Viable cell volume per culture volume
VEF	Volume-expanded-fed
WHO	World Health Organization
WI	Wistar Institute
YFV	Yellow fever virus
ZIKV	Wild-type Zika virus

## List of symbols

Symbol	Description	[Unit]
$C^*$	Saturated dissolved oxygen concentration in the bulk liquid	[mM]
$C_g$	Glucose concentration	[mM]
$C_L$	Current dissolved oxygen concentration in the bulk liquid	[mM]
CSPR	Cell-specific perfusion rate	[nL/(cell×d)]
CSVY <sub>app</sub>	Apparent cell-specific virus yield	[pfu/cell]
CSVY <sub>IAV</sub>	Cell-specific virus yield of influenza A virus	[particles/cell]
CSVY <sub>MVA</sub>	Cell-specific virus yield of MVA-CR19 virus	[pfu/cell]
D	Dilution rate	[1/h]
$d_i$	Inner diameter of each hollow fiber in the ATF module	[mm]
DO	Dissolved oxygen concentration	[%]
$\epsilon$	Permittivity	[pF/cm]
$f_n$	Number of hollow fibers in the ATF module	-
$F_{O_2}$	Pure oxygen flow rate	[cm <sup>3</sup> /min]
$F_{O_2/X}$	Ratio of pure oxygen supply per cell	[mmol/(cell×h)]
HAU	HA units	-
hpi	Hours post infection	[h]
IU	Infectious units	-
IVP	Infectious virus particles	-
$\gamma$	Shear rate	[1/s]
$k_{L,a}$	Volumetric oxygen transfer coefficient	[1/h]
$\mu$	Specific cell growth rate	[1/h]
$\mu_{max}$	Maximum specific cell growth rate	[1/h]
$\mu_{mean}$	Average specific cell growth rate	[1/h]
MOI	Multiplicity of infection (number of infectious viruses per cell)	-
N	Agitation rate	[rpm]
OTR	Oxygen transfer rate	[mmol/(L×h)]
OUR	Oxygen uptake rate	[mmol/(L×h)]
pfu	Plaque forming units	-
$P_{IAV}$	Volumetric productivity for IAV	[particles/(L×d)]
$P_{MVA}$	Volumetric productivity for MVA-CR19 virus	[pfu/(L×d)]
Q	Perfusion rate	[mL/d]
Q air	Aeration rate in bioreactor's sparger (as vessel volume per minute)	[1/min]
Q <sub>ATF</sub>	Average flow rate through the ATF's module	[L/min]
$q_g$	Cell-specific glucose consumption rate	[mmol/(cell×h)]
$q_{O_2}$	Cell-specific oxygen consumption rate	[mmol/(cell×h)]
RT	Room temperature	[°C]
t	Time	[h]
$t_2$	Doubling time	[h]
TCID <sub>50</sub>	50% tissue culture infective dose	[virions/mL]
TIP	Concentration of total IAV particles by HA	[particles/mL]
$V_E$	Medium exchange volume	[mL]
vvm	Vessel volumes per minute	[1/min]
$V_R$	Media volumes per reactor volume	-
$V_w$	Working volume	[mL]
$X_V$	Viable cell concentration	[cells/mL]

# 1 Introduction

Vaccination has an enormous contribution on public health and on the development of human population. Especially from the 20<sup>th</sup> century onwards, the impact of vaccination has been more evident with the establishment of the routine vaccination of large populations. As a deliberate practice to protect humans against diseases and to reduce mortality, vaccination has helped to control major diseases, such as smallpox, diphtheria, tetanus, yellow fever, pertussis, *Haemophilus influenzae* type B disease, poliomyelitis, measles, mumps, rubella, typhoid, rabies, rotavirus, and hepatitis B [1]. It is estimated, that between 2001 and 2020 immunization against 10 vaccine-preventable diseases in 73 low- or middle-income countries will have averted almost 20 million child deaths and save US\$ 350 billion in costs of illness [2]. In addition, immunization provides important long-term and economic benefits associated with a more productive workforce [2].

Influenza, commonly known as the flu, is one of the major causes of respiratory disease in the world. Especial vulnerability to influenza infections is observed among the elderly and very young population. For example, in the United States, infection by influenza viruses results in a cumulative hospitalization rate of 35.5 per 100,000 people, affecting mostly the elderly (88.1 per 100,000 population) or very young people (46.7 per 100,000 population) with 57% of deaths coming from pediatric cases (<http://www.cdc.gov/>) [3]. Vaccination is the primary and most effective strategy for the prevention and control of influenza.

Most of the currently licensed influenza vaccines are made using embryonated chicken eggs in production systems established in the 1940s. Embryonated chicken eggs are used as minifactories operated in parallel for influenza virus replication [4]. It is estimated that this production platform will remain in use for many years, as it has demonstrated an outstanding robustness [3]. However, in case of a pandemic, the egg-based production system might not be sufficient to meet the global demand due to egg availability, i.e. under the premise that one to two eggs yield only one vaccine dose. In this regard, the application of animal cell cultures for the production of viral vaccines provides several advantages. For example, cell culture allows for large-scale production processes that supply higher quantities of the vaccines in a shorter amount of time [5-7]. Additionally, different to the egg-based platform, cell cultures yield viruses with higher similarity to the circulating virus (less risk of antigenic modifications) [8, 9] and do not contain egg components that could induce allergic reactions [10].

Another virus that has played an important role in human vaccination is the vaccinia virus (VACV), which was the virus applied for the eradication of smallpox. Modified vaccinia Ankara (MVA) virus is a vaccinia virus strain that is unable to produce infectious progeny in most cells of mammalian origin [11-13] and is now regarded as the leading strain for a “third generation” smallpox vaccine [14]. Additionally, MVA allows for synthesis of viral early, intermediate and late gene products, which supported its development as safe and efficient viral vector [13]. As a result, MVA virus has been widely used for developing vector vaccines against infectious diseases and cancer in preclinical research [15, 16]. In addition, MVA-based vector vaccines have proven to protect against SARS-CoV, MERS-CoV, Zika virus and Ebola virus [17-20].

Similar to vaccines against influenza virus, MVA-based vaccines are mainly produced in embryonated chicken eggs or in adherent chicken embryo fibroblasts (CEF) [21]. Although productivity in these systems seems to satisfy the demand of material for current clinical trials (with high doses of around  $10^8$  pfu/mL [22, 23]), there are several scale-up limitations related with surface required to propagate the required amount of cells. Additionally, the use of adherent cells may introduce undesired animal-derived components into the production process. For this reason, the use of well-characterized animal cells, growing in suspension, represents an optimal scenario for vaccine manufacturing.

The avian cell line AGE1.CR.pIX (here abbreviated as CR.pIX) is among the best characterized suspension cell lines for vaccine production. This cell line is free of adventitious agents, and sensitive assays for reverse transcriptase activity suggested that cells do not release active endogenous retroviral particles [24, 25]. The cell line has furthermore been adapted to proliferation in suspension in chemically defined media, and propagation of recombinant and wild type MVA virus and influenza viruses to high yields has been demonstrated [24, 26-29].

Cell culture processes for the production of influenza A virus (IAV) and MVA virus using CR.pIX cells were initially performed in batch mode [26]. Infectious MVA virus occurs normally as intracellular particles or attached to the cell membrane and new infections take place mainly between adjacent cells [30]. Therefore, cell aggregation has to be induced prior to infection of suspension cells, by adding a virus production medium or 0.3 mM  $\text{CaCl}_2$  [26, 29, 31]. This additional step was not necessary for the newly developed MVA virus strain “MVA-CR19” because this new phenotype has the capacity to accumulate mainly in the cell culture’s supernatant and infect single suspension cells [32]. This new characteristic reduced the complexity of the virus harvest process, since cell disruption was not necessary [32]. Although, the virus titers in CR.pIX cells showed very competitive values of  $10^8$  pfu/mL [32], it was believed that titers similar to those obtained in CEF ( $0.1\text{--}10.0 \times 10^8$  pfu/mL, [33, 34]) could be achieved by increasing cell concentrations at the time of infection. Process intensification by increasing the concentration of infected CR.pIX cells appeared also suitable for the production of IAV, since lower yields were observed compared to other cell lines [26].



Initial attempts to increase concentrations of CR.pIX cells prior to infection with IAV were carried out using simple batch process, resulting, however, in lower cell-specific virus yields [29]. Alternatively, high cell concentrations can be achieved using perfusion systems, since they allow for a continuous medium exchange while the cells are retained within the bioreactor (using cell retention systems). The traditional fed-batch (FB) process also allows for higher cell densities and increased volumetric productivities compared to batch processes, since it supplies nutrients by pumping a concentrated feed medium in the bioreactor. Although perfusion and FB cultivation modes have different applications depending on process economics and product quality-related requirements [35, 36], it has been possible to draw on the advantages of both methods to intensify production processes of biopharmaceuticals without the need to upgrade the installed production capacity [37-41]. Perfusion cultivation mode was previously applied for the expansion of cells to higher concentrations than in batch mode and for the subsequent propagation of IAV with significant increase of virus yields [42, 43]. However, the volumetric productivity was still lower compared to the batch processes.

In this work, the application of perfusion, FB and a combination of both was evaluated in order to increase MVA-CR19 and IAV virus productivities in suspension cultures of CR.pIX cells, against conventional batch processes. The suitability of CR.pIX cells to grow to high cell densities before virus infection was the first analyzed. For this, semi-perfusion cultivations in shake flasks and perfusion cultivations in benchtop bioreactors were carried out. Since the aim to expand cells to high cell densities in perfusion should be to support maximum cell growth rate with the minimum medium utilization, the medium exchange rate was defined by the glucose uptake rate of CR.pIX cells described in the literature [44]. The second important aspect was to analyze the MVA virus propagation efficiency at high cell densities. In this regard, an initial assessment of different feeding and medium exchange strategies was carried out in shake flasks. These strategies aimed at providing not only the required nutrients for cell maintenance but also for efficient virus propagation. From this analysis, a hybrid FB/perfusion cultivation strategy during virus propagation was identified to provide the highest productivity in shake flasks. Since the main objective was to provide a scalable process, this new strategy was adapted to a benchtop bioreactor (coupled with a filtration-based cell retention system for the perfusion phase) and analyzed for productivity. There, the main challenge was the continuous recovery of the produced viral particles and, therefore, filters with different nominal pore sizes were analyzed. In a final step, the hybrid FB/perfusion strategy was applied for the propagation of IAV at high cell densities with adaptations based on the specific propagation dynamics of IAV.

## 2 Background

### 2.1 The beginnings of vaccination

The first attempts of immunization procedures date much earlier than the smallpox vaccination carried out by Edward Jenner in 1798. Some Indian buddhists of the 7<sup>th</sup> century used to drink snake venom, to become immune to its effect [1]. Other writings report the use of inoculation and variolation, to induce immunity to smallpox in 15th-century China and Turkey by either inhaling the crushed lesions or inserting them into small cuts [45]. It is believed that this practice originated in “Central Asia in the early part of the second millennium AD and then spread east to China and west to Turkey, Africa, and Europe” [1].

First proper vaccination procedures were initiated by Edward Jenner in 1798 by using cowpox for protection against smallpox. Smallpox appeared only sporadically in certain rural counties of England and the local wisdom that persons who contracted cowpox did not catch the smallpox was not widely known. Jenner, who had been an apothecary apprentice in Chipping Sodbury, England, in 1768, knew around the efficacy of cowpox against smallpox from a milkmaid [1]. He even discussed the possible relation between cowpox and smallpox with John Hunter, during his studies in London (1770 to 1773). However, in 1796 his first manuscript to the Royal Society on vaccination was rejected, since his study comprised a single individual, which was “insufficient to establish a principle” [1, 46, 47]. He continued expanding his studies during two more years and demonstrated that cowpox could be transmitted directly from one person to another, providing immunization against smallpox at a “large scale”. This results were published in *Variolae Vaccinae* in 1798 [1, 48], attracting the attention of the entire medical community on the benefits of inoculation with an animal poxvirus to prevent smallpox [1]. Table 2.1 includes the viral vaccines (blue) developed in the years following Jenner’s first vaccination procedure, according to Plotkin et al. (2013) [1].

Table 2.1. History of vaccine development. Adapted from Plotkin et al. (2013) [1].

Live attenuated vaccines	Killed whole organisms	Protein or polysaccharide	Recombinant vaccines
18 <sup>th</sup> century			
<b>Smallpox (1798)</b>			
19 <sup>th</sup> century			
<b>Rabies (1885)</b>	Typhoid (1896) Cholera (1896) Plague (1897)		
20 <sup>th</sup> century, first half			
Tuberculosis (bacille Calmette-Guérin) (1927)	Pertussis (1926)	Diphtheria toxoid (1923)	
<b>Yellow fever (1935)</b>	<b>Influenza (1936)</b> Typhus (1938)	Tetanus toxoid (1926)	
20 <sup>th</sup> century, second half			
<b>Polio (oral) (1963)</b>	<b>Polio (injected) (1955)</b>	Pneumococcus polysaccharide (1977)	Hepatitis B surface antigen recombinant (1986)
<b>Measles (1963)</b>	<b>Rabies (cell culture) (1980)</b>	Meningococcus polysaccharide (1974)	Lyme OspA (no longer available) (1998)
<b>Mumps (1967)</b>	<b>Japanese encephalitis (mouse brain) (1992)</b>	<i>Haemophilus influenzae</i> type B polysaccharide (1985)	Cholera (recombinant toxin B) (1993)
<b>Rubella (1969)</b>	<b>Tick-borne encephalitis (1981)</b>	Meningococcal conjugate (group C) (1999)	
<b>Adenovirus (1980)</b>	<b>Hepatitis A (1996)</b>	<i>H. influenzae</i> type B conjugate (1987)	
Typhoid ( <i>Salmonella</i> Ty21a) (1989)	Cholera (WC-rBS) (1991)	<b>Hepatitis B (plasma derived) (1981)</b>	
<b>Varicella (1995)</b>		Typhoid (Vi) polysaccharide (1994)	
<b>Rotavirus reassortants (1999)</b>		Acellular pertussis (1996)	
Cholera (attenuated) (no longer available) (1994)		Anthrax secreted proteins (1970)	
21 <sup>st</sup> century			
<b>Cold-adapted influenza (2003)</b>	<b>Japanese encephalitis (2009) (Vero cells)</b>	Pneumococcal conjugates (heptavalent) (2000)	Human papillomavirus recombinant (quadrivalent) (2006)
<b>Rotavirus (attenuated and new reassortants) (2006)</b>	Cholera (WC only) (2009)	Pneumococcal conjugates (13-valent) (2010)	Human papillomavirus recombinant (bivalent) (2009)
<b>Zoster (2006)</b>		Meningococcal conjugates (quadrivalent) (2005)	
<b>Dengue (2016)</b>			
<b>Ebola Zaire (based on a recombinant vesicular stomatitis virus, rVSV) (2019)</b>			

Viral vaccines are highlighted in blue color.

Another important milestone in vaccination was the development of attenuation. In 1879, Pasteur showed the attenuation of the *Pasteurella multocida* causing the chicken cholera by exposing the tissue of the dead infected chicken to dry environment. The application of this methodologies for the development of an anthrax and rabies vaccines followed from that discovery (Table 2.1) [1, 49, 50].

The few viral vaccines available until the end of the 19<sup>th</sup> century were produced in animal systems, such as calf skin for smallpox, rabbit spinal cord for rabies and mouse brain for Japanese encephalitis [1]. Developments in the following years, such as the use of fertile hen's eggs and the introduction of primary cell cultures, would define the current production processes up to today [1].

## 2.2 Current platforms for viral vaccine production

Already during the first half of the 20<sup>th</sup> century a transition from virus propagation using animals to alternatives like minced chicken embryos or embryonated chicken eggs was established. Until recently, the only acceptable substrates for vaccine production have been embryonated chicken eggs, primary cell cultures (e.g. chicken embryo fibroblasts, CEF) or human diploid cell lines (e.g. WI-38 and MRC-5 cells). Only lately, continuous cell lines were used for the production of viral vaccines for human use. For example, Vero cells, which were derived from the African green monkey kidney, have been used for the production of inactivated polio and rabies vaccines [51], and, most recently, for the production of the live-attenuated dengue vaccine [52]. The Madin-Darby canine kidney (MDCK) cells and the baby hamster kidney (BHK-21) cells are also currently applied for the production of influenza and various veterinary vaccines, respectively. Practical and economic limitations for the use of those cell lines to make larger numbers of doses of human vaccines have encouraged investigations of new manufacturing strategies and cell platforms [53].

### 2.2.1 Embryonated chicken eggs

In 1931, Ernest Goodpasture discovered that a hen's egg was an ideal production system for fowl pox virus, and a whole new, production system was born [54]. This led to the licensure of the first influenza vaccine in 1945 [55, 56]. Also, in the 1930s, Max Theiler developed the first vaccine against yellow fever virus (YFV) in embryonated chicken eggs (using the previously developed attenuated strain 17D), based on Goodpasture's method [1]. Even now, in ovo production is still widely practiced for the production of both of these vaccines (Table 2.2) [53].

Table 2.2. Summary of main types of vaccines licensed for use in humans. Adapted from Ulmer et al. (2006) [53].

Vaccine type	Selected disease targets	Vaccine preparation
Live attenuated	<b>Smallpox</b>	<b>Crude preparation of cowpox infected calf skin</b>
	Tuberculosis	<i>Mycobacterium bovis</i> BCG grown in media
	<b>Yellow fever</b>	<b>Purified, attenuated virus grown in eggs</b>
	<b>Polio</b>	<b>Purified, attenuated virus grown in tissue culture cells</b>
	<b>Chickenpox</b>	<b>Purified, attenuated virus grown in tissue culture cells</b>
	<b>Rotavirus</b>	<b>Purified, attenuated virus grown in tissue culture cells</b>
Killed	<b>Influenza</b>	<b>Purified, attenuated virus grown in eggs</b>
	Typhoid fever	Inactivated <i>Salmonella typhi</i> grown in media
	Plague	Inactivated <i>Yersinia pestis</i> grown in media
	Whooping cough	Inactivated whole-cell <i>Bordetella pertussis</i> grown in media
	<b>Influenza</b>	<b>Inactivated virus grown in eggs</b>
	<b>Polio</b>	<b>Inactivated virus grown in tissue culture cells</b>
Purified subunit	<b>Hepatitis A</b>	<b>Inactivated virus grown in tissue culture cells</b>
	Diphtheria	Inactivated toxin from <i>Corynebacterium diphtheriae</i> grown in media
	Tetanus	Inactivated toxin from <i>Clostridium tetani</i> grown in media
	Pneumococcus	Polysaccharides from 23 <i>Streptococcus pneumoniae</i> strains grown in media
	Meningococcus	Polysaccharides from four <i>Neisseria meningitidis</i> strains grown in media
	<i>Haemophilus influenzae B</i>	Polysaccharides from <i>H. influenzae</i> chemically conjugated to carrier protein
	Pertussis	Acellular extract of <i>B. pertussis</i> grown in media
Anthrax	Culture supernatant of <i>Bacillus anthracis</i> grown in media	
Recombinant subunit	<b>Hepatitis B</b>	<b>Purified, recombinant HBsAg VLP produced in tissue culture cells</b>
	<i>Borelia burgdorferi</i>	Purified, recombinant OspA produced in tissue culture cells (no longer available)

Viral vaccines are highlighted in blue color.

In ovo vaccine production relies on the infection of fertilized hens' eggs, which act as parallel minifactories where virus replicates. For the case of the seasonal influenza vaccines, this process is used for both inactivated (killed) and live attenuated (weakened) vaccines [57]. A detailed description of different influenza vaccine types is presented in Chapter 2.3.2.

A typical example of an egg-based process is the production of seasonal influenza vaccines. Before production, reassortants of the selected strains and the egg-adapted influenza A/PR8/34 (H1N1) virus are prepared to support egg-based production. The reassortants are then injected into the allantoic cavity of fertilized hen's eggs and incubated for 2–3 d to allow the viruses to replicate. After the incubation time, the allantoic fluid is harvested from the eggs and a first clarification step starts, applying deep filtration or centrifugation. To produce inactivated vaccines, viruses are chemically treated with formalin, binary ethyleneimine (BEI) or  $\beta$ -propiolactone ( $\beta$ -PL) [58] and virions are purified. The manufacturing process continues with purification and testing. For the production of attenuated vaccines, the reassorting is done with a cold-adapted influenza virus. This cold-adaptation inhibits virus replication at body temperatures [59]. This way, attenuated vaccines may not only

induce strain-specific immunity, but also T cell responses that can confer protection against a wider spectrum of influenza viruses [60, 61].

Although there were improvements in the purification process and reassortant strains were developed, the basic egg-based vaccine production process has not changed much over time. This is primarily because the low profit margins of influenza vaccine products didn't support the development of new production technologies [53]. However, considering the current manufacturing capacity estimated at 1.467 billion doses, it would be necessary to increase the current capacity by a factor of 1.5 to supply the world's population within 1 year in case of an influenza pandemic [3, 62, 63]. This capacity appears not feasible with the egg-based system, which requires one to two eggs per vaccine dose [53, 64] and relies on a scale-up based on scale-out, i.e. increasing the number of eggs and applying automation to facilitate processing [65]. Additionally, the egg-based platform still faces some limitations inherent to its animal source. For example, the adaptation of IAV strains to egg propagation can derive in mutations in the virus' hemagglutinin (HA) protein, changing the antigenicity or reducing the vaccine effectiveness [66, 67]. Also, egg-derived attenuated influenza vaccine is still contraindicated in persons with anaphylactic egg allergy [68, 69]. Accordingly, the need of a large quantity of specific-pathogen-free (SPF) hens translates in additional process control and very long production cycle time. All these factors have recently accelerated the introduction of new cell-culture based manufacturing strategies [53].

### 2.2.2 Primary cell cultures

A major breakthrough in the establishment of cell culture-based production platforms was the successful propagation of poliovirus in **primary non-neural human cells** carried out by Enders, Weller and Robbins in 1949 [70]. The demonstration that poliovirus could be grown in cell culture in a relatively safe and easy manner was one of the key scientific discoveries that led to the development of poliovirus vaccines [70, 71] and to significant advances in virus vaccine development over the last 60 years [1].

Enders' discovery led to the development of the Salk inactivated polio vaccine, the first licensed whole-virus vaccine produced in the tissue culture, which was produced in **primary monkey kidney cells (PMKC)** [71]. The application of cell culture allowed for an easier scale-up and a direct monitoring and control during the virus production process. Moreover, this platform appeared as an alternative to address the concerns on egg-related allergies.

PMKC were used in the early days of inactivated polio vaccine (IPV) manufacture. However, from 1955 to 1963 millions of people were exposed to Simian Virus 40 (SV40), derived from the used

PMKC [72]. Despite the lack of conclusive data to demonstrate that SV40 has a causative role in some human cancers, the use of PMKC was later discontinued. Therefore, the animals used to generate primary cell lines or cell banks must be screened for viruses and their sera tested for antibodies against specific pathogens. This biosafety risk demonstrates the importance of full characterization of cell substrates, which may additionally include identity/stability tests, purity and bioburden tests (including test for bacteria, fungi, mycoplasma and mycobacteria) and tests against adventitious viruses (such as retrovirus and arbovirus) [21].

**Chicken embryo fibroblasts (CEF)** used for vaccine production are obtained from 9–11 d old chicken embryos coming from pathogen free hens [73, 74]. These cells are still widely used for the propagation of viruses for vaccine production and for control tests of avian vaccines [74]. Common human vaccines such as those against measles, mumps, rubella (M-M-R<sup>®</sup> II vaccine) and rabies (RabAvert<sup>®</sup>) are still produced in CEF. Even the production of advanced vaccines, such as viral vectors based on the MVA virus, still relies on the cultivation of primary cultures of CEF [21]. However, similar to the egg-based production platform, the use of CEF requires a reliable supply of SPF eggs to minimize the risk of contamination with chicken-derived pathogens, such as the avian leucosis viruses (ALV) [73, 74]. Therefore, this platform also comprises long production cycle times and the need of strict controls of the captive herds used as the source of eggs [75].

An alternative to overcome the drawbacks of using animal-derived primary cells arrived with the **human diploid cells (HDC)** [76], which are obtained from embryos or other human tissues and possess identical chromosome sets that are free of all known adventitious agents [77]. Hayflick in 1961 [76] and Jacobs in 1967 [78] developed the two most well known HDC strains (HDCS) based on human fetal lung tissue: the Wistar Institute (WI)-38 and Medical Research Council (MRC)-5 cell, respectively. For the first time in the history of cell culture technology, cell banks were prepared from both tissue extracts to provide international standardized cells for the production of several human viral vaccines [79].

The adaptation of rabies virus to WI-38 cells permitted the development of a potent, whole-virus inactivated rabies vaccine by Koprowski, Voktor and associates during the 1960's [80]. WI-38 cells have also been used for the production of rubella virus in the Measles, Mumps, and Rubella Live Virus vaccine (M-M-R II). On the other side, MRC-5 cells have been applied for the production of the Varicella Live Virus vaccine (Varivax<sup>®</sup>), hepatitis A vaccine (Vaqta<sup>®</sup> and Havrix<sup>®</sup>), rabies vaccine (Imovax<sup>®</sup>) and polio vaccine (Poliovax<sup>®</sup>).

HDCS have a long and excellent safety record. However, senescence, the decrease of growth and viability after a certain number of cell divisions [76], is an important limitation. HDCS have demonstrated constant morphological and chromosomal characteristics through 37 to 40 passages

[77]. However, imported MRC-5 cells are generally on their 20<sup>th</sup> passage, resulting in restricted mass production [81]. Ethical concerns due to their human fetal origin and the possibility of chromosomal aberrations (e.g. aneuploidy and polyploidy) during their expansion, have also complicated the development of new HDCS. Also, intrinsic limitations of adherent cells, such as the need of growth surface and medium supplemented with bovine serum to achieve the needed number of cells, have to be considered [65].

### 2.2.3 Continuous cell lines

Different to primary cells and human diploid cells, which present senescence after a certain number of passages, continuous cell lines are cells that have the capacity to replicate indefinitely, making them theoretically immortal. Prominent examples include Vero, MDCK, BHK-21, Chinese hamster ovary (CHO) and the insect *Spodoptera frugiperda* (SF9) cells.

Continuous cell lines currently used for viral vaccine production (e.g. Vero, BHK-21, MDCK) have been generated applying multiple passaging on primary cell cultures until the continuous cell line is obtained. The immortalization mechanisms of these cells are not fully understood. However, an analysis during the generation of the continuous cell line SC-1 suggested that alterations in the p53 and Rb pathways may be involved [82].

Currently, several commercial viral vaccines are produced using continuous cell lines. For example, MDCK cells are used for the production of the influenza vaccines Optaflu®, Celtura® and Flucelvax®. Vero cells are used for the production of the Japanese encephalitis (JE) vaccines Ixiaro® and Imojev®, the poliovirus vaccine Ipol®, the rotavirus vaccines Rotateq® and Rotarix®, and the dengue vaccine Dengvaxia®.

Since some of these cell lines require adherent surfaces for growth, cultivation systems such as “roller bottles, T-flasks, cell cubes, and cell factories are widely used for the production of vaccines at industrial scale” [65]. In order to overcome the burden of surface availability during industrial scale-up [83], microcarrier technology has been established have been applied for the production of vaccines in attachment-dependent cell lines. This technology is employed, for example, for the production of rabies vaccines [65], for the production and development of new polio vaccines [84-86] and for the development of newer vaccines for chikungunya [87], using adherent Vero cells.

Advances have also been made on development of suspension cell lines. For example, Vero cells have been adapted to serum-free media [88-92] and later to grow in suspension [93]. This technology is currently used for the cell-culture-based JE vaccine Ixiaro® and Imojev® [94]. Similarly, advances



---

have been made with MDCK cells for the production of influenza vaccine [95, 96], and suspension cultures are used for the production of Optaflu®, Celtura®, and Flucelvax® in MDCK cells [97-99]. The production capacity of influenza vaccine is of multiple thousands of liters. For example, Baxter owned a 6000 L facility in the Czech Republic for the production of 20 million doses/year of flu vaccine using Vero cells on microcarriers [100] (currently used for the production of inactivated polio vaccine), Seqirus has a 2500 L scale facility in Marburg, Germany for flu in MDCK cells in suspension, and a 5000 L scale facility (reported to produce 150 million doses/year) in Holly Springs, United States [65].

Although MDCK and Vero cells are well established as vaccine production platforms, the development of alternative continuous cell lines for the production of viral vaccines has continued. One example is the duck embryonic stem cell line EB66® (Valneva), which is already used for the production of GSK influenza vaccine and has demonstrated its potential as production platform for other human and animal viruses (such as MVA virus) in suspension cultures [101]. The EB66 duck cell line was obtained from a multi step process that did not involve any genetic, viral or chemical modifications [102]. EB66 cells were selected based in the expression of specific markers for stem cells, such as telomerase, SSEA-1, EMA-1, the ability to indefinitely self-renew *in vitro* and a long-term genetic stability [103].

The cell line QOR2/2E11 has been also used for the propagation of recombinant MVA virus. These cells, which were obtained from primary cultures of quail (*Colinus virginianus*) embryo cells, were immortalized by treatment with a specific dose of UV [104, 105] and adapted to growth in suspension. Following subcloning resulted in the isolation of the lead clone QOR2/2E11, which has been used for the development of vaccine production processes [104, 105].

Additionally, recent studies have been carried out on the human lung tumor-derived A549 cell line [106] to evaluate its suitability and safety as adenovirus production platform. In this regards, Shabram and Kolman (2014) carried out a thorough characterization of A549 cells and showed comparable safety attributes to any other cell substrate for the manufacture of vaccines, although it is a tumor-derived cell line [107]. Another continuous cell line under development is the PBS-12F, a chicken embryo cell line derived from the PBS-1 cells, which were immortalized by *N*-methyl-*N'*-nitro-*N*-nitrosoguanidine (MNNG) treatment [108]. The PBS-12F cell line was adapted to growth in serum free conditions and supports the replication of human and reassortant H5N1 influenza strains with titers comparable to, and even higher than, those achievable with MDCK, Vero, and primary chicken embryo kidney (CEK) cells [109]. Alternative cell lines that have demonstrated its potential for the production of human vaccines are the novel porcine suspension cell line PBG.PK2.1 (for IAV) from

ProBioGen AG [110] and the adherent CEF-derived cell line DF-1 (for recombinant MVA) [111, 112].

Continuous cell lines have an infinite life potential *in vitro*, often display an abnormal chromosomal number and the large majority are tumorigenic [113]. Therefore, the main concern for the use of continuous cell lines is the transferability of host cell-derived oncogenic components to vaccine recipients [25]. Based on the high risk that DNA coding for transforming factors represent [25], the amount of DNA allowed in an injectable vaccine is currently limited to 10 ng per dose [25, 114]. In this regard, adjustments in the corresponding downstream processes, such as the use of more conventional harvest technologies along with column chromatography, have been carried out to achieve a high level of purification [58]. However, in a longitudinal study with monkeys injected with up to 1000 µg of DNA derived from a continuous human cell line, no appearance of tumors were observed [115]. Therefore, the limit of 10 ng of DNA per dose may overestimate the risk of potential oncogenic components [25].

### 2.2.4 Designer cell lines

Recombinant or designer cell lines such as HEK293<sup>®</sup>, PER.C6<sup>®</sup>, CAP<sup>®</sup>, DuckCelt<sup>®</sup>-T17, AGE1.CR<sup>®</sup> (CR) or AGE1.CR.pIX<sup>®</sup> (CR.pIX) are currently considered for production of various vaccines [116-121]. These novel cell substrates were originated either from human (e.g. HEK293, PER.C6 and CAP) or avian sources (e.g. DuckCelt<sup>®</sup>-T17, AGE1.CR<sup>®</sup>, AGE1.CR.pIX<sup>®</sup>).

The **human designer cell lines** HEK293<sup>®</sup>, PER.C6<sup>®</sup>, CAP<sup>®</sup> and CAP-T<sup>®</sup> were developed by transforming or stably transfecting human embryonic kidney cells (HEK293<sup>®</sup>), human embryonic retinal cells (PER.C6<sup>®</sup>) or primary human amniocytes (CAP<sup>®</sup>) with the early region 1 (E1) of human adenovirus type 5 (Ad5) [122-125]. From these, HEK293<sup>®</sup> and CAP<sup>®</sup> cells include additionally the gene sequence of the minor capsid protein IX (pIX) [126]. The CAP-T<sup>®</sup> derive from the CAP<sup>®</sup> cells, with the difference that the former contain additionally the SV40 large T-antigen [125, 127]. Because they are derived from oncogene transformed or immortalised human cells, these novel cell substrates are considered to bear a potential tumourigenic risk [21].

The **avian designer cell lines CR and CR.pIX** have a similar origin. The CR cell line derives from the engineering of retina cells, obtained from explants of a single Muscovy duck (*Cairina moschata*) embryo. To obtain the CR cells, these primary cells were immortalized with the E1 region of human Ad5 [118]. “The E1A and E1B genes were introduced into the cells by liposomal transfection of an expression plasmid without exogenous (antibiotic) selection” [25]. In addition, Jordan et al. (2013) [25] demonstrated (via immunofluorescence assays of cultures at different passages) that “only cells

that stably expressed the E1A and E1B genes survived beyond senescence, confirming the intended induced immortalization”.

As per Jordan et al. (2013) [25], “the CR cell line was further modified by transfection of an expression plasmid for the adenovirus pIX structural protein to obtain the CR.pIX cell line”. It has been proposed by Jordan et al. (2013) [25] that “some viruses, even if they are not related to adenoviruses, benefit from the presence of pIX because this protein may constitutively activate the heat shock protein 90 (Hsp90), a central factor in heat shock responses” [25, 118]. Jordan et al. (2013) [25] proposed that the activation of chaperones in the heat shock cascade may alleviate the metabolic burden that the virus replication imposes to the host cells, increasing the yield of infectious particles for some viruses.

The adaptation of CR and CR.pIX cells to proliferation in suspension was performed by “cultivation in commercial media designed for human suspension cell lines” [27]. Since commercial media did not prove to be suitable for MVA virus propagation in these cell lines, the chemically defined media CD-U2, CD-U3 (for cell proliferation) and the CD-VP4 (for MVA virus production) were developed. Using these platform media, CR.pIX cells support replication of IAV and the vaccinia virus MVA85A, a promising vaccine against tuberculosis, to high titers [26, 118]. A sound description of the metabolic performance [29, 128], influenza and MVA virus production yields [26, 28, 32] and the process development for virus production in bioreactor of both cell lines was reported previously [28, 29].

Recently, the novel DuckCelt®-T17 cell line was developed without applying the transfection of Ad5 E1A and E1B genes. This cell line was generated from primary embryo duck cells by “constitutive expression of the duck telomerase reverse transcriptase (dTERT)” [129]. This cell line was recently tested for the propagation of various human, avian and porcine influenza strains, showing satisfactory virus productivities particularly for the tested avian strains [129].

## **2.3 Influenza virus vaccine**

### **2.3.1 Influenza virus structure and replication cycle**

Influenza viruses are enveloped single-stranded, negative-sense RNA viruses, which belong to the *Orthomyxoviridae* family. Based on their structural characteristics, they are classified in types A, B, C and D. Both type A and B viruses have 8 segments in their genomes and express hemagglutinin (HA)

and neuraminidase (NA) as surface antigens, whereas types C and D viruses have 7 segments and express a HA-esterase-fusion protein on their surface [130, 131]. Moreover, influenza A viruses (IAV) are grouped according to the expression of 16 HA and 9 NA subtypes [131, 132], each one showing different genetic and antigenic characteristics [133]. The bat IAV-like viruses are a group phylogenetically close to but unable to reassort with IAV and express 18 HA and 11 NA subtypes [134, 135].

Influenza types A, B and C can infect humans, although types A and B are the most common. Type B influenza viruses are a substantial cause of annual influenza epidemics, whereas type C viruses, which also infect pigs, rarely account for human infection and epidemics [130, 131]. Influenza D viruses affect cattle and are not known to infect humans [131]. Type A and B influenza viruses can also infect a broader variety of animals including aquatic birds, pigs, horses and seals, showing a highly adapted tropism to each host [130, 133, 136]. Since both type A and B viruses cause most of the epidemics, especial attention has been put on their virology and as targets for seasonal influenza vaccination [68].

### *Structure of influenza A virus*

The RNA of IAVs is surrounded by a lipid bilayer derived from the host cell. Embedded in this lipid envelope, HA, NA and matrix 2 (M2) proteins are localized (Figure 2.1) [137]. The HA glycoprotein is responsible for virion adsorption by strongly binding to the sialic acid residues on the host cell surface [137]. “The HA glycoprotein is synthesized as an HA0 molecule that is post-translationally cleaved into HA1 and HA2 subunits; this cleavage is essential for virus infectivity” [137]. The cleavage of HA0 generates the carboxyl terminus of HA1 and the amino terminus of HA2 (necessary for membrane fusion and infectivity) ([138], as cited in [137]). The HA0 glycoproteins of low-pathogenicity avian influenza (LPAI) viruses and human influenza viruses are cleaved at a conserved arginine residue by trypsin-like proteases ([139], as cited in [137]). Therefore, infection with these viruses is restricted to tissues in which trypsin and trypsin-like proteases are present [137]. In contrast, for high-pathogenicity avian influenza (HPAI) viruses, this cleavage can be done by multiple intracellular proteases, such as furins ([140], as cited in [137]), or by non-trypsin-like extracellular proteases [137].

Together with the HA glycoprotein, the M2 protein also participates in virus uncoating for viral RNA release into the host cells. On the other side, the NA glycoprotein enables the release of new virions from the cell surface. Indeed, currently available antiviral drugs are based on neuraminidase inhibitors (Oseltamivir, Zanamivir) and M2 channel blockers (Amantadine, Rimantadine) [141].

At the inner side of the lipid envelope, matrix 1 proteins (M1) can be found, which are the most abundant proteins in the virion and associate with the viral ribonucleoprotein (vRNP) complexes. The

vRNP complexes are formed by nucleoproteins (NP), polymerase basic 1 (PB1) and 2 (PB2), and polymerase acidic proteins (PA), which are associated to the 8 segments of viral RNA (Figure 2.1). The transcription and replication of viral RNA are carried out by PB1, PB2 and PA proteins (also known as polymerase complex). The virus also encodes a nuclear export protein (NEP) [137], the non-structural proteins 1 and 2 (NS1 and NS2), which are involved in expression of viral proteins and viral replication, respectively [130, 142], and the virulence factor PB1-F2 (proapoptotic factor) [143].

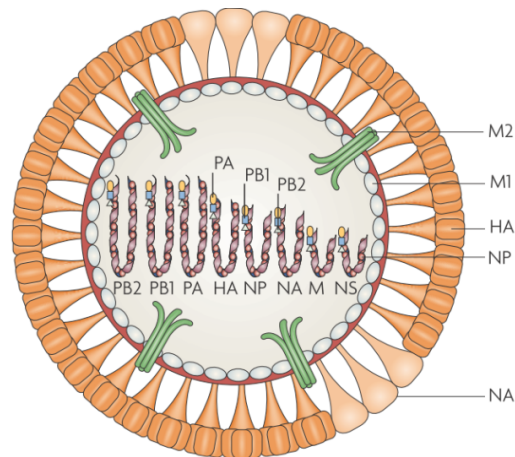


Figure 2.1. Schematic structure of influenza A virus (IAV). The IAV particle has a lipid envelope (acquired from the membrane of infected cells). Envelope proteins hemagglutinin (HA), neuraminidase (NA) and matrix protein 2 (M2) are embedded in the lipid bilayer of the viral envelope. HA and NA are the main surface glycoproteins of IAVs. The ratio of HA to NA in the viral envelope ranges from 4:1 to 5:1. Figure adapted with permission from Subbarao and Joseph (2007) [137]

Due to the lack of a proofreading mechanism of influenza RNA polymerase, frequent mutations can occur, resulting in a constantly changing antigenic appearance. Furthermore, in the case of a simultaneous infection in a single host with two or more influenza strains, reassortment of their genome segments might occur, producing new genomic combinations in the progeny [68, 143]. A so-called antigenic shift occurs, when through this combination a completely new serotype of HA is introduced into circulating human viruses. These reassorted strains may be the source of new pandemic influenza variants [143].

### *Replication cycle of influenza A virus*

Cell infection starts with the adsorption of the virions to the cell surface and the proteolytic cleavage of HA protein. Nunes-Correia reported that at 37 °C influenza virus binding to the surface of MDCK cells can achieve its equilibrium after 20 min [144]. This results in the receptor-mediated endocytosis of the virus particles approximately 20 min after infection [145], culminating with nearly 98% of bound virions being internalized 60 min after infection [144]. Once inside the cell, the interior of the virions is acidified by M2 proteins, which function as a pH-activated ion channel. Then, virion uncoating is led by this internal acidification along with the fusion of the viral envelope with the endosomal membrane enhanced by the partially cleaved HA proteins. Replication of free viral RNA begins using the cell machinery. Synthesized membrane associated proteins (HA, NA and M2) are transported to the cell membrane, whilst newly formed vRNP complexes attach the internal side of the membrane through M1 protein mediating virus budding (Figure 2.2).

Virus budding, which takes place at the apical surface membrane of infected cells [146], can be detected 5–8.5 h post infection (hpi), for influenza strains propagated in MDCK cell cultures [147-150]. This delay time is often called the “eclipse phase”. The newly synthesized virions attach again to the cell surface through the interaction between the HA and the sialic acids contained in the cell surface glycoproteins. Finally, virions are broken free due to cleavage of the bond between the sialic acid and the cell surface glycoprotein by the virus NA [151].

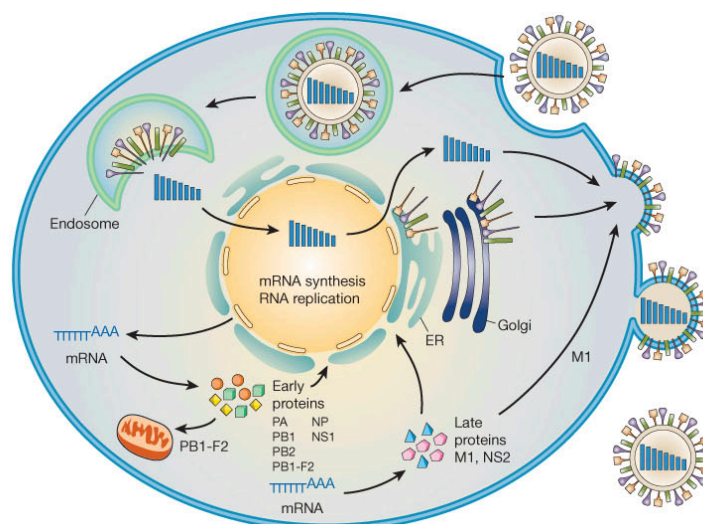


Figure 2.2. Replication cycle of influenza A virus (IAV). After endocytosis, the viral ribonucleoprotein (vRNP) complexes are released into the cytoplasm and transported to the nucleus for replication and transcription. Synthesized messenger RNAs (mRNA) are exported to the cytoplasm for translation of early viral proteins (required for replication and transcription), which are transported back to the nucleus. At late stages of the infection cycle, vRNPs are exported from the nucleus, facilitated by M1 and NS2 proteins. Virulence factor PB1-F2 associates with mitochondria. The assembly and budding of progeny virions occurs at the plasma membrane. Figure adapted with permission from Neumann, Noda and Kawaoka (2009) [152].

### 2.3.2 Cell culture-based influenza vaccine production

Seasonal influenza vaccines are tri- or tetravalent, each dose containing two IAV strains (H3N2 and H1N1) and one or two influenza B strains [68]. The content of such vaccines is established by previous analyses and recommendations given by the World Health Organization (WHO): the Global Influenza Surveillance Network (GISN) undertakes a year-round surveillance of “influenza strains in the population, and at the start of the influenza season the WHO announces, which dominant circulating strains should be included in the vaccine” [153].

Vaccines against a pandemic influenza strain, as in the case of the H1N1 pandemic in 2009, would be monovalent, containing just HA proteins from the targeted virus. Since there would be little or no immunological memory in the population against this new pandemic strain, two doses of inactivated vaccine would be needed to induce the necessary protective immunity [154].

In any of both cases, seasonal and pandemic, influenza vaccines are currently made from either inactivated virus, virus subunits (split virion), whole virion or live attenuated influenza viruses (LAIV) propagated in the allantoic cavity of 9–12 d old embryonated chicken eggs from certified farms under strict veterinary control [153]. For inactivated vaccines the virus strains are propagated separately, harvested and inactivated with formalin. To produce split-virion vaccines, the HA and NA subunits

are then released by disrupting the lipid envelope [68]. The vaccine strains are then blended containing 15 µg of each of the target viruses [155].

LAIVs grow at 25 °C and do not produce systemic symptoms of influenza disease [68, 156]. These cold-adapted influenza strains are propagated and harvested but not chemically inactivated. The three strains for the vaccine are then blended containing  $10^{6.5}$ – $10^{7.5}$  active virus particles each [155, 157]. Given their nature, LAIV's can trigger an additional immune response compared to inactivated viruses [158-160].

The production of influenza vaccine in embryonated hens' eggs is a well established process that has been carried out for more than 60 years [161] and so far has been adequate for the supply of seasonal influenza vaccines [162]. However, the egg-based process requires huge capacities and may face a shortage in the supply of embryonated eggs when an influenza pandemic occurs [99]. Therefore, a large effort was made over last 20 years by authorities and vaccine producers in the establishment of alternative production technologies, especially cell culture-based processes [163].

Particularly, the use of cell culture platforms results in reduction of lead times compared with egg-based processes and enables the establishment of robust processes under controlled conditions. Furthermore, the utilization of animal cells brings the possibility to produce influenza vaccines with avian strains and eliminate the selectivity of certain viral phenotypes during viral replication, which is generally found in embryonated eggs [164].

Currently, MDCK, Vero and PER.C6 cells have been recommended for use in commercial cell culture-based production of influenza vaccines [165]. Specially, MDCK cells and Vero cells have dominated the commercial production processes and to date, no influenza vaccines derived from PER.C6 have been approved for use in humans [166]. A summary of currently available influenza vaccines produced in cell culture is given in Table 2.3.



Table 2.3. Commercially available influenza vaccines produced in cell culture. Based on reports by Perez Rubio and Eiros (2018) [166] and Milian and Kamen (2015) [3].

Vaccine	Composition	Cell-based production platform	Manufacturer
Optaflu/ Fulcelvax	Trivalent vaccine, composed of two influenza A (H1N1, H3N2) strains and one type B strain, produced in MDCK cells [98, 167, 168]	Suspension MDCK 33016PF cell line grown in suspension in a serum-free and protein-free medium [98, 167, 168]	Seqirus (formerly manufactured by Novartis)
Celtura	Monovalent, MF59-adjuvanted, A/H1N1 pandemic vaccine. Approved by German authorities in November 2009 [168].	Analog to Optaflu [98, 167, 168]	Seqirus (formerly manufactured by Novartis)
Preflucel	Seasonal trivalent influenza vaccine formulated with inactivated H1N1, H3N2, and influenza B. Licensed in the EU in 2010 [62]	Adherent Vero cells [163]	Nanotherapeutics, Inc. (formerly manufactured by Baxter)
Celvapan	Monovalent inactivated H5N1 or H1N1. Approved for commercialization in the EU in 2009 [62]	Adherent Vero cells	Nanotherapeutics, Inc. (formerly manufactured by Baxter)
Flucelvax Quadrivalent	Tetavalent subunit vaccine: two influenza A (H1N1, H3N2) strains and two influenza B strains (Victoria, Yamagata). Approved by the FDA in 2016 [166]	MDCK cells from egg-adapted influenza viral seeds	Seqirus

The emergence of the H5N1 and H1N1 influenza pandemic strains in recent years has motivated the development of new platforms for influenza vaccine production. One example is Sanofi's Flublok<sup>®</sup> (originally developed by Protein Science Corporation), which is the first recombinant hemagglutinin (HA) vaccine licensed by the FDA and is produced using a platform using the insect cells and the baculovirus expression system technology [169]. As described in Chapter 2.2.4, designer cell lines grown in suspension, such as CR and CR.pIX (ProBioGen AG, Berlin, Germany), have been also intensively explored as alternative production platforms of whole influenza virus, with very promising results [26, 28, 99].

For cell-culture based IAV production, fast cell growth, high viability and appropriate cell metabolism are to be considered. According to Genzel et al. (2009) [99], the optimization of influenza virus infection and propagation should focus on:

- Quality of virus seeds: they should provide a high infectivity and contain a low proportion of non-infectious or defective particles, which can hinder virus propagation and thus reduce virus production yields [170].
- Trypsin activity: the proteolytic cleavage of the influenza HA glycoprotein enables the fusion of the viral and endosomal membranes, leading to the release of viral RNA into the host cell's

cytoplasm. For *in vitro* cell infections, this proteolytic cleavage is enabled by the addition of trypsin to the cultivation medium at time of infection (TOI).

- Fast virus propagation to high hemagglutinin (HA) titers ( $>2.4 \log_{10}$  (HAU/100  $\mu$ L)) and infectious virus titers ( $>1 \times 10^8$  virions/mL, TCID<sub>50</sub>)
- Stable virus titers (no unspecific virus degradation)
- Composition of cultivation broths for efficient purification (low DNA and protein content desirable)

## 2.4 MVA virus for vaccine production

The modified vaccinia Ankara (MVA) virus is an attenuated strain of vaccinia virus (VACV) that belongs to the *Orthopoxvirus* genus of the *Poxviridae* family. VACV is the virus that was used to achieve the global eradication of smallpox [171].

MVA virus was obtained from the strain chorioallantois vaccinia virus Ankara (CVA) [172], which derived directly from VACV. CVA was maintained by alternating passages in the skin of calf and donkeys at the Turkish vaccine institute in Ankara [25] and in 1953, in Germany, attenuated by serial passaging on chicken-derived material [25, 173]. MVA was obtained from passage 516 by plaque isolation [25]. This new isolate showed a loss of 15% of its genome at six deletion sites [25, 174, 175] and other minor disruptions in several genes, which limited significantly its host range [25]. This way, replication of MVA in human cells was blocked or severely impaired [11, 12, 25].

As per Jordan et al. (2013) [25], despite the inability of MVA virus to replicate in human cells, its viral genes are expressed very efficiently, resulting in a robust T-cell mediated immune response [13, 176-178] that is not inhibited by preexisting immunity [179]. In addition, vaccinia viruses can be manipulated genetically by homologous recombination, accepting inserts of at least 25,000 bp [13, 25, 180, 181]. These characteristics made MVA a suitable candidate as a vector vaccine.

### 2.4.1 Vaccinia virus structure and replication cycle

VACV has a complex structure and a assembly pathway with several forms of infectious viruses from each infected cell [182]. The VACV genome, viral enzymes and factors for transcription of the early group of genes are packaged in the core of infectious virus particles [182, 183]. A detailed description of both structure and replication cycle is presented in the following sections.

### Structure

VACV is an enveloped brick-shaped virus with a size of approximately  $350 \times 270$  nm. Figure 2.3 shows the structure of the intracellular mature virus (IMV) of VACV, which is one of the infectious forms present during the virus replication cycle (Figure 2.4). The IMV has a double membrane envelope, forming a 30 nm-thick surface layer, which surrounds the inner core [30]. The core contains a large double-stranded DNA genome of approximately 200 kb and viral enzymes, including DNA-dependent RNA polymerase and RNA-processing enzymes (Figure 2.3). VACV contains no helical or icosahedral nucleocapsid [30].

Another infectious form of VACV, the extracellular enveloped virus (EEV), contains an additional lipid bilayer membrane that is wrapped around the entire IMV particle [30] (Figure 2.4). Both IMV and EEV can initiate the infectious cycle [184], but differ in their surface glycoproteins and in the number of wrapping membranes, and may enter the cells by different mechanisms [184, 185]. A detailed description of the VACV replication cycle is presented in the following chapter.

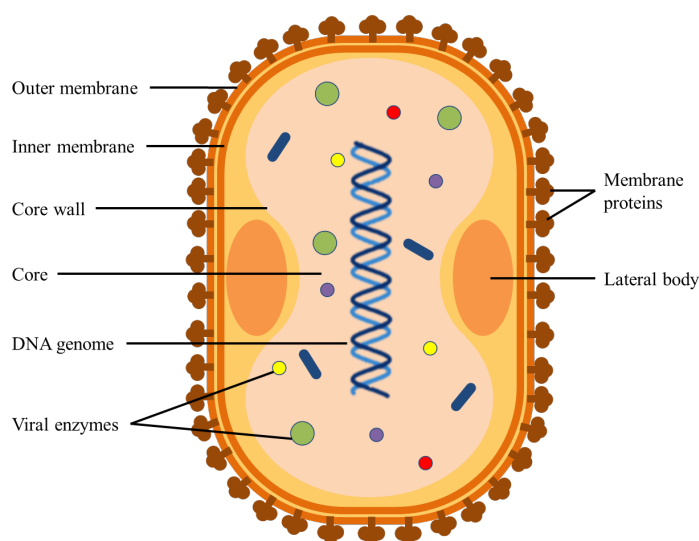


Figure 2.3. Schematic structure of an infectious intracellular mature vaccinia virion (IMV). Figure adapted from Harrison et al. (2004) [30].

### Replication cycle

Like all poxviruses, VACV replicate in the cytoplasm using their own machinery, depending only minimally on the host cell for DNA and RNA replication [30]. A schematic representation of the single-cell replication cycle of vaccinia virus is presented in Figure 2.4. IMV and EEV bind to and enter their host cells by recognition of glycosaminoglycans (GAGs) present on the surface of the target cells. Following membrane fusion and virus internalization, virus uncoating takes place, and the viral core is released into the cytoplasm [30]. Non-permissive poxvirus infections generally abort at a point

downstream of the binding/fusion step [185]. The core contains, the viral genome, the viral DNA-dependent RNA polymerase, “initiation” proteins necessary for specific recognition of the promoters of viral early genes, and several RNA processing enzymes that modify viral transcripts [30]. Once in the cytoplasm, the core synthesizes early viral mRNAs, which are subsequently extruded in an ATP-dependent manner and translated by the cellular protein-synthesizing machinery [186, 187]. During this early replication phase, approximately half of the viral genes are expressed [30]. Some early proteins have a sequence similar to cellular growth factors and can induce proliferation of neighboring cells or counteract host immune defense mechanisms [30]. The synthesis of early proteins also induces the uncoating of the core, which leads to the release of a nucleoprotein complex containing the viral genome [30]. Early gene expression ceases at this point and existing early proteins catalyze the replication of the viral DNA genome, which serves as template for further viral DNA replication [30]. Newly synthesized viral DNA molecules serve as templates for transcription of viral intermediate-phase genes. The transcription activation of intermediate genes also requires the “intermediate transcription factors”, which are “early” proteins that, according to Harrison et al. (2004) [30], “confer specificity for intermediate promoters on the viral RNA polymerase, as well as a host-cell protein (Vtlf2) that relocates from the infected cell nucleus to the cytoplasm”.

The proteins encoded by intermediate mRNAs include those necessary for transcription of late-phase genes [30]. The latter genes encode the structural virions proteins, virion enzymes and other essential proteins (e.g. early initiation proteins) to be incorporated into virus particles during assembly [30]. Once these proteins are synthesized by the cellular translation machinery, the assembly of progeny virus particles begins within the so-called “viral factories” [30].

As described by Harrison et al. (2004) [30], the initial virus assembly results in formation of the immature virus (IV) (Figure 2.4), which is a spherical particle delimited by a membrane obtained from an early compartment of the cellular secretory pathway [30]. This virus particle matures into the brick-shaped IMV, which is released only on cell lysis [30] (Figure 2.4). The IMV can acquire a second, double membrane from a trans-Golgi or early endosomal compartment to form the intracellular enveloped virus (IEV) [30] (Figure 2.4). The IEVs move to the cell surface on microtubules where fusion with the plasma membrane forms cell-associated enveloped virus (CEV) (Figure 2.4). These CEV induce an actin polymerization that promotes a direct transfer to neighboring cells to continue with virus propagation [30] (Figure 2.4). Alternatively CEV can also be released from the membrane as EEV [30].

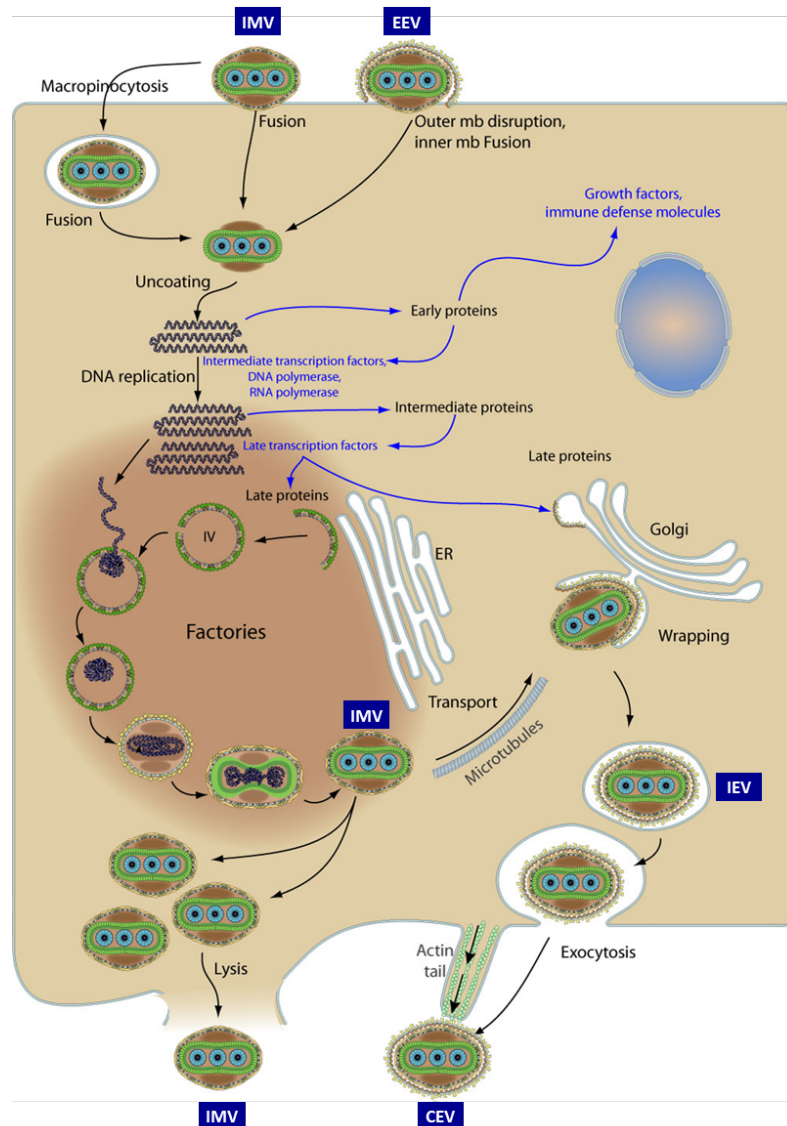


Figure 2.4. Replication cycle of vaccinia virus (VACV). Vaccinia infectious particles exist as intracellular mature virus (IMV) IMV and as extracellular enveloped virus (EEV). From McFadden 2005 [185]: the binding of IMV and EEV is determined by several viral proteins and by glycosaminoglycans (GAGs) on the surface of the target cell or by components of the extracellular matrix. Fully permissive viral replication is characterized by three waves of viral mRNA and protein synthesis (known as early, intermediate and late), which end with the morphogenesis of the IMV (see *Replication cycle* for a detailed description) [185]. IMVs are transported via microtubules and wrapped in a Golgi-derived membrane to form the intracellular enveloped virus (IEV). The IEV fuses to the cell membrane forming the cell-associated enveloped virus (CEV), which is either extruded to a neighboring cell by actin-tail polymerization or is released in the form of an EEV. IMV can also be released by cell lysis. Figure adapted from [ViralZone](#), SIB Swiss Institute of Bioinformatics, 2020 (licensed under [CC BY 4.0 International License](#)).

### **2.4.2 MVA virus as vector vaccine**

Vector vaccines are based on well-characterized infectious agents suitable for genetic manipulation and known to be stably attenuated [25, 51, 188, 189]. They should be ideally replication-deficient in the intended recipient, so that they can be given even to immune-compromised patients in both therapeutic and prophylactic treatments [25]. Nevertheless, vector vaccines should remain functional in the intended recipient, even in cases of a pre-existing immunity or the reactivation of the immune response against the vector [25, 188, 189].

Viruses investigated for immunization against infectious and neoplastic diseases include sendai virus, alphaviruses, measles virus, adenoviruses of different animal species, nonintegrative lentiviral vectors, vesicular stomatitis virus, and poxviruses (vaccinia virus, MVA, and avian poxviruses) [25, 190, 191]. Especially promising vectors are the highly attenuated poxviruses, including modified vaccinia virus Ankara (MVA) [23]. MVA virus vectors have a very efficient immunogenicity and are safe for use in humans. On the one hand, as reported by Gómez et al. (2013) [22], “they express gene products within cells that are efficiently presented by both MHC class I and class II pathways, leading to activation of CD4<sup>+</sup> and CD8<sup>+</sup> T cells”. Moreover, the safety of MVA virus for use in humans has been demonstrated during the smallpox eradication campaign of the World Health Organization and, more recently, in numerous clinical trials for the treatment of various diseases [25] (e.g., [192-196]).

The increasing application of recombinant MVAs into clinical trials has been possible thanks to ongoing advances in vector technology, quality control and better immune monitoring [180]. “Various recombinant MVA that express different viral heterologous antigens have been generated and extensively tested in pre-clinical and clinical trials as candidate vaccine against diseases such as AIDS, influenza, severe acute respiratory syndrome (SARS) and human respiratory syncytial virus (RSV) infection [15, 197-199]” [200]. In addition, MVA-based vector vaccines have proven to elicit virus neutralizing antibodies against SARS-CoV, MERS-CoV, Zika virus and Ebola viruses in animal models [17-20].

### **2.4.3 MVA virus production**

While MVA’s host restriction increases safety, it also impacts its manufacturing. As reported by Jordan et al. (2013) [25], “vectors that are highly attenuated amplify only to very low levels or not at all at the site of injection and therefore have to be given at high doses for optimal stimulation of the immune system [201]”. In this regard, the expected doses range for the use of MVA as a vector

vaccine may be around  $10^8$  pfu/mL [22, 23], and should be preferably produced in media free of animal-derived components [200].

Currently, MVA virus, similar to other viruses adapted to avian substrates (e.g. IAV or YFV), is mainly produced in embryonated chicken eggs or CEF [21] with infectious titers within the range of  $0.1\text{--}10.0 \times 10^8$  pfu/mL [33, 34]. However, the use of variable primary animal-derived material is not an optimal scenario for the manufacturing processes and safety of the product. Furthermore, as described by Jordan et al. (2013) [25], “primary cells are difficult to adapt to advanced cultivation strategies in modern bioreactors”.

To overcome this problem, two cell culture-based production platforms were developed. On the one hand, the embryonic avian cell lines EB14 (chicken embryonic stem cells) [202] and EB66 (duck embryonic stem cells) [31] have shown to be highly permissive to the recombinant strains MVA-GFP (expressing green fluorescent protein) and MVA-HCV (expressing antigens for hepatitis C virus). Both cell lines exhibited MVA virus titers of  $1.0 \times 10^8$  pfu/mL in suspension cultures using a chemically defined medium.

On the other hand, two fully permissive avian suspension cell lines, CR and CR.pIX were developed by Jordan et al. (2009) [118] and adapted to proliferation in a chemically defined medium to enable the establishment of robust high-yield production processes [26, 27, 203]. Especially high MVA virus yields were observed in CR.pIX cells cultures, reaching peak titers of  $3.2 \times 10^8$  pfu/mL [26].

Because MVA spreads preferably to the neighboring cells via cell-to-cell contact (see Chapter 2.4.1), both EB66 and CR.pIX production platforms employed similar biphasic cell culture formats, where cells were expanded during 72 h and cell aggregates were induced at TOI (Figure 2.5). Cell aggregation was achieved with the addition of one volume of virus production medium (supplemented for example with 0.3 mM  $\text{CaCl}_2$  for EB66 cells [31]) prior to virus infection. In both cases, an optimal multiplicity of infection (MOI) of 0.05 was identified [26, 31]. Since most of the MVA infectious virions appear within infected cells (i.e. as IMV, IEV, CEV), virus harvest is performed by homogenization of the cell broth (typically 48–72 hpi) followed by a clarification step [31].

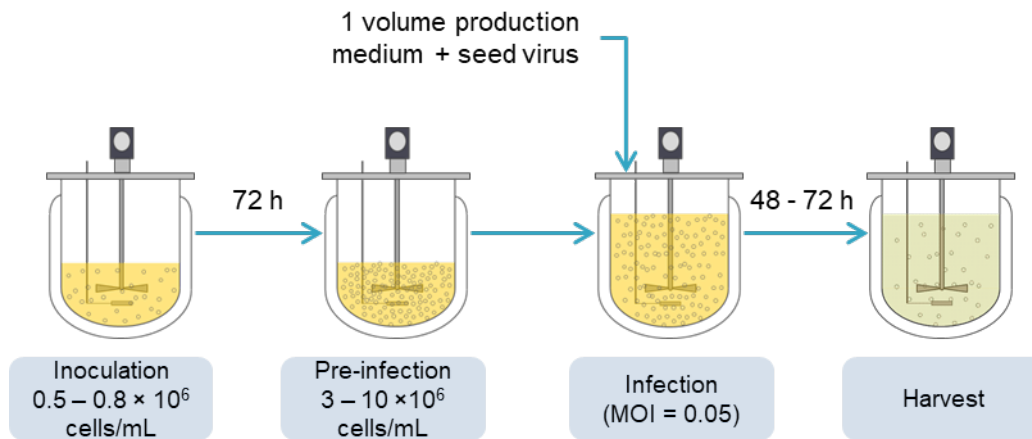


Figure 2.5. Biphasic process for the production of MVA virus in suspension cultures of CR.pIX and EB66 cells. Cells are first expanded during 3 d. Then, virus infection is initiated by adding the seed MVA virus together with 1 volume of production medium (CR.pIX process) or prior to addition of production medium (EB66 process) at a multiplicity of infection (MOI) of 0.05. Produced MVA viruses are harvested at the time of maximum virus titer, typically after 48–72 hpi, by cell disruption and clarification [26, 31].

Jordan et al. (2013) carried on further studies on the replication of serial MVA virus (wild-type) passages in a chemically defined medium using suspension CR cells [32]. It was observed that virus titer increased continuously along the tested 20 passages and that most of the infectious virus particles were released in the culture's supernatant (i.e. as EEV), rather than associated or within infected cells (as observed in the typical cell aggregate-based process) [32]. As a result, a MVA strain (MVA-CR19) was obtained, which propagates also in non-agglomerated CR.pIX suspension cells. With this new isolate, that represents a different genotype of MVA [32], titers in the order of  $10^8$  pfu/mL were obtained at a conventional cell density (CCD) of around  $2.0 \times 10^6$  cells/mL (after dilution with cell propagation medium). As a higher fraction (75%) of infectious MVA-CR19 is released into the supernatant, harvest of infectious units does not require whole-cell lysates anymore, facilitating the subsequent downstream processing [32].



---

## 2.5 High cell density approaches in animal cell culture processes

According to Griffiths et al. (1992) [204], the term “high cell density” (HCD) can be applied for concentrations of animal cells in the order of  $10^7$  cells/mL. Alternatively, the CCD achieved in a typical batch cultivation of a specific cell line, can serve as a reference to define this threshold [205]. For example, for many of the cell lines used in vaccine production in batch mode, a CCD in the range of  $2 \times 10^6$  cells/mL to  $4 \times 10^6$  cells/mL is obtained [205]. Therefore, in general, cell concentrations one order of magnitude higher than those obtained by the established cultivation processes can be considered as “high cell densities” [205]. This chapter describes the application of HCD for the production of biologicals (i.e. recombinant proteins and viral vaccines) and corresponds to an extended and revised version of the section “Virus production at high cell densities” from a previous publication by the present author, Vazquez Ramirez, and Tapia (2016) [205].

### 2.5.1 Cultivation options for the production of recombinant proteins at high cell densities

The operation of bioreactors at HCD is one approach to intensify processes for the production of biologicals [205]. In this regard, HCD processes allow for the use of compact bioreactors with high volumetric productivities [206, 207] when operating at viable cell concentrations of  $10^7$ – $10^8$  cells/mL [208]. Those cell concentrations can be achieved in fed-batch (FB) or perfusion mode. The selection of the adequate HCD cultivation mode normally depends on the specific requirements of the intended product and the technical demand that their application in large scale implies [36]. As the expertise and technologies for industrial application of both FB and perfusion evolve, new production strategies combining FB and perfusion have been explored. In the following, the benefits of both cultivation modes (as stand-alone or in combination) on process intensification are described.

#### *Fed-batch processes*

In FB cultivation mode, nutrients such as glucose, amino acids and vitamins with trace elements are added to avoid their depletion. The nutrient supplementation can be carried out either continuously throughout the process or in a non-continuous way by single bolus additions at defined time points. In order to prevent substantial dilution in the bioreactor, nutrients are added mostly in a concentrated form [209, 210]. Based on that, FB bioreactors are initially filled at 50–70% of their maximum capacity and started as batch until substrates have reached growth-limiting values [211].

A sound metabolic understanding of the cell line of interest is necessary to define robust FB processes. On the one hand, the metabolic analysis allows for the definition of nutrient-concentrated feed media to avoid single additions of each component and, thus, to reduce process complexity and control. On the other hand, the deep understanding of cellular metabolism enables the definition of the feeding strategies (e.g. start of feeding, duration of feeding, addition mode – continuous or bolus –, feeding rates) that fulfill nutrient requirements and minimize the accumulation of undesired metabolites, such as lactate and ammonium.

By supplementing limiting nutrients in FB bioreactors, the cells undergo a longer growth phase [211], reaching concentrations in the order of  $10^7$  cells/mL, and higher product concentrations and product yields than in simple batch [211]. Nevertheless, a larger effort for equipment and on-line process control is required than in simple batch [211].

Fed-batch cultivation mode has been applied for long time in the biopharmaceutical industry and thus a large amount of literature and expertise on FB is available. This historical preference has been supported by the ease of its operation and validation. Based on that, it is expected, that the application of fed-batch will be preferred over perfusion, when product quality and process economic savings are not under stake [36].

### *Perfusion processes*

Perfusion is a cultivation mode that allows for a continuous medium renewal, while cells are retained in the bioreactor. Therefore, compared to FB, perfusion has the potential to achieve higher concentrations of viable cells and allows for longer cultivation length. Accordingly, the volumetric production rate in perfusion can be 4–10 times higher as compared to FB [212]. Regarding the product of interest, perfusion allows for a lower residence time in the bioreactor (due to the option for continuous product harvesting), which is an important aspect for labile recombinant proteins [35].

In recombinant protein production, the development and optimization of perfusion processes has been carried out for more than 20 years [206, 207, 213], and a high number of cell culture-derived products (mainly CHO cell-derived) have been introduced into the market [36, 213]. Given the short residence time, perfusion has been applied for the production of labile proteins, such as factor VIII (Kogenate-FS<sup>®</sup>, Bayer) and enzymes, such as Cerezyme<sup>®</sup> (Genzyme), produced in animal cell cultures [35, 212, 214]. Given its high volumetric production rates, perfusion is applied for the production of some highly demanded or low-titer monoclonal antibodies (mAbs), such as Infliximab (Recicade<sup>®</sup>, Jansen Biotech) and Abciximab (ReoPro<sup>®</sup>, Jansen Biotech), respectively [36, 212].

High cell concentrations in perfusion cultures are achieved due to the continuous medium exchange, which allows for a constant nutrient-enriched environment (e.g. constant glucose concentration) avoiding the accumulation of unwanted by-products (such as lactate and ammonium) [215], while keeping the cells in the bioreactor using different retention systems (Figure 2.6, Figure 2.7 A).

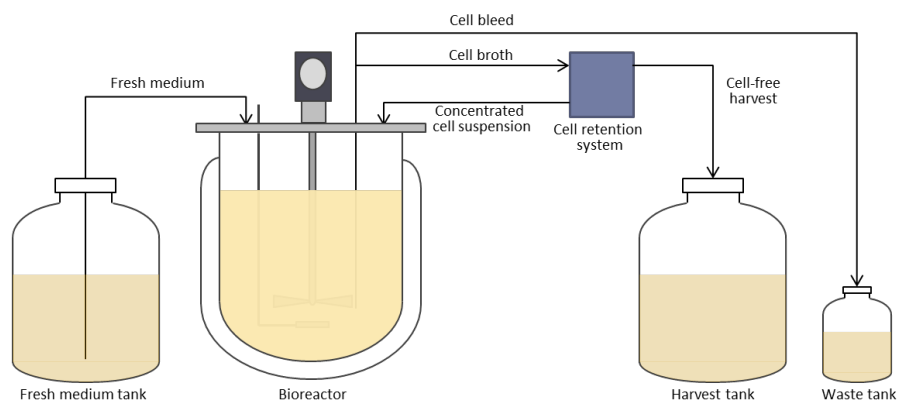


Figure 2.6. Schematic representation of a perfusion process. The cell broth flows continuously through the cell retention system. One fraction of the cell broth volume is removed as a cell-free harvest and the concentrated cell suspension is returned to the bioreactor. The cell-free harvest is continuously collected in the harvest tank while the fresh medium is automatically re-fed, maintaining a constant working volume in the bioreactor. Once a desired cell concentration is reached, it is maintained constant by removing cells from the bioreactor (cell bleeding) at defined flow rate.

As mentioned already in a previous publication, “the production of recombinant proteins in perfusion is typically performed at high medium exchange rates of 1–3 media volumes per reactor volume ( $V_R$ ) per day or a cell-specific perfusion rate (CSPR) of 0.05–0.5 nL/(cell×d) [216]. To maintain cultures in a proliferative state at constant high cell densities a controlled and continuous removal of cells from the bioreactor is performed, the so-called “cell bleed” [208, 217, 218]” [219] (Figure 2.6, Figure 2.7 A).

For the industrial production of recombinant proteins in perfusion-based bioreactors, a large variety of retention systems can be found [36]. “In general, filtration-based systems (i.e. internal and external spin filter, alternating tangential flow filtration – ATF – and tangential flow filtration – TFF –), gravity settlers and acoustic filters have been extensively used in industry as well as in academia [36, 208, 213]. Some of these systems have potential drawbacks such as filter clogging (filtration-based systems), and limited scalability (gravity settlers and acoustic filters). Nevertheless, ATF and TFF systems apply cross-flow filtration, which reduces the risk of filter clogging, and can be easily scaled-up, based on the surface area of the hollow fiber cartridge [213]” [205]. ATF and TFF are typically operated with microfiltration hollow fiber modules (0.2 to 0.65  $\mu\text{m}$  pore size) in order to assure product harvest whilst retaining cells to very high cell concentrations in the order of  $10^8$  cells/mL [208]. Recent studies with novel large pore size hollow fiber modules (5 and 10  $\mu\text{m}$ ) have even shown a 100% product recovery in the harvest in a 18 d perfusion process without an evident membrane

clogging [220].

“Other options for perfusion cultivation of animal cells are fixed-bed reactors and entrapping retention systems. These systems, however, are known for heterogeneities regarding the distribution of medium components and gases [221] as well as for their operational complexity [213]. Nevertheless, a recently developed fixed-bed bioreactor (CellTank®, PerfuseCell) has shown homogeneous concentration of metabolites allowing cultivation of CHO K1 cells at concentrations up to  $2 \times 10^8$  cells/mL [222]” [205].

Current industrial perfusion processes are operated at approximately  $20 \times 10^6$  cells/mL. However, recent advances in technology and process optimization show a trend towards much higher cell concentrations. Most likely, future industrial perfusion processes will target  $50\text{--}80 \times 10^6$  cells/mL [35].

### ***Intensified Fed-Batch processes***

Several strategies to intensify the traditional CHO-cells FB processes (with seeding cell concentrations of  $0.4\text{--}1 \times 10^6$  cells/mL) have been proposed and some are most likely being applied in manufacturing. Interestingly, most of them include the use of perfusion at a certain stage of the seed train and/or production stage. For example, the “n-1 perfusion/high-seed fed-batch”, consists on the application of perfusion at the n-1 stage of the seed train to expand cells up to around  $60 \times 10^6$  cells/mL, allowing the inoculation of the FB production bioreactor at around  $10 \times 10^6$  cells/mL [37, 40, 223]. This strategy has the potential to optimize the upstream manufacturing capacity utilization and to increase the volumetric productivity while maintaining or improving product quality [37].

The “concentrated FB” strategy consists in the use of a filtration-based perfusion (with ATF or TFF) bioreactor, which is perfused with a blend of basal and FB-medium [38]. However, instead of using a microfiltration module, which only retains cells, concentrated FB employs an ultrafiltration module to also retain the product of interest. The waste removal, nutrient supplementation and cell/product retention allows the cells in the bioreactor to reach concentrations around  $1.5 \times 10^8$  cells/mL and yields titers 3 times higher than in the standard FB [38, 39]. However, the observed gains may result in a significant increase on the cost of goods (COG) in large scale, which are mostly related to the used of higher amounts of concentrated FB-medium and the adaptation of a FB bioreactor for operation in perfusion [38].

The “hybrid perfusion FB” strategy comprises a three-day perfusion phase followed by a conventional fed-batch culture using highly concentrated feeds, with both phases performed in the production bioreactor [41]. In their report, Hiller et al. [41] used a TFF for the proof of concept, however, an ATF

---

system is also suitable for this application. As described by Hiller et al. (2017) [41], by using this strategy, “the overall productivity of the culture is approximately doubled when compared with a highly optimized state-of-the-art FB process”. Very high cell concentrations  $> 80 \times 10^6$  cells/mL can be reached, and therefore adaptations in the sparging system may be needed when scaling up to large-scale stainless steel FB bioreactors [41].

As described before, there has been a trend in the application of ATF and TFF systems not only for the realization of long-term perfusion production processes but also for the intensification existing traditional FB processes. This valuable knowhow generated in traditional CHO cell-based cultivations have served as a based for the intensification of viral vaccines production processes.

### **2.5.2 Current high cell density approaches for the production of viral vaccines**

“Most biologicals produced in animal cell culture are continuously synthesized during the cell proliferation phase. Recombinant proteins, for example, are typically produced in batch or fed-batch mode, where the product is accumulated in the culture broth and harvested once peak concentrations are reached [215]” [205, 219]. “In contrast, most cell culture-derived viral vaccines are produced in biphasic processes” [219]. In the initial “cell growth phase”, the host cells are propagated to a desired cell concentration before the addition of the seed virus. The “virus replication phase” starts with the addition of the seed virus and comprises the following internalization of the virus’ genetic material into the host cell, the synthesis of viral RNA/DNA and viral proteins as well as the release of progeny virus particles [224]. In a typical process at CCD both phases are operated in batch mode [205]. “Furthermore, it has to be taken into account that the replication process of lytic viruses results in cell death due to apoptosis followed by cell degradation and release of contaminants such as cellular DNA and host cell proteins” [205].

Given the partition of most of the virus production processes in a cell growth phase and a virus replication phase, and the nature of the synthesis of the product of interest (virus particles), different production profiles and kinetics are to be expected in perfusion mode compared to the typical recombinant protein production process [205] (Figure 2.7).

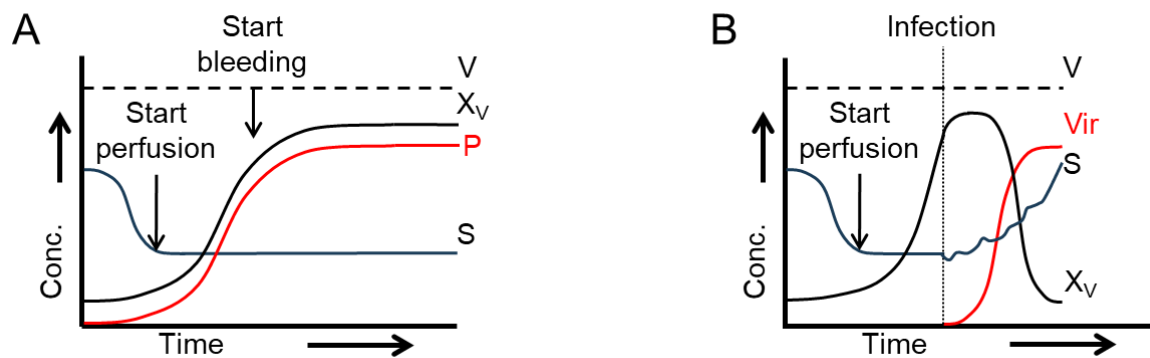


Figure 2.7. Schematic representation of the perfusion-based HCD production of recombinant proteins and viruses. (A) Concentration profiles of different performance parameters in a perfused bioreactor for the production of recombinant proteins. Cells are cultivated in batch before perfusion is started. When fresh medium is perfused, maintaining a constant volume ( $V$ ) in the bioreactor, a relatively constant substrate ( $S$ , glucose) concentration and a sustained exponential growth of viable cells ( $X_V$ ) are expected. Cell bleed is started to maintain a constant high cell concentration (steady state) that is still supported by the perfusion rate. The product concentration ( $P$ ) follows a similar profile as  $X_V$  during the steady state as long as the cells maintain a constant production rate. (B) Concentration profiles of different performance parameters in a perfused bioreactor for the production of viruses. Cells are first expanded to a desired high concentration using perfusion prior to virus infection. The virus ( $Vir$ ) propagation starts and cell concentration declines as cell lysis and apoptosis progress. At this point perfusion has to be adjusted to balance substrate and by-product concentrations for optimal virus propagation. Horizontal dashed line: bioreactor working volume, vertical dashed line: time of infection, arrows indicate the time point of start of perfusion and cell bleed. Figure adapted with permission from Tapia and Vazquez-Ramirez (2016) [205].

The fundamental differences described in Figure 2.7 play an important role in the adaptation of HCD process strategies that are typically applied in recombinant protein production, into the viral vaccine field. For example, if perfusion is applied for the production of virus particles, the cells need first to be propagated to concentrations that cannot be achieved in batch mode. Then, specific process strategies should be applied during the virus propagation phase, given the differences in the replication dynamics of each virus, the metabolic requirements for efficient virus replication and the extensive cell death rate (which will define the termination of the production process). The optimization of these specific process strategies should aim to prevent the “cell density effect”, which is a reduction in the cell-specific virus yields observed when increasing the concentration of the cells to be infected [205, 225, 226].

A summary of approaches for virus production at HCD and their main characteristics is given in Table 2.4. This table comprises relevant publications until the completion of the experimental part of the present work. More recent publications (from 2019 onwards) are also included but not considered in the discussion, since they correspond to follow-up projects that resulted from the outcomes of the present work. In the following chapters a summary of processes for expansion of cells to HCD (historically applied in virus production development) and for the optimization of cell-specific virus yields is presented.

Table 2.4. Overview on viruses produced in HCD cultures reported in literature. Modified with permission from Tapia and Vazquez-Ramirez (2016) [205].

Virus	Cell line	Type	Max cell concentrations ( $10^6$ cell/mL)	Bioreactor type	Cell expansion	Virus Infection/propagation	Virus harvest during propagation	Highest yields	Comments	Reference
Adenovirus	HEK293	Suspension	8	STR/TFF	Perfusion	Halting/Perfusion	No	$7.8 \times 10^9$ IVP/mL at 35 °C	5.5 times higher than the batch control in spinner	Cortin et al. 2004 [227]
Adenovirus ONYX-411 (recombinant oncolytic vector)	HeLaS3 human tumor cell	Suspension	14.8	STR/ATF	Perfusion	Halting/Perfusion	No (intracellular viral vectors)	$6 \times 10^{11}$ VP/mL	Titer 7-fold higher than those achieved in fed-batch	Yuk et al. 2004 [228]
Adenovirus type 5 (Ad5)	HEK293	Suspension	3	STR/Acoustic settler	Perfusion	Perfusion	No (intracellular viral vectors, high MOI = 20 at infection)	16,200 VP/cell $6.0 \times 10^9$ VP/mL	Cell-specific and volumetric yields comparable to batch. However infection at a cell concentration of $6 \times 10^6$ cells/mL led to a 5-fold reduction in specific productivity	Henry et al. 2004 [229]
Adenovirus type 5 (Ad5)	HEK293	Suspension	7.8	STR/TFF	Perfusion	Halting/Perfusion	No	$4.4 \times 10^{10}$ IVP/mL $5.600$ IVP/cell	Cell specific yield 4.3 times higher than batch	Galvez et al. 2012 [230]
Adenovirus type 5, 26, 35 (Ad5, Ad26, Ad35)	PER.C6	Suspension	16	STR/ATF	Perfusion	Perfusion	No (intracellular viral vectors)	50,000 to 150,000 VP/cell, $1.0 \times 10^{12}$ VP/mL for rAd26	Ratio VP/IVP of 20:1	Van Herk and Luitjens 2011 [231]
A/PR/8/34 influenza (H1N1) virus	MDCK	Adherent	6.2	STR	Repeated FB	Repeated FB	Discontinuous	13,630 VP/cell 5,248 HA/100 $\mu$ L	Cell-specific and volumetric yields higher than batch	Bock et al. 2011 [232]
A/PR/8/34 influenza virus	HEK293	Suspension	6	STR/Acoustic settler	Perfusion	Perfusion	Continuous	3,960 VP/cell	Cell-specific yield increased 4-fold	Petiot et al. 2011 [233]
A/New Caledonia/20/99 Influenza (H1N1) virus	MDCK	Adherent	8	Fixed bed	Recirculation	Medium exchange before infection Recirculation	No/washout with PBS and	2.89 log <sub>10</sub> (HAU/100 $\mu$ L) and $7.8 \times 10^7$ TCID <sub>50</sub> /mL	Novel disposable packed-bed bioreactor	Sun et al. 2013 [234]
A/PR/8/34 influenza virus	CAP	Suspension	26.9	STR/ATF	Perfusion	Perfusion	No	4,086 VP/cell $1.18 \times 10^{12}$ VP/L d	Cell-specific and volumetric productivity comparable to batch	Genzel et al. 2014 [42]

Virus	Cell line	Type	Max cell concentrations (10 <sup>6</sup> cell/mL)	Bioreactor type	Cell expansion	Virus Infection/propagation	Virus harvest during propagation	Highest yields	Comments	Reference
A/PR/8/34 influenza virus	CR	Suspension	28.1	STR/ATF	Perfusion	Perfusion	No	1,708 VP/cell 7.0 × 10 <sup>11</sup> VP/L d	Cell-specific and volumetric productivity comparable to batch	Genzel et al. 2014 [42]
A/PR/8/34 (H1N1) & A/Mexico/4108/2009 influenza virus	MDCK	Adherent / Suspension	40/28	Hollow fiber	Recirculation	Periodic harvest	Discontinuous	3.87 and 3.14 log <sub>10</sub> (HAU/100 µL) 1.8 × 10 <sup>10</sup> and 1.3 × 10 <sup>7</sup> TCID <sub>50</sub> /mL for A/PR/8/34 and A/Mexico/4108/2009, respectively	Both higher yields (HA and TCID <sub>50</sub> ) were obtained with MDCK suspension cells	Tapia et al. 2014 [235]
A/PR/8/34 (H1N1) influenza virus	CR-pIX	Suspension	50	Single-use orbital shaken bioreactor/ATF	Perfusion	Perfusion	No	3,059 VP/cell 2.0 × 10 <sup>12</sup> VP/L d	Disposable bioreactor. First report on orbital shaken bioreactor coupled with ATF	Coronel et al. 2019 [236]
A/PR/8/34 (H1N1) influenza virus	CR-pIX	Suspension	38	Single-use orbital shaken bioreactor/TFF	Perfusion	Perfusion	No	3,487 VP/cell 2.2 × 10 <sup>12</sup> VP/L d	Disposable bioreactor. First report on orbital shaken bioreactor coupled with TFF	Coronel et al. 2019 [236]
A/PR/8/34 (H1N1) influenza virus	PBG.PK2.1	Suspension	40–49	STR/ATF	Perfusion	Perfusion	No	3,053 to 4,805 VP/cell 3.9 to 4.0 log <sub>10</sub> (HAU/100 µL)	Yields comparable to other cell lines (CAF, PER.C6 or HEK293)	Grämicher et al. 2019 [110]
A/PR/8/34 (H1N1) influenza virus	MDCK.Xeno	Suspension	41.5–58.7	125 mL Shake flask	Semi-perfusion	Semi-perfusion	Discontinuous	13,600 VP/cell 4.19 log <sub>10</sub> (HAU/100 µL)	MDCK.Xeno cells were generated after adaptation of MDCK.SUS2 to the animal component free medium Xeno™-S001S	Bissinger et al. 2019 [237]
Moloney Murine Leukemia Virus (MoMLV) retrovirus vector	293GPG	Suspension	11	STR/Acoustic settler	Perfusion	Perfusion	Continuous	3 to 4 × 10 <sup>7</sup> IVP/mL	20-fold increase in specific productivity compared to adherent cells. Cell line produces infectious virus constitutively, no need of infection	Ghani et al. 2006 [238]
<i>Parapoxvirus ovis</i>	BK	Adherent	7	STR	Periodic medium exchange	VE-Fed-Batch	No	1.06 × 10 <sup>8</sup> VP/L d	20-fold increase in volumetric productivity, compared to batch	Pohlscheid et al. 2008 [239]



Virus	Cell line	Type	Max cell concentrations (10 <sup>6</sup> cell/mL)	Bioreactor type	Cell expansion	Virus Infection/propagation	Virus harvest during propagation	Highest yields	Comments	Reference
Poliovirus (PV) type 1, 2 & 4	Vero	Adherent	2	STR	Semi-batch*	Fed-Batch (Glucose/Gln)	No	356 DU/mL for PVI	1.5- to 2-fold increase in cell-specific and volumetric yield compared to batch	Thomassen et al. 2014 [86]
Rabies	Vero	Adherent	5	STR/spin filter	Recirculation	Perfusion	Continuous	1.38 × 10 <sup>8</sup> FFU/mL	2.6-fold higher specific productivity than batch	Rourou et al. 2007 [88]
Yellow fever virus 17D (YFV), produced in Vero cells	EB66®	Suspension	57	STR/TFF	Perfusion	Perfusion	No	3.1 × 10 <sup>7</sup> pfu/mL 0.05 pfu/cell 3.2 × 10 <sup>7</sup> pfu/L d	Manual perfusion control. Low cell growth and viability observed in a replication experiment	Nikolay et al. 2018 [240]
Yellow fever virus 17D (YFV)	EB66®	Suspension	95	STR/ATF	Perfusion	Perfusion	No	7.3 × 10 <sup>8</sup> pfu/mL 8 pfu/cell 4.5 × 10 <sup>9</sup> pfu/L d	Manual perfusion control	Nikolay et al. 2018 [240]
Wild-type Zika virus (ZIKV)	EB66®	Suspension	160	STR/ATF	Perfusion	Perfusion	No	1.0 × 10 <sup>10</sup> pfu/mL 65 pfu/cell 6.0 × 10 <sup>10</sup> pfu/L d	Automated control of CSPR based on on-line viable cell concentrations	Nikolay et al. 2018 [240]

VP: Total viral particles

IVP: Infectious viral particles

FFU: Fluorescent focus units

DU: D-antigen units

HA: Hemagglutinin

pfu: Plaque forming units

\* Semi-batch: daily media replacement

### ***Examples of high cell density cultivations of adherent and suspension cells***

The main limitation for cell growth in adherent cells is the availability of the growth surface, whereas the maximum growth of suspension cells is mainly limited by the total amount of nutrients in the growth medium and the accumulation of growth inhibiting compounds. Additional “limitations for HCD processes using suspension cells such as space, reactor design and operation as well as aeration have to be considered as discussed previously by Ozturk et al. (1996) [207]” [205].

Therefore, the main strategy to achieve high densities of adherent cells has been the increase of the growth surface, for example by using microcarriers for cell anchorage in stirred tank bioreactors (STR) [205]. “The use of microcarriers offers the additional advantage that it allows an easy exchange of medium by sedimentation of carriers after switching off the stirrer of cultivation vessels or stopping the rocking unit of wave systems. For instance, an increase from  $1.8 \times 10^6$  cells/mL to  $1.1 \times 10^7$  cells/mL could be achieved for adherent MDCK cells when increasing the concentration of the microcarrier Cytodex 1 from 2.0 g/L to 12.5 g/L using a repeated fed-batch process [232]” [205]. Microcarriers also facilitate the exchange of exhausted culture medium by fresh culture medium based on an estimated cell-specific perfusion rate as described before [241]. “In another example, the proliferation of Bovine Kidney (BK) cells on Cytodex 3 for the propagation of *Parapoxvirus ovis* up to  $7.0 \times 10^6$  cells/mL was carried out using a periodic medium exchange [239] based on the minimum glucose concentration measured. Finally, a recirculation-based feeding mode was applied for the propagation of Vero cells grown on microcarriers at around  $6.0 \times 10^6$  cells/mL for subsequent infection with various poliovirus serotypes [86]. In this process, fresh medium of a STR was circulated through the cultivation bioreactor at increasing rates depending on cultivation time” [205].

“Although similar to the recirculation strategy followed by Thomassen et al. (2014) [86], Tapia et al. (2014) [235] reported a special case for the proliferation of both adherent and suspension MDCK cells in a single-use hollow fiber bioreactor for propagation of pandemic influenza virus [235]. Here, cell concentrations of around  $3.0 \times 10^7$  cells/mL were obtained by recirculation of fresh medium through the hollow fibers providing nutrients to the cells and diluting accumulated toxic compounds” [205].

Regarding suspension cells, Nadeau and Kamen (2003) [242] reported the use of perfusion systems in the production of adenoviral vectors in HEK293 and PER.C6 cells. However, cell concentrations did not exceed  $6.0 \times 10^6$  cells/mL, no significant increase in volumetric yield was observed and a decrease in cell-specific yields (cell density effect) was observed compared to batch cultivations [205]. “External cell retention systems such as acoustic filters [233], or the ATF system [42] have been used in various vaccine production processes established in research laboratories. Using an acoustic filter, suspension HEK293 cells have been grown to concentrations approaching  $6.0 \times 10^6$  cells/mL before

infection with a recombinant Ad 5 [243] and IAV [233], respectively. In this case, cell growth continued even after infection reaching 11 [243] and  $14 \times 10^6$  cells/mL [233]. In another study, the designer cell lines CR and CAP were cultivated to 4.8 and  $3.3 \times 10^7$  cells/mL, respectively for the propagation of IAV [42] using an ATF system. Significant efforts have also been reported regarding options to intensify vaccine production processes using PER.C6 cells. Although this cell line can be cultivated up to  $1.0 \times 10^7$  cells/mL in batch [244] and above  $1.0 \times 10^8$  cells/mL in perfusion mode using an ATF system [245, 246], current production of adenoviral vectors (serotype 26 and 35) are carried out only at a PER.C6 cell concentration of around  $1.6 \times 10^7$  cells/mL [247]” [205]. One reason for that moderate HCD applied for the propagation of adenoviruses, might be the recurrence of the cell density effect reported in other suspension cells (such as HEK293) in perfusion [229, 243].

Although ATF and TFF systems share a similar separation principle, i.e. tangential flow filtration, a larger effort might be anticipated when setting up the optimal process parameters for TFF systems, more specifically, when defining the pump type and flow rate used for the recirculation of the cell suspension through the hollow fiber module. For example, legacy TFF systems use peristaltic pumps in the recirculation loop, which may expose the cells to a larger shear stress, affecting cell growth and viability [248, 249]. Therefore, adjustments might be needed in the flow rate and number of rollers in the pump head used [208]. To prevent the negative effect of shear stress, low-stress magnetic levitated pumps were used by Nikolay et al. (2018) [240] and Coronel et al. (2019) [236] in the cell growth phase and during the propagation of YFV in EB66 cells and IAV in CR.pIX cells, respectively (Table 2.4). However, Nikolay et al. (2018) [240] observed an unexpected decrease in cell growth and viability during the cell growth phase, when testing an alternative culture medium. This effect was not observed with an ATF system, indicating a possible influence of the TFF system [240]. In this regard, acceptable cell growth and viability were reported previously by Karst et al. (2016) [250] and Coronel et al. (2019) [236], when connecting the outlet port from the bottom of the bioreactor (most likely not available in Nikolay’s experiments [240]) to the TFF magnetic levitated pump, as recommended by the pump manufacturer (personal communication).

“The theoretical maximum cell concentration, which can be obtained for animal cells, is considered to be around  $10^9$  cells/mL [207]. Given that the supply of cells with critical substrates and the removal of growth-inhibiting compounds can always be guaranteed by appropriate feeding and perfusion strategies, the maximum cell concentration largely depends on the volumetric oxygen transfer coefficient ( $k_{La}$ ) that the cultivation system supports. Accordingly, depending on the cell line, the use of conventional stirred tank or wave bioreactors with  $k_{La}$  values up to 55 1/h should allow achieving cell densities in the order of  $1 \times 10^8$  cells/mL. As expected, experiments show that it is challenging to obtain such high concentration in these cultivation systems, and that additional issues, such as accumulation of  $CO_2$  to toxic concentrations have to be taken into account. For example, Clincke et al.

[208] have reported previously on CHO cell cultivations exceeding  $2 \times 10^8$  cells/mL, where a suitable aeration/agitation strategy and CO<sub>2</sub>-stripping needed to be implemented” [205].

### ***Examples to obtain high cell-specific virus yields***

“To achieve high virus titers, cells should typically be infected during the late exponential growth phase. In addition, an optimal supply of nutrients at TOI is required [224]. The latter can be achieved by a complete medium exchange prior to addition of the virus seed [232, 239] or by an intensive medium renewal during the cell proliferation phase [86]. Use of a perfusion rate of two  $V_R$  per day starting immediately after virus infection also helped to improve adenovirus yields in HEK293 cells [251]. Here, losses of infectious virus particles in the clarified fraction at the early phase of infection were compensated by infecting with an MOI two times higher (MOI = 20) than in the reference process in batch (MOI = 10)” [205].

“In order to support virus propagation, FB mode and/or discontinuous medium exchange have been carried out, especially in processes based on immobilized cells. For example, infecting MCDK cells grown on Cytodex 1, Bock et al. (2011) [232] demonstrated that performing a repeated fed-batch process during the first 2 to 10 hpi, allowed to obtain cell-specific IAV yields 3-fold higher compared to a conventional batch process. Similarly, Pohlscheidt et al. (2008) [239] applied a so-called “volume-expanded-fed” (VEF) batch strategy for the propagation of a *Parapoxvirus ovis* strain in BK cells grown on Cytodex 3. This cultivation strategy consisted in the discontinuous addition of medium to a final volume four times larger than the initial operation volume. Here, total virus yield was increased 40-fold, while virus titers and volumetric productivity were increased in one and two orders of magnitude, respectively, in comparison to a batch process [239]. Compared to a typical FB process (with lower volume additions), the VEF batch strategy resulted in an almost 6-fold increase in total virus yield” [205]. Discontinuous medium exchange and virus harvest during virus propagation has been also successfully applied to maintain high cell-specific virus yields of IAV in MDCK cells [235]. The daily harvesting of virus-containing supernatants was possible for both adherent and suspension (MDCK-SUS2) MDCK cells cultivated in a hollow fiber bioreactor (HFBR). The IAV was collected via multiple harvests of the extra-capillary space during a virus production time of up to 12 d. Cell-specific virus yields between 2,000 and 8,000 virions/cell were obtained for adherent MDCK cells, and between 11,000 and 19,000 virions/cell for suspension MDCK.SUS2 cells [235]. These cell-specific virus yields were comparable to those obtained in the typical batch production mode in STR and other HCD systems [235]. These observations highlighted the benefits of discontinuous virus harvest “not only for the production of viruses that propagate exclusively in mitotic cells and have a long replication cycle, such as the mink enteritis virus (MEV) [205, 252]” [205], but also for fast-propagating types, such as IAV.

“When operating processes with suspension cell lines, continuous virus harvest/medium exchange is a viable option. In this regard, acoustic filters have been used for cell retention and harvesting of a cell-free virus broth. For example, IAV produced in HEK293 cells was continuously harvested with the clarified supernatant with cell-specific yields of around 4000 virions/cell [42, 233]. Here, to avoid virus losses in the clarified fraction, medium exchange was not carried out for some hours after infection to allow for an efficient uptake of virions into cells. As addressed before, other commercially available separation systems used at industrial scale, e.g. gravity settlers or spin filters [36], could also allow for continuous virus harvesting when infecting suspension cells at concentrations of around  $2 \times 10^7$  cells/mL [213]. Furthermore, continuous virus harvests at cell concentrations in the order of  $10^8$  could be also possible using new types of bioreactors such as the perfusion bioreactor CellTank®” [205].

“An alternative approach to perform virus propagation using perfusion systems is the retention of both cells and virus particles within the bioreactor. This can be achieved using ATF and TFF perfusion systems. Similar to acoustic filter-based processes [42, 233], for ATF- and TFF-based processes a medium exchange should be avoided for a few hours after addition of virus seeds to allow for an efficient uptake of virions into cells [42, 110, 205, 236]. For the case of the ATF-based set-up proposed by Genzel et al. [42], it was shown that continuous medium exchange resulted in high cell-specific yields of IAV at laboratory scale [42]. Similar results were later obtained for YFV (with ATF and TFF) [240], ZIKV (with ATF) [240], and IAV (with ATF and TFF) [110, 236] using different cell lines and bioreactor types (see Table 2.4 for additional information). However, the choice of a suitable hollow fiber membrane seems to be a crucial factor, since the pore size of membranes seems to have an influence on productivity [42]. It is evident, that when using membrane-based separation systems, a sound characterization of cell retention during the growth phase must be carried out since any change in porosity and average pore size will have a negative impact on virus retention or harvest titers. Whether it is beneficial to continuously harvest virus particles or to retain them within the bioreactor during the whole virus production phase has to be determined in advance and characteristics of filtration modules have to be chosen accordingly. It might be even beneficial to use different pore sizes for the cell-growth than for the virus-production phase” [205].

## 2.6 On-line monitoring and control for cell culture-based vaccine production processes

Process understanding and process control has gained much attention by regulatory agencies responsible for the production of biologics during the last decade. In that respect, new regulatory initiatives such as Process Analytical Technology (PAT), Quality by Design (QbD), and Real-time Release (RTR) have been set on place, trending towards establishment of platform technologies [253]. The PAT regulatory framework includes guidelines that encourage innovation on the use of on-, in-, or at-line measurements and control strategies. These measurements should then be directed to the gain in quality, safety, and efficacy in the form of: cycle time reduction, prevention of rejects, implementation of RTR, improved safety with increased use of automation and improved efficiency from continuous processing [253].

Several PAT tools have been developed and applied to monitor cell cultivation processes over the last years [254]. For example, for biomass monitoring, a correlation between cell concentration and metabolic rates of a culture (e.g. oxygen uptake rate) has been proposed [255-257]. However, dielectric spectroscopy (DS) offers more direct measurements of viable biomass, since it is based on the on-line detection of the capacitance or permittivity ( $\epsilon$ ) that only intact viable cells exhibit [258-260]. More specifically, DS-based biomass measurements rely on the capacity of the cells to act as capacitors. This is, viable cells with an intact membrane get polarized when submitting them to an electromagnetic field at a defined frequency ( $f$ ) and release an electric signal when returning to their basal state, after the electromagnetic field is interrupted [258]. Depending on the applied frequency, different levels of cell polarization are achieved, which has a direct effect on the resulting permittivity signal, producing the so-called  $\beta$ -dispersion [261] (Figure 2.8 A). The frequency at which viable cells reach 50% of their maximum polarization rate (i.e. maximum permittivity signal) is known as the characteristic frequency ( $f_c$ ) [261] (Figure 2.8). The resulting capacitance or permittivity signal relates directly with the volume of cells with intact cytoplasmic membranes and the electrical properties of the membranes [258, 260, 262]. A linear correlation between permittivity and viable cell concentration (i.e. cells/mL) can be expected if the cell size distribution is relatively constant during the cell culture. However, since cell size distribution can vary during the cell culture, the total viable cell volume per culture volume (VCV) represents a more suitable reference [260] (Figure 2.8 B).

The existing capacitive sensors apply these cell dielectric properties, so that the permittivity value obtained at the  $f_c$  is correlated to the VCV [260, 263]. Figure 2.8 illustrates the polarization of viable cells exposed to different frequencies and the resulting  $\beta$ -dispersion spectra of the observed permittivity.

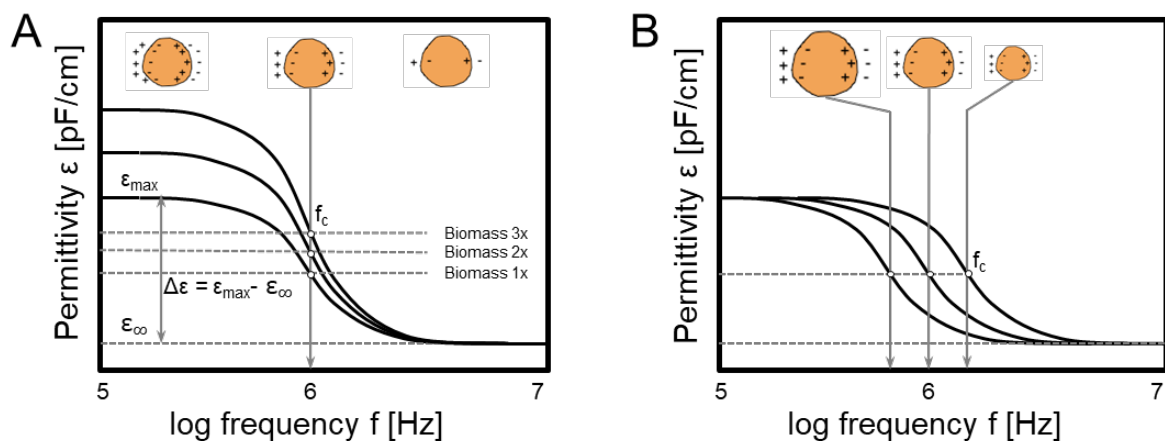


Figure 2.8. Schematic illustration of the  $\beta$ -dispersion spectrum of the observed permittivity. A: at low frequencies cells are fully polarized ( $\epsilon_{\max}$ ), whereas at high frequencies little polarization is achieved. The minimum permittivity signal possible is that from the cultivation medium, represented by  $\epsilon_{\infty}$ . Increasing the cell concentration increases the VCV and consequently leads to an overall increase in  $\Delta\epsilon$ . B: Comparison of three cell suspensions with same permittivity (i.e. same VCV) but composed of cells with different cell sizes. The characteristic frequency ( $f_c$ ) increases when cell size decreases. Figure modified with permission from Cannizzaro et al. (2003) [261].

On-line biomass measurements using DS have been successfully implemented for the automatic control of CSPR for the optimization of perfusion processes. CSPR can be modulated either by controlling the medium feeding flow rate based on the on-line viable cell concentration [241] or by controlling the cell bleeding at a fixed feeding flow rate [216]. The first strategy was applied recently for the control of CSPR during the production of yellow fever and Zika virus at HCD [240, 264].

A more detailed study on the application of DS using a multi-frequency analysis showed the potential of monitoring different metabolic state based on the intracellular conductivity ( $\sigma_i$ ) [259]. There, a correlation of alterations in the nutrient environment (e.g. nutrient limitations) on the intracellular content (i.e. intracellular conductivity,  $\sigma_i$ ) could be observed. This way, the on-line signal  $\sigma_i$  could be used as an indicator of changes in the physiological state and, more specifically, changes in the nutrient availability of mammalian cell cultures [259]. Additionally, the evolution of other dielectric properties during the cell culture has been analyzed for the production of viral particles. Especially, important changes in the cell culture's characteristic frequency ( $f_c$ ) has shown to correlate with the occurrence of viral replication phases during the propagation of lentiviral vectors [265], reovirus, influenza virus and baculovirus in animal cell culture [266].

Finally, spectroscopy-based methods such as near infrared spectroscopy (NIRS) and Raman spectroscopy can also be applied for online cell culture monitoring and control in virus production, similar to processes for recombinant protein production with animal and microbial cells [254, 267]. For example, Mercier et al. (2016) [262] demonstrated the application of NIRS in monitoring of glucose, lactate and total cell concentrations for cultivation of PER.C6 cells in perfusion. Monitoring of optical density and particle size using NIRS [254, 268], might also be of interest for the production of viral particles in cell culture. In the field of Raman spectroscopy in mammalian cell culture development, the monitoring of a wide range of process relevant analytes such as glucose, lactate, ammonia and viable cell concentration [269], and aminoacids [270] has been demonstrated. Given the detailed chemical information of virus particles that is possible to obtain with Raman spectroscopy (e.g. detection of virus DNA/RNA [271], virus protein-nucleic acid interaction [272] and virus lipids [273]), the monitoring of virus titers and other virus replication-related processes may also be feasible during cell culture-based virus production.



## 3 Materials and Methods

This chapter presents an overview of the cell line, the cell cultivation methods and materials, and the analytical methods used for the determination of cell culture performance and virus yields. Several methods were adapted from previous publication of the present author [200, 219].

### 3.1 Cells and medium

“The AGE1.CR.pIX<sup>®</sup> cell line (here named CR.pIX) was kindly provided by ProBioGen AG. This cell line was derived from the avian cell line AGE1.CR<sup>®</sup> (CR), which was generated from Muscovy duck retina cells [118]. The CR.pIX cells differ from their progenitor CR cells in that they express the pIX protein of human adenovirus [118]. Suspension CR.pIX cells were cultivated in chemically defined CD-U3 medium (Biochrom GmbH) with a glucose concentration of 33–40 mM, supplemented with glutamine (Sigma, Lot SLBS8600) and alanine (Sigma, Lot BCBS2461V) to a final concentration of 2 mM. In addition, recombinant insulin-like growth factor (LONG-R3IGF, Sigma, Lot LOS6008) was added at 10 ng/mL final concentration” [219].

### 3.2 Cultivations in shake flasks

CR.pIX cells were expanded in baffled shake flasks. Cell cultures with a working volume ( $V_w$ ) of 50 mL were performed in shake flasks with a nominal volume of 125 mL (#215-2273, VWR International, LLC), whereas 110 mL cultures were performed in 250 mL shale flasks (#215-2277,, VWR International, LLC). All shake flasks where incubated at 37 °C, 5% CO<sub>2</sub> and 185 rpm agitation speed in a Multitron incubation orbital shaker (Infors AG) with 5 cm shaking diameter. Cell passaging was performed every 3–4 d at a seed concentration of  $0.8 \times 10^6$  cells/mL. For one cell expansion run, the dissolved oxygen concentration (DO, in %) and the pH were monitored on-line using a PreSens shake-flask reader SFR (PreSens Precision Sensing GmbH, Regensburg, Germany). The sensor device was installed in the orbital shaker and the cell culture was performed with the above-mentioned conditions.

For infection experiments at CCD, shake flasks were inoculated to  $0.8\text{--}0.9 \times 10^6$  cells/mL and cultivated for 72 h to reach around  $4.0 \times 10^6$  cells/mL before infection. Then infection was carried out as indicated in 3.4.

For experiments at HCD, cells were cultivated in batch for 72 h before starting semi-perfusion. As a non-continuous process, the semi-perfusion comprised a medium exchange every 8–24 h. The amount of medium exchange was calculated based on a constant cell-specific perfusion rate (CSPR) [207] taking into account the steady state mass balance for substrates as described by Kompala and Ozturk [212] with glucose as the major energy source for CR.pIX cells [274] as:

$$CSPR = \frac{D}{X_V} = \frac{q_g}{(C_{gM} - C_{gR})} \quad (1)$$

Where  $D$  is the dilution rate (in 1/h),  $X_V$  is the viable cell concentration (in cells/mL),  $q_g$  is the estimated cell-specific glucose consumption rate of  $8.54 \times 10^{-11}$  mmol/(cell×h) for CR.pIX cells in perfusion [200],  $C_{gM}$  is the glucose concentration in CD-U3 medium (33–40 mM), and  $C_{gR}$  the expected glucose concentration in the bioreactor (6 mM). From equation 1, a CSPR of 0.060 nL/(cell×d) ( $2.5 \times 10^{-9}$  mL/(cell×h)) was obtained and used throughout all perfusion calculations.

As  $D$  is the ratio between the perfusion rate ( $Q$ , in mL/h) and the culture's working volume ( $V_w$ , in mL) in a continuous process, the perfusion rate  $Q$  at any time point ( $t$ , in h) during cell growth can be expressed as:

$$Q = X_V \times e^{\mu \times t} \times V_w \times CSPR \quad (2)$$

A constant specific cell growth rate ( $\mu$ ) of 0.026 1/h was considered based on previous reports [29] and confirmed during semi-perfusion cultivations. In semi-perfusion, the volume of medium to exchange ( $V_E$ , in mL) for a certain time frame, should be equal to the amount of medium exchanged in a continuous perfusion process during the same time frame:

$$\frac{dV_E}{dt} = X_V \times e^{\mu \times t} \times V_w \times CSPR \quad (3)$$

Therefore, solving equation 3,  $V_E$  can be defined as:

$$V_E = \frac{X_V}{\mu} \times (e^{\mu \times \Delta t} - 1) \times V_w \times CSPR \quad (4)$$

Using equation 4 at every sampling time, a new  $V_E$  was calculated for the subsequent period ( $\Delta t$ ) of 8–24 h. The calculated volume was removed from the cell culture and centrifuged at  $200 \times g$  for 5 min.

The supernatant was discarded, the cell pellet re-suspended in the same volume of fresh medium and returned to the shake flask. Fluctuations in the concentration of medium components were avoided by regularly adjusting the frequency of medium exchange (maximum 60%  $V_w$ ). In order to assure a homogeneous cell population at TOI, cells used for each virus infection experiment were expanded in parallel in 250 mL shake flasks (110 mL  $V_w$ ). Additionally, at each time point of medium exchange, cells from all shake flasks were pooled, sampled and the exchange volume calculated based on the pooled cell concentration. When a minimum target concentration of  $50 \times 10^6$  cells/mL was achieved, cells were distributed to 125 mL shake flasks (50 mL  $V_w$ ) and infected accordingly.

At TOI, for infections comprising a total or a partial medium exchange, the corresponding volume of cell broth was centrifuged at  $200 \times g$  for 5 min and the cell pellet re-suspended in the respective volume of fresh medium containing the virus. When required, pH and DO were monitored on-line using an SFR<sup>®</sup> system (PreSens).

### 3.3 Cultivations in bioreactors

#### 3.3.1 Characterization of the bioreactor

For a better control of process parameters, cultivations were performed in a 1 L (nominal volume) benchtop bioreactor (BIOSTAT<sup>®</sup>B plus, Sartorius AG) [219]. Therefore, an initial characterization of the bioreactor with regards to the anticipated process parameters for HCD cultivations was carried out. Specifically, the bioreactor's volumetric oxygen transfer coefficient ( $k_La$ ) was calculated for the planned cultivation conditions (based on previous cultivation conditions of CR cells grown in perfusion mode [42]) and different sparger oxygen flow rates (Table 3.1, see Chapter 4.1.1 for results). These values were then compared to the required  $k_La$  expected for high density cultivations of CR.pIX cells (see Chapter 4.1.2)

Table 3.1 Parameters for the measurement of the bioreactor  $k_La$  for the cultivation of CR.pIX cells

Parameter	Description
Culture medium	CD-U3 with 1 mL antifoam
Operation volume	0.8 L
Aeration rate (pure oxygen)	1, 4, 8, 16 and 30 cm <sup>3</sup> /min
Aeration device	Micro-sparger: sintered stainless steel frit, 20 $\mu$ m pore size
Impeller	3-blade segment impeller, axial downward flow
Stirring rate	142 rpm
Temperature	37 °C

### 3.3.2 Standard process parameters

Prior to bioreactor inoculation, CR.pIX cells were expanded as indicated in Chapter 3.1. Then, cells were seeded in the bioreactor at  $0.8 \times 10^6$  cells/mL, with a working volume ( $V_w$ ) of 0.6–0.8 L and cultivated at 37 °C and pH  $7.2 \pm 0.2$ . “Dissolved oxygen concentration was controlled at 40% by pulsed aeration with pure oxygen through a 20  $\mu\text{m}$  pore size micro-sparger (Table 3.1) unit to a maximum of 29–38  $\text{cm}^3/\text{min}$ ” [219]. The stirring speed was started with 120 rpm at inoculation and adjusted manually up to 160 rpm to maintain the DO set point. “Samples of 6–8 mL were taken with a syringe through a Luer-Lock-septum in 12 or 24 h intervals and stored at -80 °C until analysis” [219].

### 3.3.3 Operational set-up of the perfusion bioreactor with an ATF2 system

For perfusion cultivations, “cells were initially cultivated in batch mode until a glucose concentration of 14–17 mM (60–72 h after inoculation) was reached. At that point, perfusion was started using an ATF2 perfusion system controlled by the C24U-V2.0 controller from Refine Technology and polysulfone hollow fiber cartridges with pore sizes of 500 kDa” [219] and 0.65  $\mu\text{m}$ , or polyethersulfone hollow fiber cartridges ranging from 500 kDa to 0.65  $\mu\text{m}$  (Appendix 1).

#### *Perfusion control during the cell growth phase*

Regarding the operation of the ATF system, the average flow rate of the cell broth through the hollow fiber module ( $Q_{ATF}$ , in mL/s) was defined considering the shear rate ( $\gamma$ , in 1/s) produced by the hollow fiber to the CR.pIX cells, according to equation 5:

$$\gamma = \frac{4 \times Q_{ATF}}{f_n \times \pi \times r^3} \quad (5)$$

where  $f_n$  is the number of hollow fibers and  $r$  the fiber lumen radius (in cm). In order to minimize negative effects on shear stress,  $Q_{ATF}$  values of 0.5 or 1 L/min (16.7 or 8.3 mL/s) were used for large hollow fiber modules, whereas 0.1 L/min (1.7 mL/s) were applied for small modules (Table 3.2). A detailed summary of the characteristics of the hollow fiber modules used in this study is presented in the Appendix 1.

Table 3.2. Summary of characteristics and operational properties of the hollow fibers used for all ATF experiments

Experiment ID <sup>a</sup>	Module <sup>b</sup>	$f_n$ <sup>c</sup>	$d_i$ [mm] <sup>d</sup>	$Q_{ATF}$ [L/min] <sup>e</sup>	$\gamma$ [1/s] <sup>f</sup>
HBM1	L500	50	1	1.0	3395
HBM2					
HBI1					
HBM3	L65U	75	0.75	0.5	2683
HBI2 (virus propagation)	L65U	110	0.75	0.5	1829
HBM4 (cell growth)	L20U	75	1	0.5	1132
HBI2 (cell growth)	S500	12	1	0.1	1415
Correlation $\varepsilon/VCV$	S50U	14	1	0.1	1213
HBM4 (virus propagation)	S65U	20	0.75	0.1	2012

<sup>a</sup> H: high cell density, B: bioreactor, M: MVA-CR19, I: influenza virus A/PR/8/34 (H1N1)

<sup>b</sup> Internal code. Surface: S (small), L (large); pore size: 65U (0.65  $\mu\text{m}$ ), 50U (0.50  $\mu\text{m}$ ), 20U (0.2  $\mu\text{m}$ ), 500 (500 kDa)

<sup>c</sup> Number of fibers in the hollow fiber module

<sup>d</sup> Internal diameter of each hollow fiber

<sup>e</sup> Flow rate within the module's lumen

<sup>f</sup> Shear rate

Perfusion control in the bioreactor was achieved by applying the control loops for external pumps and bioreactor weight, available in the BIOSTAT®B plus module, as described in Figure 3.1. In summary, external pump B (harvest) was set at the calculated perfusion rate (as described below) and the bioreactor's volume was maintained constant through the weight control using the feeding pump A (medium feed), assuring a feeding rate identical to the harvest rate (Figure 3.1).

Similar to semi-perfusion cultivations, perfusion flow rates were calculated applying equation 2 (see Chapter 3.2) and adjusted manually every 12 or 24 h on pump B. For that, viable cell densities were measured off-line and the corresponding flow rates for that sampling time were calculated to assure a CSPR of around 0.06 nL/(cell $\times$ d), which is the optimal exchange rate for CR.pIX cells observed in Chapter 4.2.1 (based on the glucose consumption rate of CR.pIX cells [200]) [219]. Expected viable cell densities and the corresponding perfusion flow rates after 12 or 24 h were calculated taking into account a maximum cell-specific growth rate of  $\mu = 0.026$  1/h [29, 219]. A constant increase of pump B speed between two sampling times was achieved using a linear ramp-up profile in the BIOSTAT®B plus module. The cell growth phase ended when the target cell concentration of  $> 25 \times 10^6$  cells/mL was reached.

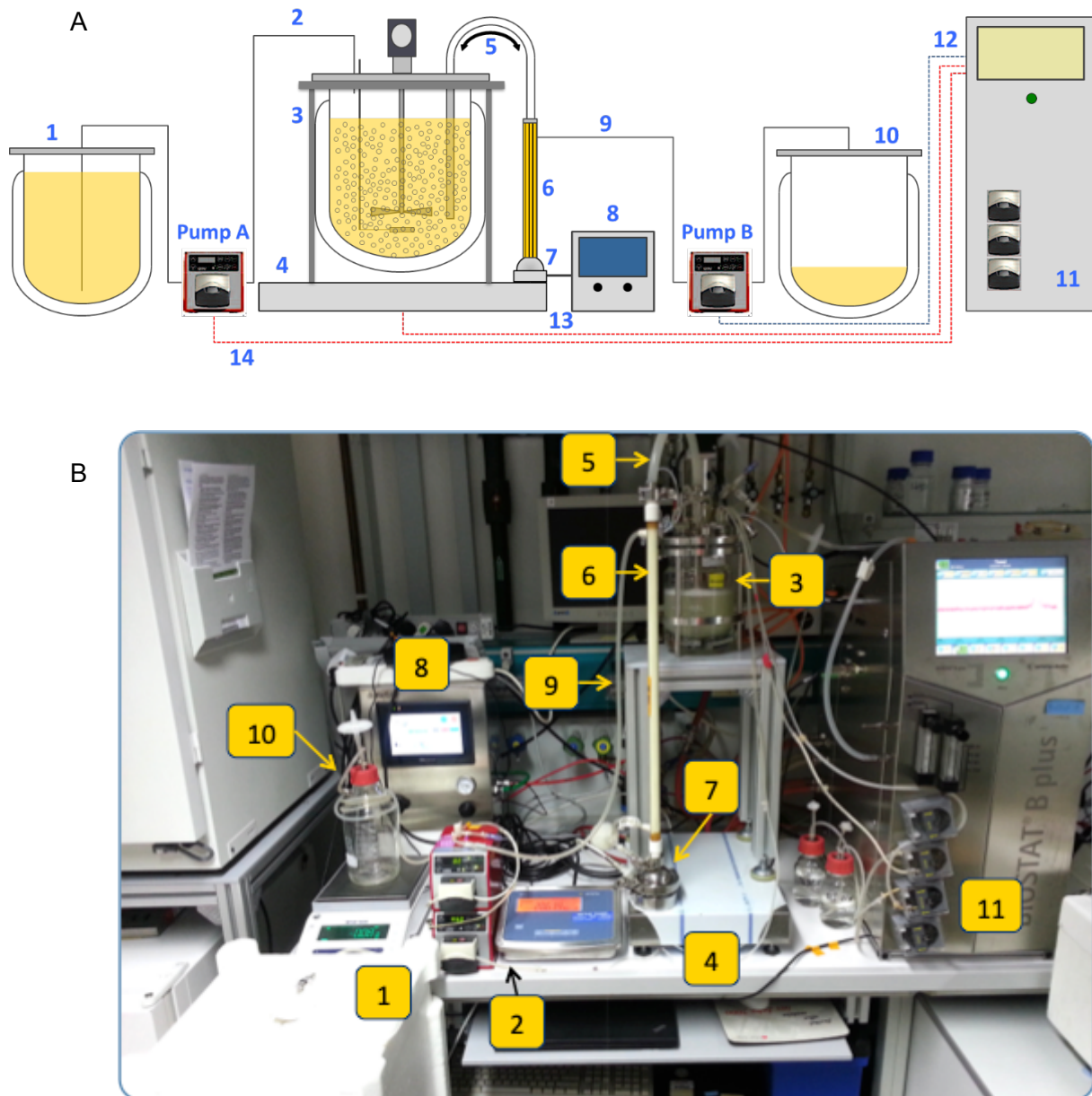


Figure 3.1. Schematic process diagram (A) and example photograph (B) of the ATF-based perfusion bioreactor layout for the cultivation of CR.pIX cells at HCD. Cell retention and continuous harvest of clarified broth was achieved using the ATF2 system, which consisted of a hollow fiber module (6), an alternating diaphragm pump (7) and the C24U-V2.0 control unit (8). The cell suspension was pumped in an alternating mode (5) between the bioreactor (3) and the hollow fiber module (6) at an average flow rate of 1 L/min. The cell-free permeate (9) was continuously pulled using pump B and collected in the harvest container (10). The flow rate profile for the permeate line (9) was adjusted daily via the bioreactor's control unit (11), which controlled the speed of pump B through the control line (12). The bioreactor's mass was maintained constant using the weight signal (13) from the bioreactor's scale (4) and the automatic addition of fresh CD-U3 medium (1) by pump A through medium line (2): pump A was automatically switched on by the control unit (11) through the feedback loop (14) when the bioreactor's mass decreased from the initially defined set point, and turned off when the set point was reached. Red dotted lines: bioreactor's mass control loop. Blue dotted line: control signal for external pump A.

---

### ***Medium supply during the virus propagation phase***

Bioreactors at HCD were operated with or without a medium exchange before virus infection. For bioreactors with medium exchange, the perfusion rate was set to  $0.5 V_R/h$  or  $0.28 V_R/h$  two or three hours before infection, respectively, to allow for total exchange of medium of 1 or  $0.85 V_R$ . This should help to reduce the risk of nutrient limitation and to dilute unwanted by-products that could negatively affect virus propagation. The application of one or the other strategy is mentioned for the corresponding experiments in Chapter 4 “Results and Discussion”.

After medium exchange, the bioreactors were infected either with MVA-CR19 or IAV A/PR/8/34 (H1N1). For MVA-CR19 bioreactors operated in perfusion mode during the virus propagation phase, the perfusion rate from 0 to 36 hpi was calculated using equation 2 (see Chapter 3.2), applying the same cell growth rate as for the cell growth phase ( $\mu = 0.026$  1/h). From 36 hpi a specific cell death rate ( $\mu_d = -0.028$  1/h) was used instead (based on reports of IAV propagation in perfusion cultures of CR cells [44]). For influenza bioreactors operated in perfusion mode during the virus propagation phase, the perfusion rate was calculated using equation 2 (see Chapter 3.2) and a  $\mu_d = -0.028$  1/h was used starting from 0 hpi.

## **3.4 Virus handling**

### **3.4.1 MVA-CR19 virus**

All infections with MVA-CR19 virus were carried out with the working bank #22.08.2013 ( $4.41 \times 10^8$  pfu/mL) derived from a virus seed [32] kindly provided by ProBioGen AG. Before infection, seed virus aliquots were treated for 1 min in a sonication water bath to break up virus aggregates. All cultivations were infected at an MOI of 0.05. Infections at CCD ( $4.0 \times 10^6$  cells/mL) were performed as described by Lohr (2014) [29], diluting the cell culture 1:2 with fresh CD-U3 medium containing the defined amount of virus. Hence a final concentration of  $2.0 \times 10^6$  cells/mL was obtained after infection. For infections in shake flasks at HCD, the seed virus was diluted in the fresh medium that was used for the corresponding total or partial medium exchange at TOI. For infection in bioreactors at HCD, the virus was diluted in fresh medium with a volume equal to 5–6% of the  $V_w$ , and added to the cell culture after the medium exchange.

For quantification of the concentration of infectious intracellular and extracellular virus particles (here lysate), a cell disruption procedure was applied. Cell-containing samples were treated with three

freeze/thaw cycles (-80 °C/room temperature, RT), followed by a 1 min incubation in a sonication water bath (45 kHz, RT) and centrifugation at  $1500 \times g$ , 10 min, RT, to discard cellular debris. For the quantification of viruses released by host cells (here supernatant), infected cell-containing samples were centrifuged at  $200 \times g$ , 5 min, RT, supernatant was retrieved and treated also with three freeze/thaw cycles before storage [32]. All virus samples were stored in aliquots of 0.5–1 mL at -80 °C.

### 3.4.2 Influenza A virus

All studies with human IAV were performed with MDCK-derived virus seed A/PR/8/34 H1N1 (Robert Koch Institute, Amp. 3138) that was adapted to CR.pIX cells over three passages. The infectious titer of the adapted virus seed was determined in MDCK cells by a TCID<sub>50</sub> (50% tissue culture infective dose) assay as  $1.48 \times 10^7$  virions/mL.

“All bioreactor experiments were performed at an MOI of  $1 \times 10^{-3}$  in presence of  $1 \times 10^{-6}$  U trypsin/cell (Gibco, #27250-018; prepared in PBS to 500 U/mL) to facilitate progress of infection” [219]. For virus titration, samples of 0.5–1 mL were withdrawn from infected cultures and centrifuged at  $200 \times g$ , 5 min, RT, to discard cellular biomass. The supernatant was retrieved and stored at -80 °C.

## 3.5 Analytics

### 3.5.1 Cell concentration and viability

#### *Off-line measurements*

As described previously by Vazquez-Ramirez et al. (2019) [219], viable cell concentrations  $X_V$ , “cell viability (in %) and average cell diameter (in  $\mu\text{m}$ ) were determined with the cell counter Vi-CELL™ XR (Beckman Coulter) using a previously validated measuring program with a relative standard deviation (for  $X_V$ ) of 2.5% for CR and CR.pIX cells [29]”. Sample volumes of 0.5 and 1 mL were withdrawn from shake flasks and bioreactor cultivations, respectively. The applied program was validated for a range of 0.25 to  $10.0 \times 10^6$  cells/mL and therefore proper dilutions were made with PBS (for shake flask cultivations) or with cell-free permeate (for perfusion bioreactors) to assure measurements of maximum concentrations of around  $5 \times 10^6$  cells/mL. Table 3.3 presents the applied dilution steps according to the expected cell concentration.



Table 3.3. Dilution steps for the measurement of cell concentration using the cell counter Vi-CELL™ XR

$X_v$ in sample [10 <sup>6</sup> cells/mL]	Dilution step	Sample volume [mL]	PBS or permeate volume [mL]
0.25–5	NA	0.5–1.0	NA
5–10	1:2	0.5	0.5
10–20	1:4	0.5	1.5
20–80	1:10	0.2	1.8
> 80	1:20	0.1	1.9

### *On-line measurements*

For some cultivations, on-line monitoring of viable cell densities was evaluated using an Incyte® capacitance probe connected to an Arc View 265 controller (Hamilton Bonaduz AG), as described previously by Vazquez-Ramirez et al. (2019) [219]. The on-line system was configured to provide the cell culture's permittivity ( $\epsilon$ , in pF/cm), which correlates directly to the total viable cell volume per culture volume (VCV, in  $\mu\text{L}/\text{mL}$ ) [219]. The on-line permittivity was converted to VCV applying a correlation factor  $\text{VCV}/\epsilon$  of 1.2 obtained from an initial calibration (Appendix 2).

On-line VCV values were compared with the off-line VCV calculated using cell diameters measured with the Vi-CELL™ XR analyzer, considering each cell as a spherical particle. For an accurate calculation, the cell diameter distribution was taken into account. Therefore, “cells analyzed from a total of 100 images (per sample) were clustered in diameter classes in the range of 8.1–29.9  $\mu\text{m}$ ” [219] as described previously [275].

### **3.5.2 Extracellular metabolites**

Samples of 1 mL were taken “with a syringe through a Luer-Lock-septum in 12 or 24 h intervals and stored at -80 °C until analysis. A validated assay using a BioProfile 100 Plus Nova analyzer (Nova Biomedical, United States) was used to determine glucose and lactate concentrations” [219]. The glucose concentration in bioreactor was closely monitored to confirm the suitability of the applied perfusion rate to avoid glucose concentrations below 6 mM (see 3.2). Lactate concentration was also monitored to avoid accumulation in the bioreactor. Glutamine, glutamate and ammonium concentrations were measured (as supportive information) as described previously [26] and are available in the experimental data sheets. Table 3.4 summarizes the standard deviations obtained from the method validation.

Table 3.4. Standard deviations derived from the method validation for the measurement of metabolite concentrations using the BioProfile 100 Plus Nova analyzer.

Metabolite	Standard deviation of the method
Glucose	0.39 mM <sup>a</sup>
Lactate	0.30 mM <sup>a</sup>
Glutamine	12.8% <sup>b</sup>
Glutamate	4.5% <sup>b</sup>
Ammonium	0.03 mM <sup>a</sup>

<sup>a</sup>Absolute standard deviations are shown for parameters with a homogenous variance

<sup>b</sup>Relative standard deviations are shown for parameters with a non-homogenous variance

Prior to the analysis of extracellular metabolites during the virus propagation phase, the corresponding samples were inactivated at 80 °C for 3 min and analyzed immediately or stored at -80 °C until analysis was performed.

### 3.5.3 MVA-CR19 virus titration

Prior to titration, samples were thawed and treated for 1 min in a sonication water bath (45 kHz). Infectious MVA-CR19 virus titration was performed in Vero cells (African green monkey kidney cells; ATCC CCL-81) using a variation of the TCID<sub>50</sub> procedure from Reed and Munch (1938) [276], as described by Jordan et al. (2009) [118]. The resulting titers are expressed in pfu/mL. The standard deviation was  $\pm 0.4 \log_{10}$  [219], which corresponded to a relative standard deviation (RSD) of 92.1%. Based on that, differences in MVA-CR19 virus titer  $\geq 10$ -fold were considered as significant.

### 3.5.4 Influenza A virus titration

#### *Hemagglutinin assay*

The main application for IAV preparations is the production of inactivated vaccines, “where the total concentration of the viral hemagglutinin protein (HA) as an antigen is decisive” [219]. HA titers were determined by a hemagglutination assay as previously described by Kalbfuss et al. (2008) [277] and expressed as  $\log_{10}$  HA units per test volume ( $\log_{10}$  (HAU/100  $\mu$ L)). The standard deviation of the method was  $\pm 0.081 \log_{10}$  (HAU/100  $\mu$ L) [277], which corresponded to a RSD of 18.7%.

The hemagglutination assay applies a standard erythrocyte concentration of  $2 \times 10^7$  cells/mL. For the estimation of the total IAV particle concentrations based on the HA titers, it is assumed that one virus particle binds to one erythrocyte. Therefore, the concentration of total IAV particles measured by HA (*TIP*, in particles/mL) was estimated using equation 6:

$$TIP = 2 \times 10^7 \times 10^{(\log_{10} (HAU/100 \mu L))} \quad (6)$$

### ***TCID<sub>50</sub> (50% tissue culture infective dose) assay***

The concentration of infectious IAV was determined by TCID<sub>50</sub> as described by Genzel and Reichl [278]. The resulting titers are expressed in virions/mL. The dilution error of the TCID<sub>50</sub> assay was  $\pm 0.3 \log_{10}$  [279].

### **3.5.5 Virus productivity estimations**

#### ***MVA-CR19 virus***

The overall cell-specific virus yield for MVA-CR19 virus ( $CSVY_{MVA}$ , in pfu/cell) was calculated based the total produced infectious particles (by TCID<sub>50</sub>) from the cell lysates and the maximum cell number measured after infection. For infected cultures where periodic harvests were carried out,  $CSVY_{MVA}$  was calculated as follows:

$$CSVY_{MVA} = \frac{\sum_{t_0}^{t_n} (TCID50_{H,t_n} \times V_{H,t_n})}{X_{V,max} \times V_w} \quad (7)$$

Where  $t_n$  is the process time,  $TCID50_{H,t_n}$  is the TCID<sub>50</sub> of a harvest at time  $t_n$ ,  $V_{H,t_n}$  is the harvest volume collected (in mL) at time  $t_n$ ,  $X_{V,max}$  is the maximum cell concentration (in cells/mL) after infection and  $V_w$  the bioreactor's working volume (in mL) at  $X_{V,max}$ . For infected cultures where no periodic harvests were carried out,  $TCID50_{H,t_n}$  was the highest virus titer and  $V_{H,t_n}$  the reactor volume at the highest virus titer.

In order to trace the progression of the specific virus yield along the virus propagation phase, “apparent” cell-specific virus yields ( $CSVY_{app,t_n}$ , in pfu/cell) were calculated considering the number of virus particles produced until a defined time  $t_n$  and the number of cells infected at 0 hpi, according to equation 8:

$$CSVY_{app,t_n} = \frac{\sum_{t_0}^{t_n} (TCID50_{H,t_n} \times V_{H,t_n})}{X_{V,t_0} \times V_{w,t_0}} \quad (8)$$

Where  $X_{V,t_0}$  and  $V_{w,t_0}$  are the viable cell concentration and bioreactor's working volume, respectively, at 0 hpi. Taking into account the relative standard deviations of the methods for MVA-CR19 virus titration (92.1%) and for viable cells density (2.5%), the RSD of the calculation of  $CSVY_{MVA}$  and  $CSVY_{app,t_n}$  was 92.1%.

The volumetric productivity ( $P_{MVA}$ , in pfu/(L×d)) was calculated using the total produced infectious particles (by TCID<sub>50</sub>), the total volume of medium spent during the cell growth and virus replication phase ( $V_{M,T}$ , in L), and the total process time including cell growth phase ( $t_p$ , in d), by:

$$P_{MVA} = \frac{\sum_{t_0}^{t_n} (TCID_{50_{H,t_n}} \times V_{H,t_n})}{V_{M,T} \times t_p} \quad (9)$$

Considering the error contributions of the volume and time measurements as negligible, the RSD of  $P_{MVA}$  was considered the same as the RSD of the method for MVA-CR19 virus titration (92.1%).

### ***Influenza A virus***

The overall cell-specific virus yield for IAV ( $CSVY_{IAV}$ , in particles/cell) was determined using the concentration of total IAV particles ( $TIP$ ) and the maximum cell number obtained after infection. For infected cultures where periodic harvests were carried out,  $CSVY_{IAV}$  was calculated as follows:

$$CSVY_{IAV} = \frac{\sum_{t_0}^{t_n} (TIP_{H,t_n} \times V_{H,t_n})}{X_{V,max} \times V_w} \quad (10)$$

Where  $TIP_{H,t_n}$  is the  $TIP$  of a harvest at time  $t_n$ ,  $V_{H,t_n}$  is the harvest volume collected (in mL) at time  $t_n$ ,  $X_{V,max}$  is the maximum cell concentration (in cells/mL) after infection and  $V_w$  the bioreactor's working volume (in mL) at  $X_{V,max}$ . For infected cultures where no periodic harvests were carried out,  $TIP_{H,t_n}$  was the highest virus titer and  $V_{H,t_n}$  the reactor volume at the highest virus titer. Taking into account the relative standard deviations of the methods for IAV titration (18.7%) and for viable cells density (2.5%), the RSD of the calculation of  $CSVY_{IAV}$  was 18.9%.

The volumetric productivity ( $P_{IAV}$ , in particles/(L×d)) was calculated using the total produced virus particles (by HA), the total volume of medium spent during the cell growth and virus replication phase ( $V_{M,T}$ , in L), and the total process time including cell growth phase ( $t_p$ , in d), by:

$$P_{IAV} = \frac{\sum_{t_0}^{t_n} (TIP_{H,t_n} \times V_{H,t_n})}{V_{M,T} \times t_p} \quad (11)$$

Considering the error contributions of the volume and time measurements as negligible, the relative standard deviation of  $P_{IAV}$  was considered the same as the RSD of the method for IAV titration (18.7%).

### **3.5.6 Determination of infection rates using flow cytometry**

The percentage of infected cells at different time points post infection was determined with flow cytometry. A total amount of  $1 \times 10^6$  infected cells were fixed using 1–2% formaldehyde for 30 min at 4 °C. Fixed cells were washed once with phosphate buffered saline (PBS) and permeabilized with 0.5% Tween 20 in PBS at 4 °C for 5 min. The cells were immuno-stained with 1:100 diluted FITC-conjugated polyclonal anti-vaccinia antibody (1952402357, Quartett GmbH) in staining buffer containing PBS plus 1% fetal calf serum (FCS) for 1–2 h in the dark at RT. Flow cytometry was performed with an ImageStream®X Mark II Imaging Flow Cytometer (Merck Millipore) at a wavelength of 488 nm at 5 mV intensity. Data analysis was performed using the integrated IDEAS® and FlowJow software.

## 4 Results and Discussion

This chapter describes the results obtained during the development of a cultivation strategy that allows for high-yield virus production processes at HCD. It starts with a section dedicated to the characterization of the benchtop bioreactor used for HCD cultivations, comprising the determination of the expected bioreactor's  $k_La$  and the calculation of the maximum possible cell concentration that can be achieved in the bioreactor. Then, initial results on the assessment of CSPR-based perfusion (in a benchtop bioreactor with ATF) and semi-perfusion (in shake flasks) cultivations are shown. Based on these results, the CSPR-based perfusion process was optimized and applied first for the propagation of MVA-CR19 virus. These results are presented and discussed in a third section, together with other feeding strategies, which were assessed in small-scale (shake flask) cultivation systems to allow for a higher experimental throughput. These alternative strategies aimed at improving MVA-CR19 virus yields using different ways of medium supply and virus harvest. The scale-up of the most promising feeding strategy up to the benchtop bioreactor is also presented in the third section. In a fourth section, the applicability of the strategy defined with MVA-CR19 for the propagation of IAV is presented. Finally, in the fifth section the application of a pH-based strategy for perfusion control, and the on-line monitoring of cellular biomass and changes of cells dielectric properties during virus propagation are described.

The results on the assessment of the small-scale cultivation strategies for MVA-CR19 virus (Chapters 4.2.2 to 4.4.2) are based on a previous publication by the present author in Vazquez-Ramirez et al. (2018) [200]. The results describing the benchtop bioreactor, for the production of MVA-CR19 and IAV (Chapters 4.4.3 to 4.5.2), are also available in a follow-up publication from Vazquez-Ramirez et al. (2019) [219].

## 4.1 Characterization of the benchtop bioreactor BIOSTAT<sup>®</sup>B plus

### 4.1.1 Estimation of the volumetric oxygen transfer coefficient

The volumetric oxygen transfer coefficient  $k_L a$  of the bioreactor was determined using the dynamic method considering the cultivation parameters described in Table 3.1.

In a STR, the oxygen transfer rate ( $OTR$ , in mmol/L×h) from the gas to the liquid phase is described by:

$$OTR = k_L a \times (C^* - C_L) \quad (12)$$

Where  $C_L$  (mM) represents the current oxygen concentration in the bulk liquid and  $C^*$  (mM) the oxygen saturation concentration in the bulk liquid in equilibrium to the bulk gas phase, according to Henry's law [280]. For a well-mixed bioreactor, the mass balance for the dissolved oxygen in the liquid phase can be established as:

$$\frac{dC}{dt} = OTR - OUR \quad (13)$$

Where  $\frac{dC}{dt}$  is the accumulation rate of oxygen in the liquid phase,  $OTR$  represents the oxygen transfer rate from the gas to the liquid (in mmol/(L×h)), described according to equation 12, and  $OUR$  is the oxygen uptake rate of the cultivated cells. This last term can be expressed as:

$$OUR = q_{O_2} \times X_V \quad (14)$$

Where  $q_{O_2}$  is the specific oxygen uptake rate of the growing cells and  $X_V$  the viable cell concentration.

In the absence of biomass or with non-respiring cells, when biochemical reactions do not take place,  $OUR = 0$ . In this case, equation 13 can be simplified to:

$$\frac{dC}{dt} = k_L a \times (C^* - C) \quad (15)$$

When integrating equation 15 the following linear equation is obtained:

$$\ln \frac{C^* - C_2}{C^* - C_1} = -k_L a \times (t_2 - t_1) \quad (16)$$

Equation 16 can be applied to determine the  $k_L a$  value at certain aeration, temperature and stirring conditions using the dynamic method. This method consists in the initial sparging of nitrogen to allow the oxygen desorption from the liquid phase (i.e. culture medium). When completely desorbed, oxygen supply is started until the oxygen saturation concentration in the liquid is reached. For such a case  $C_1 = 0$  and  $t_1 = 0$ , thus equation 16 can be expressed as:

$$\ln\left(1 - \frac{C_L}{C^*}\right) = -k_L a \times t \quad (17)$$

Equation 17 describes the time course of dissolved oxygen from the restart of aeration to the saturation point and  $k_L a$  can be determined from the slope of the  $\ln(A)$  versus time, with  $A = 1 - \frac{C_L}{C^*}$ .

The dynamic method was performed on the bioreactor vessel filled with 0.8 L of CD-U2 medium (with an almost identical composition to the CD-U3 medium used throughout CR.pIX cell cultivations), and with all inlet/outlet ports and on-line probes (pH and DO) installed. Additionally, analysis was carried out under cultivation conditions described in Chapter 3.3. Although oxygenation of the STR during cultivation was set at  $1 \text{ cm}^3/\text{mL}$ , additional  $k_L a$  values for 4, 8, 16 and  $30 \text{ cm}^3/\text{mL}$  were also determined for a broader characterization.

Since the DO probe was initially calibrated to 0% at total desorption and to 100% at oxygen saturation (with air),  $C^*$  was considered as 100% for the calculation of  $k_L a$ . The time course of oxygen concentration and the resulting linear regression of  $\ln(A)$  for different oxygen flow rates can be observed in Figure 4.1 A and B, respectively. A summary of all tested flow rates and its corresponding experimental  $k_L a$  can be found in Table 4.1.

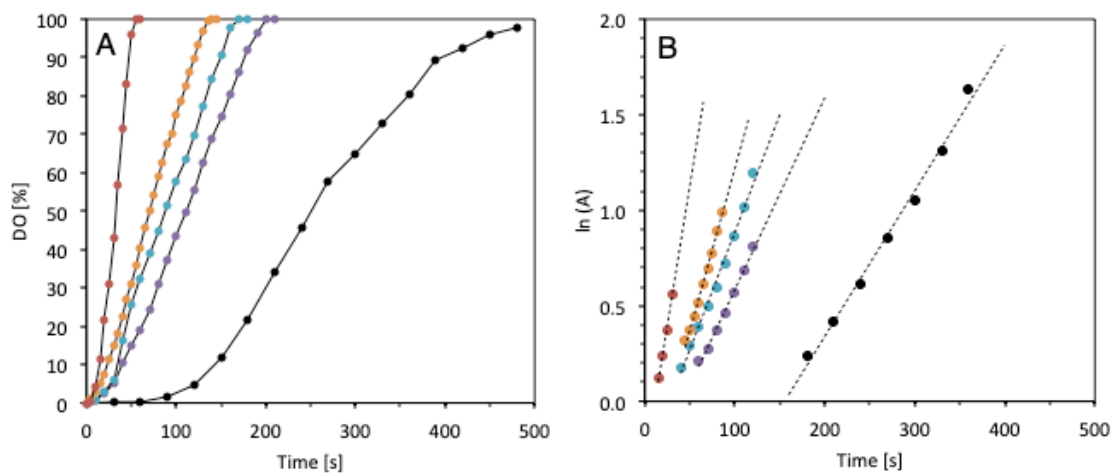


Figure 4.1. Dissolved oxygen concentration (DO) in a 0.8 L Biostat® B Plus bioreactor at different oxygen flow rates. A: Time course of DO values for different oxygen flow rates.  $1 \text{ cm}^3/\text{mL}$  (black),  $4 \text{ cm}^3/\text{mL}$  (purple),  $8 \text{ cm}^3/\text{mL}$  (turquoise),  $16 \text{ cm}^3/\text{mL}$  (orange),  $30 \text{ cm}^3/\text{mL}$  (dark red). B: linear correlations for different oxygen flow rates, where  $A = 1 - \frac{C_L}{C^*}$ .



Table 4.1.  $k_L a$  values at different oxygen flow rates for a Biostat® B Plus benchtop bioreactor at 0.8 L working volume and under operation conditions defined in Table 3.1.

Flow rate O <sub>2</sub> [cm <sup>3</sup> /min]	Flow rate O <sub>2</sub> [vvm]	Corresponding air flow rate* [vvm]	$k_L a$ [1/s]	$k_L a$ [1/h]
1	$1.25 \times 10^{-3}$	$5.95 \times 10^{-3}$	$7.56 \times 10^{-3}$	27.5
4	$5.00 \times 10^{-3}$	$2.38 \times 10^{-2}$	$1.01 \times 10^{-2}$	36.2
8	$1.00 \times 10^{-2}$	$4.76 \times 10^{-2}$	$1.23 \times 10^{-2}$	44.3
16	$2.00 \times 10^{-2}$	$9.52 \times 10^{-2}$	$1.96 \times 10^{-2}$	70.5
30	$3.75 \times 10^{-2}$	$1.79 \times 10^{-1}$	$2.92 \times 10^{-2}$	105

\* Estimated value, considering the content of oxygen (21%) in air

Based on this analysis, the  $k_L a$  value expected under the applied cultivation conditions was 27.5 1/h (Table 4.1), which was higher than other  $k_L a$  values reported for similar benchtop Biostat B bioreactors with stainless steel microspargers [281-283] (Table 4.2). This was possible by using a microsparger with a 5-times lower pore size (20  $\mu\text{m}$ ), despite the use of an almost 10-times lower aeration rate (0.006 vvm). Additionally, the application of higher agitation speeds and the use of pure oxygen in the gas phase also allowed for higher  $k_L a$  values (Table 4.2). The  $k_L a$  of 27.5 1/h differed from the value previously reported by Vazquez-Ramirez et al. (2018) [200] (10.9 1/h). This is due to the applied methods. While the former value was derived from experimental data, the latter was based on an empirical correlation proposed by Van't Riet (1979) [284]. For all further calculations,  $k_L a = 27.5$  1/h was used.

Table 4.2. Summary of  $k_L a$  values for BIOSTAT® bioreactors with different nominal volumes and settings

Reactor type	Sparger type	N [rpm]	Q air [vvm]	Medium	$k_L a$ [1/h]	Source
BIOSTAT® Bplus 1 L	Microsparger, pore 20 $\mu\text{m}$ (Stainless steel)	142	0.006	O <sub>2</sub> -Medium (CD-U3 with antifoam)	27.5	This report
BIOSTAT® B 5 L	Microsparger, pore 100 $\mu\text{m}$ (Stainless steel)	100	0.05	Air-RPMI 1640	9.7	[283]
		50	0.05		9.4	
		100	0.10		10.4	
BIOSTAT® B 5 L	Microsparger, pore 100 $\mu\text{m}$ (Stainless steel)	50	0.10	Air-DMEM	10.1	[282]
		100	0.05		10.0	
		50	0.05		9.0	
BIOSTAT® B 5 L	Microsparger, pore 100 $\mu\text{m}$ (Stainless steel)	100	0.10	Air-DMEM	10.0	[282]
		50	0.10		10.0	
		100	0.10		10.0	
BIOSTAT® B 5 L	Microsparger, pore 100 $\mu\text{m}$ (Stainless steel)	60	0.05	Air-CHOMaster HPI	8.0	[281]
BIOSTAT® C 5 L	Drilled-hole sparger	50–60	Not reported	Air-GMEM (+/- serum)	4.80	[232]

#### 4.1.2 Maximum cell concentration supported by the bioreactor

At the time the bioreactor's  $k_L a$  was determined, a large data set of bioreactor cultivations of CR cells at HCD had already been published [42]. Considering the close relationship between CR and CR.pIX cells, the  $q_{O_2}$  of the CR.pIX cells was assumed similar to the CR cells and thus a comparable  $OUR$  is expected at identical  $X_V$  values (based on equation 14). Furthermore, same cultivation parameters (sparger type, cultivation temperature and stirring rate) used in the reported CR cells cultivations were applied for the bioreactor cultivations with CR.pIX cells in the present work. Therefore, the oxygen flow rates  $F_{O_2}$  (through the microsparger) applied for the CR-cell run DPM3 (reported by Genzel et al. (2014) [42]), were analyzed to estimate  $q_{O_2}$ . This analysis is explained in the following.

The DPM3 run was performed in perfusion mode using an ATF2 system, with perfusion starting at 42 h of cultivation [42]. In order to minimize cell damage due to high sparging flow rates, pure oxygen was used at very low flow rates to maintain oxygen concentration at 40% (around 0.4 mM) for the experiment DPM3. The maximum oxygen flow rate was set at  $1.0 \text{ cm}^3/\text{min}$  ( $1.25 \times 10^{-3} \text{ vvm}$ ), which is considerably lower than the typical aeration rates applied for animal cells (0.01–0.1 vvm). During the cell growth phase, the DPM3 run required a maximum oxygen flow rate of  $0.49 \text{ cm}^3/\text{min}$  to reach  $28.1 \times 10^6 \text{ cells/mL}$  (Figure 4.2). This corresponds to almost 50% of the maximum aeration capacity of the bioreactor, showing a high potential to support higher cell concentrations with the chosen set-up (Table 3.1).

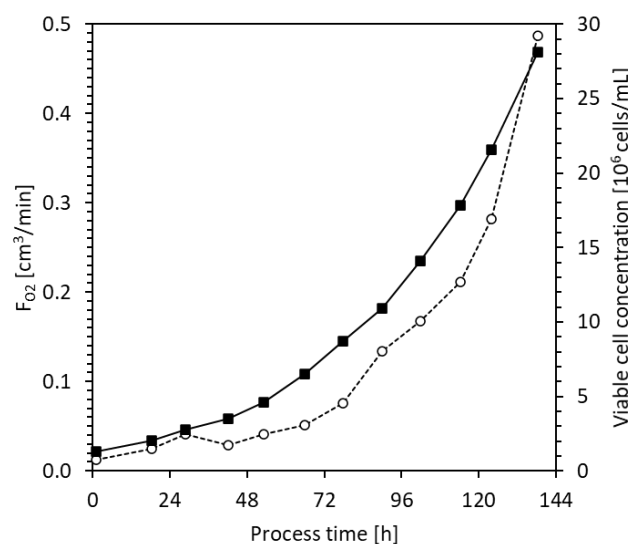


Figure 4.2. Pure oxygen flow rates along the cultivation of CR cells (DPM3 run). The oxygen flow rate (empty circles) increased exponentially throughout the cultivation and aligned with the exponential profile of the viable cell concentration (full squares). Time 0 represents the time of cell inoculation. Dataset obtained from Genzel et al. (2014) [42].

The  $F_{O_2}$  values during the complete DPM3 run process were periodically recorded with cycles of 60 seconds. In the case, that  $q_{O_2}$  of CR cells remained constant during the whole process, regardless the increase in cell concentration, the ratio of  $F_{O_2}$  per amount of cells  $F_{O_2/X}$  (in  $\text{mmol}/(\text{cell}\times\text{h})$ ) was also expected to remain constant. In this regard, an average ratio  $F_{O_2/X}$  of  $3.01 \times 10^{-11} \text{ mmol}/(\text{cell}\times\text{h})$  was observed up to a cell concentration of  $6.48 \times 10^6 \text{ cells/mL}$  (Figure 4.3). However, above that threshold a linear increase was observed (Figure 4.3), indicating either an actual increase of  $q_{O_2}$  or a decrease in the efficiency of the oxygen transfer (i.e. a decrease in the bioreactor's  $k_L a$ ) at  $X_V > 6.48 \times 10^6 \text{ cells/mL}$ . The linear correlation between  $F_{O_2/X}$  and  $X_V$ , for  $X_V \geq 6.48 \times 10^6 \text{ cells/mL}$ , can be described by the following equation:

$$F_{O_2/X} = 1.36 \times 10^{-18} \times X_V + 2.15 \times 10^{-11} \quad (18)$$

Where  $X_V$  is given in  $\text{cells/mL}$  and  $F_{O_2/X}$  in  $\text{mmol}/(\text{cell}\times\text{h})$ .

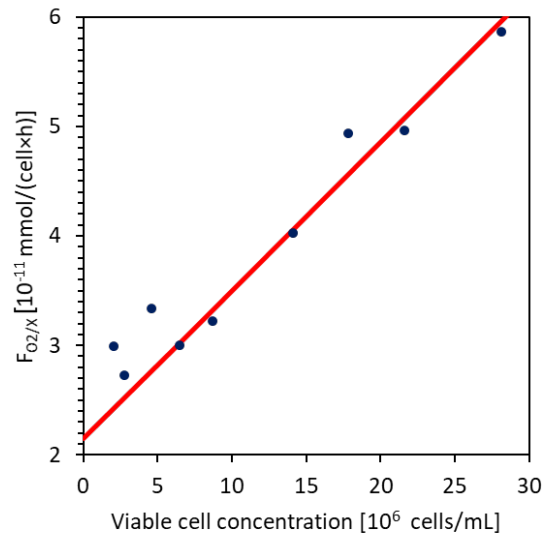


Figure 4.3. Oxygen supply rate per cell and hour at different concentrations of CR cells (DPM3 run). Oxygen supply rate per cell ( $F_{O_2/X}$ , blue dots) remained relatively constant up to a concentration of  $6.48 \times 10^6 \text{ cells/mL}$ . At higher concentrations, a linear increase was observed, suggesting an increase in the specific oxygen consumption rate ( $q_{O_2}$ ) or a decrease in the bioreactor's  $k_L a$ . The linear correlation between  $F_{O_2/X}$  and  $X_V$ , for  $X_V \geq 6.48 \times 10^6 \text{ cells/mL}$  is depicted as red line.

For the calculation of the maximum cell concentration based on the bioreactor's  $k_L a$  (27.5 1/h) and the cultivation parameters (Table 3.1), it is assumed that  $OTR = OUR$ , therefore (from equations 12 and 14)  $X_V$  can be expressed as:

$$X_V = \frac{k_L a \times (C_L^* - C_L)}{q_{O_2}} \quad (19)$$

Assuming that  $q_{O_2}$  follows the same linear correlation of  $F_{O_2/X}$  with respect to the cell concentration, the slope obtained in equation 18 was used to define the increase of  $q_{O_2}$  (in mmol/(cell×h)) along the cell growth as:

$$q_{O_2} = 1.36 \times 10^{-18} \times X_V \quad (20)$$

Substituting  $q_{O_2}$  in equation 19, the maximum cell concentration possible was defined as:

$$X_V = \sqrt{\frac{k_L a \times (C_L^* - C_L)}{1.36 \times 10^{-18}}} \quad (21)$$

Where  $C_L^*$  was  $10.0 \times 10^{-4}$  mmol/mL and  $C_L$  was  $4.0 \times 10^{-4}$  mmol/mL. Based on the  $k_L a$  of 27.5 1/h (Table 4.1) obtained for the maximum aeration possible for all bioreactor cultivations (1.0 cm<sup>3</sup>/min pure oxygen through microsparger), the maximum cell concentration for the cultivation system was predicted to  $110 \times 10^6$  cells/mL. Therefore, oxygen limitation was not expected for the cultivation of CR.pIX cells to achieve cell concentrations around the targeted  $50 \times 10^6$  cells/mL.

In summary, the measured  $k_L a$  of the bioreactor used for perfusion cultivations was higher than the values observed in the literature for similar systems, due to the application of pure oxygen and the use of a micro-sparger. The observed profile in the reactor's oxygen input was a suitable parameter to infer the oxygen demand of CR.pIX cells along their growth phase. It was useful to forecast a maximum cell concentration for the given bioreactor's  $k_L a$  and to provide a certainty for sufficient oxygen supply to cultivate CR.pIX cells at the minimum target cell concentration of  $50 \times 10^6$  cells/mL.

## 4.2 Definition of the semi-perfusion and perfusion processes for the cultivation of CR.pIX cells at high cell density

The establishment of a perfusion process using a CSPR based on the glucose demand of the CR.pIX cells was carried out in a 0.8 L bioreactor using the set-up described in Table 3.1. The suitability of the perfusion rates obtained using equation 2 and the manual control was evaluated especially with regard to the real CSPR and the glucose and lactate concentrations obtained during the cultivation. In addition, related parameters such as the resulting specific cell growth rate and the total volume of medium spent during cell propagation were evaluated.

Based on the evaluation of this first bioreactor run, standard operation parameters for future perfusion (in bioreactor) and semi-perfusion (in shake flasks) cultivations were established.

#### 4.2.1 Definition of the perfusion process in bioreactor

A CSPR-based strategy for the propagation of CR.pIX cells at HCD was initially assessed in a 0.8 L bioreactor with a target cell concentration of  $25 \times 10^6$  cells/mL. The bioreactor was inoculated at a cell concentration of  $1.3 \times 10^6$  cells/mL and perfusion was started soon after inoculation (6.75 h post inoculation) to avoid any accumulation of lactate or ammonium before reaching the target cell concentration. CD-U3 medium with a glucose concentration of 39.6 mM was applied for perfusion at a theoretical CSPR of 0.062 nL/(cell×d), according to equation 1.

As expected, by starting perfusion at an early stage (i.e. 6.75 h post inoculation), the glucose concentration had a moderate reduction (to 21.2 mM) with respect to its initial value at inoculation (33.5 mM), whereas lactate was undetectable for almost the whole cell propagation phase (Figure 4.4). However, these cultivation conditions led to a  $\mu = 0.016$  1/h (doubling time,  $t_2 = 43.3$  h), which was among the lowest rates for CR.pIX cells cultivated in batch mode in 1 L bioreactors, reported by Lohr (2014) [29]. In that study, Lohr obtained an average  $\mu = 0.0196$  1/h ( $t_2 = 35.4$  h) from 5 bioreactor cultivations [29]. The aim of the cell growth phase is to expand the cells at the highest  $\mu$  possible in order to minimize process time and medium utilization. Therefore the perfusion process should aim at the same or higher  $\mu$  values with respect to reference cultivations in batch mode.

The observed low  $\mu$  value suggested that the minimization of lactate concentrations to almost undetectable values had no positive influence on the cell growth rate. Moreover, the early beginning of perfusion and the medium overfeeding (due to a failed pump calibration) from 0.1 to 1.6 d after inoculation (Figure 4.4), seemed to affect the cell growth negatively (increased shear stress in the ATF system) and dilution of endogenous cell growth factors.

Despite the unintended over-feeding during the first 1.5 d, the implemented perfusion control, using manual adjustments with a linear increase between two samples, led to an average CSPR of 0.065 nL/(cell×d) (ranging 0.047–0.080 nL/(cell×d)) (Figure 4.4, A). A reduction to 0.055 nL/(cell×d) was performed from day 6 observing a faster decline of glucose concentration (Figure 4.4, A) but no negative effect on the cell growth rate (Figure 4.4, B).

The obtained average CSPR fitted the expected value of 0.062 nL/(cell×d), demonstrating that a constant CSPR-based feeding covers accurately the glucose requirements of the cells to produce the expected cell biomass concentrations. Additionally, it demonstrated its potential as a robust feeding strategy that includes the option for periodic adjustments every 12 to 24 h.

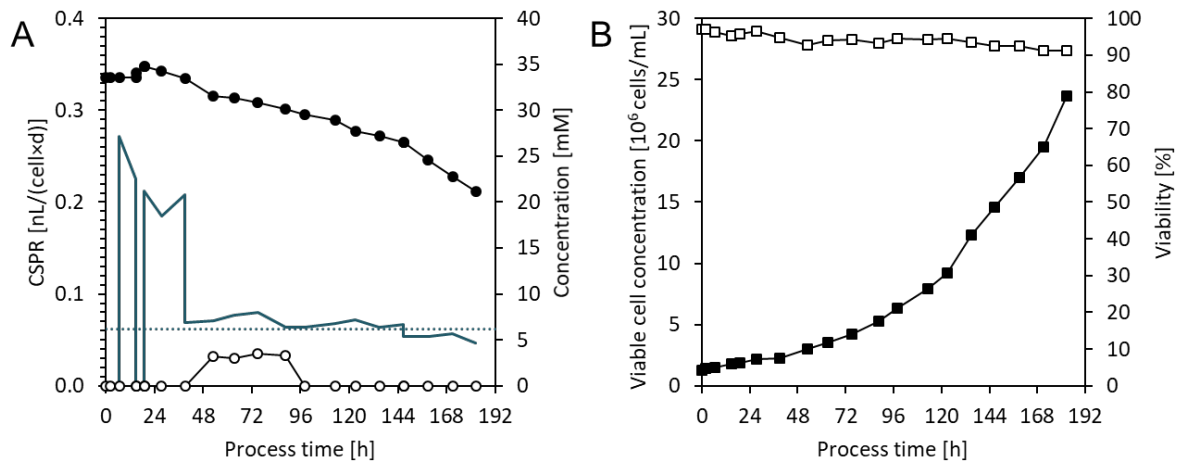


Figure 4.4. CR.pIX cell kinetics applying a CSPR-based manual perfusion control in a 0.8 L bioreactor. A: glucose (full circles) and lactate (empty circles) concentrations, real (continuous turquoise line) and theoretical (dashed turquoise line) cell-specific perfusion rate (CSPR). B: viable cell concentration (full squares) and viability (empty squares).

As a result, the medium utilization was minimized to 3.14 L (3.9  $V_R$ ) (Figure 4.5), which was considerably lower compared to the 8.10 L (9  $V_R$ ) used to propagate CR cells up to  $23.7 \times 10^6$  cells/mL at the same specific growth rate [42].

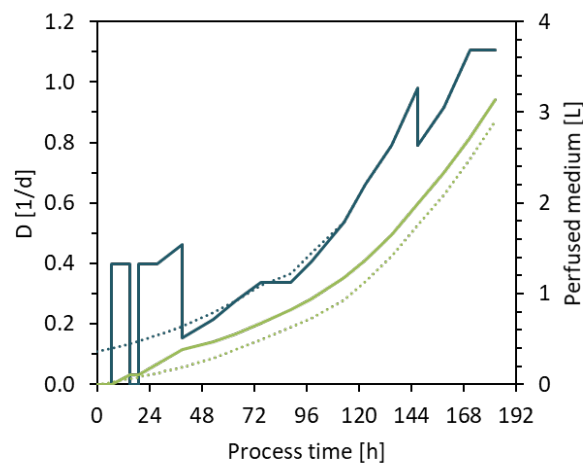


Figure 4.5. Medium spent applying a CSPR-based manual perfusion control in a 0.8 L bioreactor. Real (continuous turquoise line) and theoretical (dashed turquoise line) dilution rate (D). Real (continuous green line) and theoretical (dashed green line) accumulated spent medium.

From the results obtained in this first assessment, a CSPR of around 0.060 nL/(cell×d) was selected for further perfusion (bioreactor) and semi-perfusion (shake flasks) cultivations. Starting the ATF perfusion system soon after inoculation affected cell growth by extending the lag phase up to 1.6 d after inoculation. For that reason, the beginning of the perfusion or semi-perfusion mode was set at 2.5 d for following cultivations. Finally, the manual control of perfusion rate in bioreactor approximately every 12 h was suitable to maintain a stable CSPR during the cultivation.

This cultivation was subsequently infected with IAV. These results are presented in Chapter 4.5, where the process optimization for IAV propagation is introduced. This cultivation comprises a virus propagation phase performed also applying perfusion and is identified in the following as “HB11”.

#### 4.2.2 Definition of the semi-perfusion process in shake flasks

As described in a previous work by Vazquez-Ramirez et al. (2018) [200], “conditions for batch cultivation of CR.pIX cells in baffled shake flasks were previously optimized [28] and concentrations up to  $10 \times 10^6$  cells/mL with a viability of 95% were routinely obtained. However, whether these conditions, especially the shaking frequency (185 rpm), could fulfill oxygen transfer requirements to achieve cell concentrations up to  $50 \times 10^6$  cells/mL was not clear. Also, the suitability of a manual medium exchange by centrifugation (semi-perfusion) to mimic perfusion in shake flasks had to be demonstrated”.

Hence, the  $k_L a$  for the described cultivations at 37 °C, a shaking frequency ( $n$ ) of 185 rpm and maximum volumes ( $V_{max}$ ) of 125 and 150 mL was estimated applying an empirical correlation described for shake flasks with same geometrical configuration by Schiefelbein et al. (2013) [285]:

$$k_L a = a \cdot e^{-0.5 \left( \left( \frac{n-x_0}{b} \right)^2 + \left( \frac{V_{max}-y_0}{c} \right)^2 \right)} \quad (22)$$

with coefficients  $a$ ,  $b$ ,  $c$  and  $x_0$  and  $y_0$  according to Table 4.3. Equation 22 resulted from the mathematical fitting, using a Gaussian function, of the experimentally estimated  $k_L a$  values with different shaking frequencies ( $n$ ) and filling volumes ( $V_{max}$ ) applied. Hence, the empirical coefficients represent the standard coefficients defined by the Gaussian function.

Table 4.3. Empirical parameters for the estimation of  $k_L a$  in 125 mL and 250 mL baffled disposable shake flasks at 37 °C and a filling level of 40%. Modified from Schiefelbein et al. (2013) [285]

Coefficient	Value
$x_0$	271.60
$y_0$	257.66
$a$	256.42
$b$	67.41
$c$	221.02

Based on the theoretical calculation,  $k_L a$  values of 90.9 and 128.5 1/h would be expected for of 125 mL and 250 mL shake flasks, respectively, with a filling level of 40%. These values are up to 5 times higher than the estimated  $k_L a$  of 27.5 1/h for the bioreactor described above (Chapter 4.1.1) and, therefore, sufficient oxygen supply was expected in the shake flasks used for HCD cultures.

“Subsequently, the scale-down to 110 mL ( $V_w$ ) shake flasks was analyzed considering the specific cell growth rate, glucose and lactate concentrations, DO and pH as key parameters. Applying a constant CSPR of 0.060 nL/(cell×d), a maximum cell concentration of  $45.4 \times 10^6$  cells/mL (Figure 4.6 A) with a specific cell growth rate of 0.018 1/h was achieved. Constant medium renewal allowed maintaining the glucose and lactate concentrations at similar levels as in the HCD bioreactor cultivation (Figure 4.6 B). In addition, the pH values were in a range of  $7.2 \pm 0.2$  (Figure 4.6 C), which corresponded to the set-point of typical bioreactor cultivations (see Chapter 3.3.2). As expected, the DO was maintained at very high levels ( $>85\%$ , Figure 4.6 C). Therefore no oxygen limitation was anticipated for the following HCD cultivations” [200].

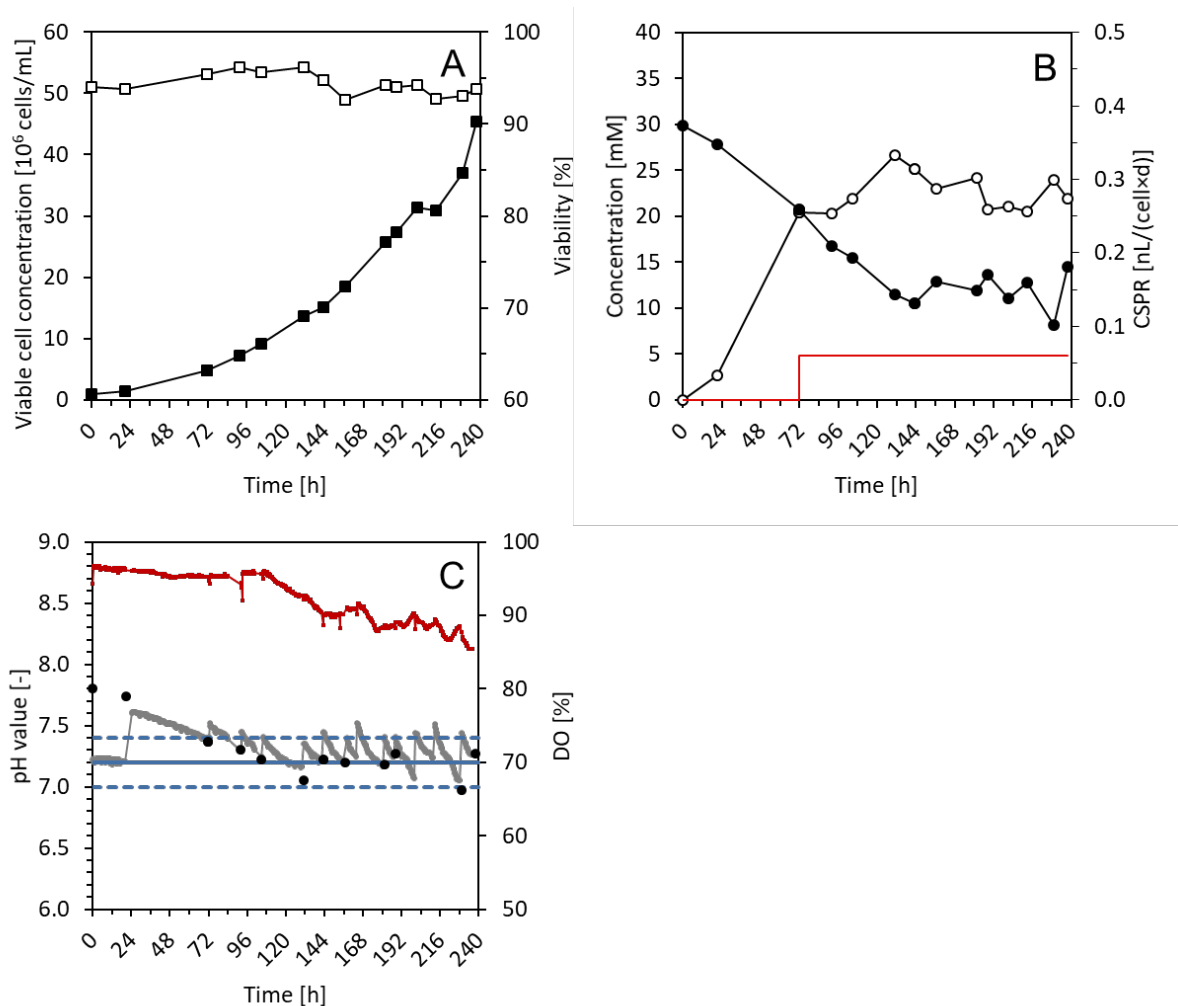


Figure 4.6. Cultivation of CR.pIX cells to high cell densities applying semi-perfusion in 250 mL shake flasks (110 mL  $V_w$ ). A: viable cell concentration (full squares) and viability (empty squares), B: glucose (full circles) and lactate (empty circles) concentrations, theoretical cell-specific perfusion rate (CSPR) (red line); C: on-line DO (red dots), on-line (gray dots) and off-line pH (black dots), optimal pH (continuous blue line), dashed lines:  $\pm 0.2$  pH units. On-line DO and pH were monitored with the PreSens shake-flask reader SFR (PreSens Precision Sensing GmbH, Regensburg, Germany) as described in Chapter 3.2. Figure adapted with permission from Vazquez-Ramirez et al. (2018) [200].



### 4.3 Propagation of MVA-CR19 virus in batch cultures

As a reference, cultivations using CR.pIX cells at CCD were carried out in three independent 50 mL ( $V_w$ ) shake flask (referred as **CSM2** in the following). Here a maximum average titer of  $3.9 \times 10^8$  pfu/mL was obtained at around 72 hpi (Figure 4.7). “This was around 24 h later compared to reports from Jordan et al. [32] who used the same virus isolate, cell line and infection strategy” [200] as for the cultivation set CSM1 (Table 4.4). Despite the difference in virus replication dynamics, the CSM2 set showed a similar virus titer,  $CSVY_{MVA}$  and  $P_{MVA}$  compared to the reported CSM1 cultivation set (Table 4.4). Additionally, the  $CSVY_{MVA}$  and the  $P_{MVA}$  obtained for CSM2 were also comparable to reported results of MVA wild-type (MVA-wt) propagated in CR.pIX cells in shake flasks (CSW) [29] and bioreactor (CBW) [26, 29] (Table 4.4). Thus, the results obtained were considered as representative for CCD infections.

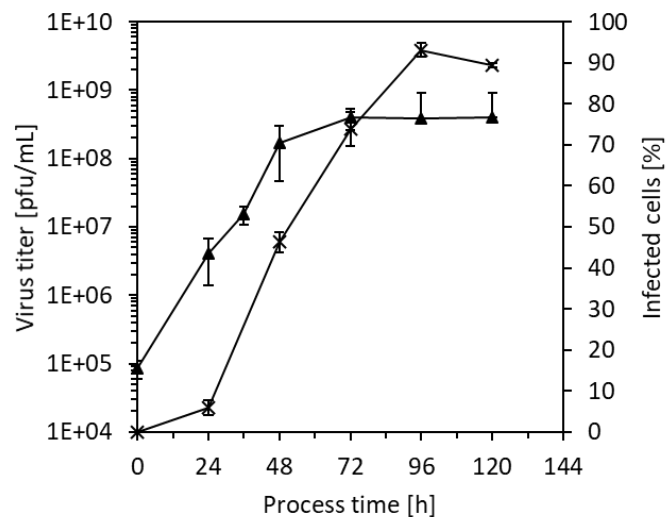


Figure 4.7. MVA-CR19 virus propagation in CR.pIX cells infected at CCD ( $2.0 \times 10^6$  cells/mL) in shake flasks. Virus titer (full triangles) and percentage of infected cells with respect to total cells (crosses) obtained for the experiment CSM2 are presented. Each point represents the mean value and error bars the standard deviation of three independent cultivations. Time 0 represents the time of virus infection. Figure adapted with permission from Vazquez-Ramirez et al. (2018) [200].

Table 4.4 Overview of different cultivation runs for MVA production in CR.pIX suspension cells at conventional cell densities (CCD). Adapted with permission from Vazquez-Ramirez et al. (2018) [200].

Experiment ID <sup>a</sup>	Working volume [mL]	Harvest titer [pfu /mL]	$t_T$ [d] <sup>b</sup>	Max. cells [ $10^6$ cells/mL]	CSVY <sub>MVA</sub> [pfu/cell] <sup>c</sup>	P <sub>MVA</sub> [pfu/(L×d)] <sup>d</sup>
CSW <sup>c</sup> [29]	50	$2.7 \times 10^8$	5.0	2.7	100	$5.4 \times 10^{10}$
CBW <sup>f</sup> [26, 29]	1000	$1.0 \times 10^8$	5.0	2.0	50	$2.0 \times 10^{10}$
CSM1 <sup>g</sup> [32]	50	$3.0 \times 10^8$	5.0	2.0	150	$6.0 \times 10^{10}$
<b>CSM2<sup>h</sup></b>	50	$3.9 \times 10^8$	6.0	3.0	130	$6.6 \times 10^{10}$

<sup>a</sup> C: conventional-cell-density, S: shake flask, B: bioreactor, W: MVA-wt, M: MVA-CR19

<sup>b</sup> Total time from cell inoculation to maximum titer

<sup>c</sup> Cell-specific virus yield

<sup>d</sup> Volumetric productivity

<sup>e</sup> Average of four independent cultivations.

<sup>f</sup> Single bioreactor cultivations

<sup>g, h</sup> Average of three independent cultivations

## 4.4 Propagation of MVA-CR19 virus in high cell density cultures

### 4.4.1 MVA-CR19 virus propagation applying perfusion

Since perfusion was used for the cell growth phase in all HCD cultivations in bioreactors (using an ATF perfusion system), the most feasible option was to proceed with a similar perfusion strategy during the virus propagation phase (i.e. a full perfusion process). In this regard, reports have shown that the medium renewal strategies during both cell growth and virus propagation phases have an impact in final virus yields [86, 239]. Hence, the reduction of perfusion rates using a glucose/glutamine-concentrated CD-U3 medium during the cell growth phase was analyzed in the cultivation HBM1. These data were then compared to the cultivation HBM2, performed with a standard CD-U3 medium and a constant CSPR of 0.06 nL/(cell×d). The effect of the perfusion during the virus propagation phase using a non-concentrated medium was additionally investigated for both HBM1 and HBM2, with the difference that only HBM2 comprised a medium exchange right before infection with MVA-CR19. In both cases, cells and viral particles were retained in the bioreactor using a 500 kDa hollow fiber module L500 (Table 3.2) in the ATF system.

#### Options for perfusion during the cell growth phase

In a first cultivation (in the following referred as **HBM1**), possible medium savings were analyzed when performing perfusion with a CD-U3 medium either 5- or 10-fold concentrated with glucose and glutamine, during the cell growth phase. Initially, during process time -181 – -123 h, the culture was fed at the target CSPR (0.06 nL/(cell×d)) with normal CD-U3 medium. This perfusion rate led to a

$\mu_{\max}=0.030$  1/h (Table 4.5). However, the cell growth was clearly altered when feeding with a 10-fold concentrated medium. Here, cells did not grow during process time -123 – -87.5 (Figure 4.8 A). During this time frame, glucose concentration was significantly increased from 7 to 22 mM (Figure 4.8 B), although the CSPR was adjusted accordingly to avoid an obvious substrate (i.e. glucose) overfeeding (Figure 4.8). Similarly, lactate increased from 22 to 52 mM was observed. This alteration in the cellular metabolism was very likely correlated with the considerable increase in osmolality resulting from the feeding of concentrated medium (Figure 4.8 C).

The negative effect of the concentrated medium on cell growth could be reversed when resuming the feeding with a non-concentrated medium during process time -87.5 – -57.5 h. Cell growth continued at the rate observed before addition of concentrated medium. Glucose/lactate concentrations and osmolality leveled out similarly (Figure 4.8). Once having reestablished optimal cell growth conditions, perfusion with a 5-fold glucose/glutamine-concentrated medium was assessed during process time -57.5 – -46 h with same negative results as seen before. Therefore, it seemed clear that the highly concentrated medium was not improving cell growth, and thus exclusively non-concentrated medium was used in the following (Figure 4.8 A, B). For this cultivation, no medium exchange was performed prior to virus infection.

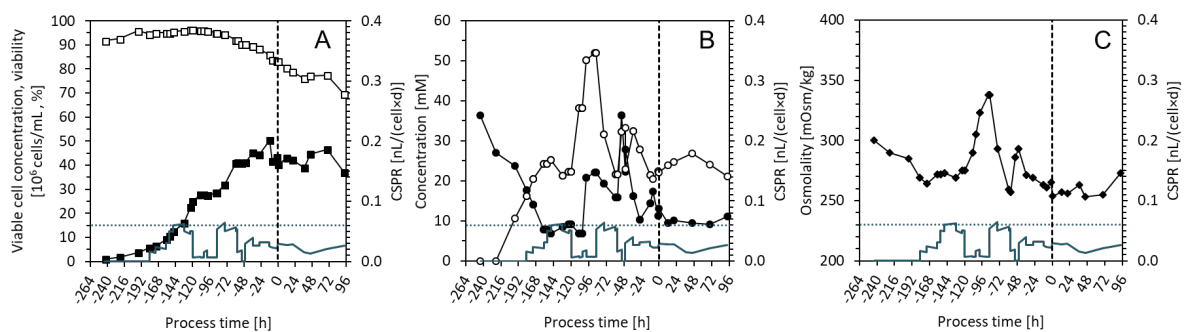


Figure 4.8. Cell growth kinetics, glucose/lactate concentration and osmolality in a HCD perfusion culture of CR.pIX cells (HBM1), before and after infection with MVA-CR19 virus. A: viable cell concentration (full squares) and viability (empty squares). CR.pIX cells were expanded in perfusion and infected at  $42 \times 10^6$  cells/mL in a 1 L bioreactor (0.8 L  $V_w$ ). Time of infection: 0 h (vertical dashed line). B: glucose (full circles) and lactate (empty circles) concentrations. C: osmolality (diamonds). Real (continuous turquoise line) and theoretical (dashed turquoise line) cell-specific perfusion rate (CSPR).

An additional cultivation (in the following referred as **HBM2**) was performed with a target CSPR of 0.06 nL/(cell×d), with a non-concentrated CD-U3 medium, plus additional perfusion increases prior to and post infection. As described previously by Vazquez-Ramirez et al. (2018) [200], „for a concentration targeting  $50 \times 10^6$  cells/mL in the perfusion bioreactor, the medium feeding regime described in Chapter 3.3.3 (see “Perfusion control during the cell growth phase”) led to a constant

$\mu=0.019$  1/h ( $t_2 = 36.5$  h)”. Around process time -50 – -36 h, a failure in the perfusion control led to a short overfeeding and to a dilution of the cell culture (Figure 4.9 A, B). As corrective measure, “medium addition was stopped for 2 h and medium removed through the hollow fiber unit to recover the original  $V_w$  of 0.8 L. Perfusion was then re-started using the initial regime and  $57 \times 10^6$  cells/mL at 95% viability were finally obtained 247 h after inoculation (Figure 4.9 A)” [200]. As expected, this perfusion control led to a very stable CSPR with an average value of 0.057 nL/(cell×d) and a very low standard deviation (Table 4.5), demonstrating the robustness of the feeding strategy chosen. The medium utilization was around  $8.8 V_R$ , which is considerably lower “compared to the almost  $32 V_R$  reported previously for CR cells (parental cell line of CR.pIX cells), where  $50 \times 10^6$  cells/mL at a similar specific growth rate of 0.020 1/h ( $t_2 = 34.6$  h) were obtained [42]” [200].

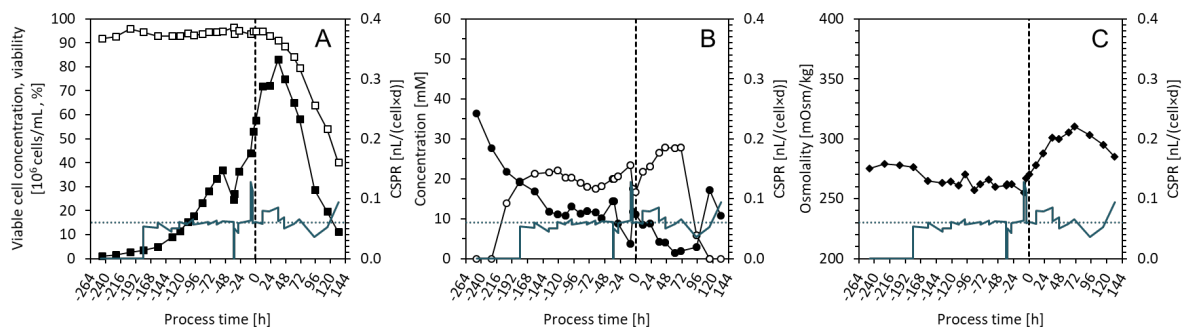


Figure 4.9. Cell growth kinetics, glucose/lactate concentration and osmolality in a HCD perfusion culture of CR.pIX cells (HBM2), before and after infection with MVA-CR19 virus. A: viable cell concentration (full squares) and viability (empty squares). CR.pIX cells were expanded in perfusion and infected at  $57 \times 10^6$  cells/mL in a 1 L bioreactor (0.8 L  $V_w$ ). Time of infection: 0 h (vertical dashed line). B: glucose (full circles) and lactate (empty circles) concentrations. C: osmolality (diamonds). Real (continuous turquoise line) and theoretical (dashed turquoise line) cell-specific perfusion rate (CSPR). Figure adapted with permission from Vazquez-Ramirez et al. (2018) [200].

Three hours before infection, the perfusion rate increased to achieve a total medium exchange of  $0.85 V_R$  as stated in Chapter 3.3.3 (see „Medium supply during the virus propagation phase“) of Materials and Methods. “The extensive medium exchange during the last 3 h before infection resulted in an increase in the glucose concentration from 3.72 to 11.0 mM. Despite the adjustment of the perfusion rate to an average CSPR of 0.06 nL/(cell×d) after infection, the glucose concentration showed a decrease from 11.0 to 8.49 mM during the first 12 hpi. In order to prevent a glucose limitation during the early stage of virus replication, the CSPR was increased by 50% from 12 to 36 hpi (Figure 4.9 B). Afterwards, the perfusion rate was re-adjusted to the target CSPR” [200].

Table 4.5. Summary of process parameters and performance of HBM1 and HBM2 runs during the CR.pIX cell expansion in a perfusion in bioreactor.

Experiment ID <sup>a</sup>	Working volume [mL]	Hollow fiber module	Seed cell concentration [10 <sup>6</sup> cells/mL]	$\mu_{\text{mean}}$ [1/h]	$\mu_{\text{max}}$ [1/h]	Actual average CSPR [nL/(cell×d)]	Duration [h] <sup>b</sup>
HBM1	800	500 kDa	0.9	0.026 (n=8, SD=0.006)	0.030	0.030 (n=16, SD=0.019)	338
HBM2	800	500 kDa	0.8	0.019 (n=12, SD=0.005)	0.026	0.057 (n=24, SD=0.006)	247

<sup>a</sup>H: high cell density, B: bioreactor, M: MVA-CR19

<sup>b</sup>Time from cell inoculation to infection

n: number of data points considered for the average calculations

In summary, when applying a 5- or 10-fold concentrated medium, no clear benefit with respect to medium savings was observed, since none of them supported a constant exponential cell growth rate and a cell viability above 90%. In contrast, the use of basal CD-U3 medium at a fixed CSPR allowed for a higher cell growth rate and viability, still with considerable medium savings. Therefore, the basal composition of CD-U3 medium was used for all following studies.

### Options for perfusion during the virus propagation phase

After infection using an MOI = 0.05, virus propagation developed differently for both HBM1 and HBM2 cultivations. More specifically, the virus propagated faster in HBM2 than HBM1 during the first 48 hpi (Figure 4.10 A). However, no difference in virus titer was observed for later time points. A clear difference during the first 48 hpi was also observed in the viable cell concentration and the viability. For the case of the HBM1 cultivation, the culture viability had a tendency to decrease even before infection, which might have impaired virus propagation during the first 36 hpi and therefore no significant viability decay was observed during this period (Figure 4.8 A). In contrast, for the HBM2 bioreactor, viability dropped clearly only after virus infection (Figure 4.9 A). Beyond the 36 hpi, viable cell concentrations and cell viabilities in HBM1 increased slightly in parallel with the accumulation of viruses. In contrast, this effect was much earlier for the HBM2 cultivation, soon after virus inoculation. This observation suggested that indeed cells in better shape are more permissible for infection and/or competent for further virus propagation. For the case of the HBM2 cultivation, cells were carefully fed until the TOI and further infection environment could have been improved by the extensive medium exchange performed during the last 3 h before infection (see „medium supply during the virus propagation phase“ in Chapter 3.3.3). The HBM1 cultivation did not undergo a medium exchange prior to virus infection, and a slight increase in cell viability and viable cell concentration was observed only 36 hpi, most likely as a result of the continuous feeding. This recovery in cell concentration and viability in the HBM1 cultivation might have finally supported further virus propagation.

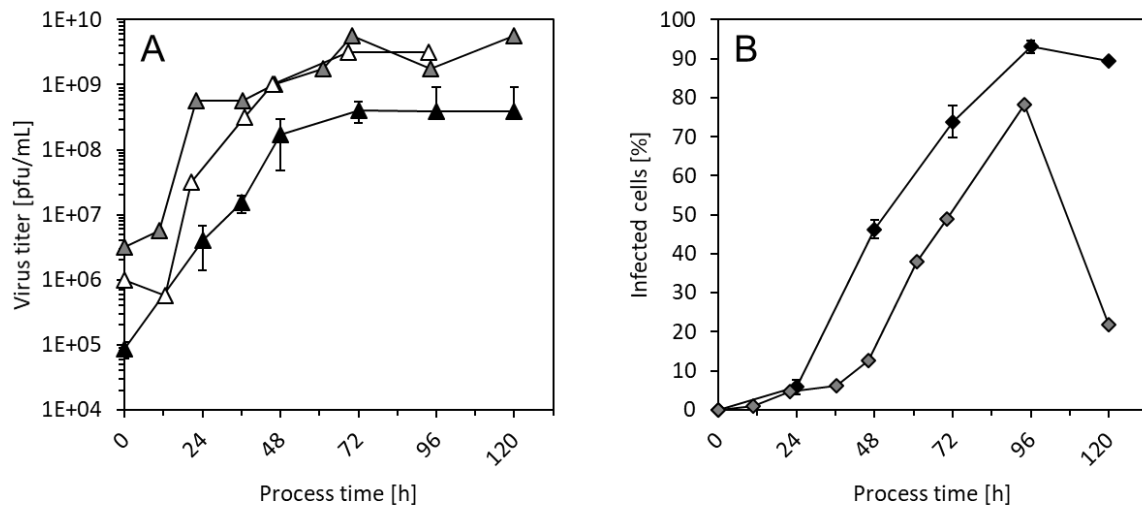


Figure 4.10. Comparison of the propagation of MVA-CR19 virus in HCD perfusion and CCD cultures of CR.pIX cells. Two HCD perfusion cultivations (HBM1 and HBM2) and the CCD cultivation set CSM2 (see Table 4.4) are presented. A: virus titers for HBM1 (white triangles), HBM2 (gray triangles), CSM2 (black triangles) cultivations. B: percentage of infected cells for HBM2 (gray diamonds), CSM2 (black diamonds) cultivations. Data from CSM2 represent the mean values and error bars the standard deviation of three independent cultivations. Time 0 represents the time of virus infection. Figure adapted with permission from Vazquez-Ramirez et al. (2018) [200].

For HBM1 cultivation a maximum virus titer of  $3.2 \times 10^9$  pfu/mL was obtained at 69 hpi, whereas for HBM2 a maximum virus titer of  $5.6 \times 10^9$  pfu/mL was obtained at 70 hpi (Figure 4.10 A). These titers were around 10-fold higher than the maximum achieved for the reference infections at CCD in shake flasks ( $3.9 \times 10^8$  pfu/mL) at 72 hpi (Figure 4.10 A) [200].

As observed in Table 4.6,  $CSVY_{MVA}$  values of 68 and 67 pfu/cell were obtained for HBM1 and HBM2, respectively, which were around 40% lower than for the reference infections at CCD in shake flasks (Table 4.4, CSM2), and other reported values (Table 4.4, CSM1, CSW). For the HBM2 cultivation, the concentration of viable cells increased significantly after infection up to  $83 \times 10^6$  cells/mL (Figure 4.9 A). In addition, the percentage of infected cells was very low during the first 36 hpi (Figure 4.10 C). This suggested a delay in the virus uptake and onset of intracellular virus replication [200].

Similarly, the obtained volumetric productivities at HCD (Table 4.6) seemed also lower compared to the CCD experiments (Table 4.4). One reason for that could be the total amount of medium employed for biomass expansion and during virus propagation. Despite the application of limited CSPR during cell growth and virus propagation phases of HBM1 reactor,  $P_{MVA}$  was not improved (Table 4.6) compared to the reference CCD experiments (Table 4.4).

Table 4.6. Overview of MVA-CR19 virus production yields obtained in HCD perfusion cultivations of CR.pIX cells in bioreactor (HBM1 and HBM2).

Experiment ID <sup>a</sup>	Working volume [mL]	Harvest titer [pfu/mL]	$t_T$ [d] <sup>b</sup>	Max. cells [ $10^6$ cells/mL]	CSVY <sub>MVA</sub> [pfu/cell] <sup>c</sup>	P <sub>MVA</sub> [pfu/(L×d)] <sup>d</sup>
HBM1	800	$3.2 \times 10^9$	13	47	68	$1.8 \times 10^{10}$
HBM2	800	$5.6 \times 10^9$	13	83	67	$2.4 \times 10^{10}$

<sup>a</sup>H: high cell density, B: bioreactor, M: MVA-CR19

<sup>b</sup>Total time from cell inoculation to maximum titer

<sup>c</sup>Cell-specific virus yield (for calculation refer to Chapter 3.5.5 Virus productivity estimations)

<sup>d</sup>Volumetric productivity (for calculation refer to Chapter 3.5.5 Virus productivity estimations)

Based on the results obtained from HBM1 and HBM2 cultivations, two key factors seemed to be important for the optimization of MVA-CR19 productivity at HCD [200]:

- a. “An optimization of infection conditions to achieve fast virus replication after the addition of the seed virus.
- b. A minimization of medium utilization over the entire virus propagation phase without compromising final virus titers”.

In order to address these two targets, the application of several feeding strategies during the virus replication phase was investigated [200]. A detailed description of these strategies is presented in in Chapter 4.4.2.

#### 4.4.2 MVA-CR19 virus propagation applying alternative feeding strategies

Alternative feeding strategies during virus propagation at HCD were assessed aiming at the optimization of the MVA-CR19 virus replication and the reduction of medium utilization. In order to increase the experimental throughput, this assessment was performed in shake flasks, applying the semi-perfusion methodology for CR.pIX cell expansion to HCDs. Regarding the MVA-CR19 virus expansion, first, two feeding strategies to maintain glucose supply during virus propagation were analyzed: 50% medium exchange before infection (ME50) and fed-batch with 10-fold glucose/glutamine-concentrated medium (FB10). Finally, three strategies aiming at maximizing virus yields were investigated: fed-batch with basal medium (FB), daily medium exchange (DME) and a combination of FB and DME (F+D). All feeding strategies were also performed in shake flasks.

##### Strategies to maintain glucose supply during virus propagation

CR.pIX cells were cultivated to  $37 \times 10^6$  cells/mL in  $2 \times 250$  mL shake flasks (110 mL  $V_w$ ) using semi-perfusion [200]. Before infection, both 110 mL cell suspensions were pooled and equally distributed in  $4 \times 125$  mL shake flasks (50 mL  $V_w$ ). During virus propagation, two different strategies

for the supply of glucose (major energy source for CR.pIX cells [274]) were analyzed with regard to the limitation of glucose and its effect on virus yields. One pair of shake flasks was fed with bolus additions of a 10-fold glucose- and glutamine-concentrated CD-U3 medium (**FB10 strategy**, Figure 4.11 A) and another pair with a single medium exchange of 50% at TOI (**ME50 strategy**, Figure 4.11 B) [200]. Each pair was infected with one of the two available MVA-CR19 seed-virus banks (MC19a and MC19b) at an MOI of 0.05.

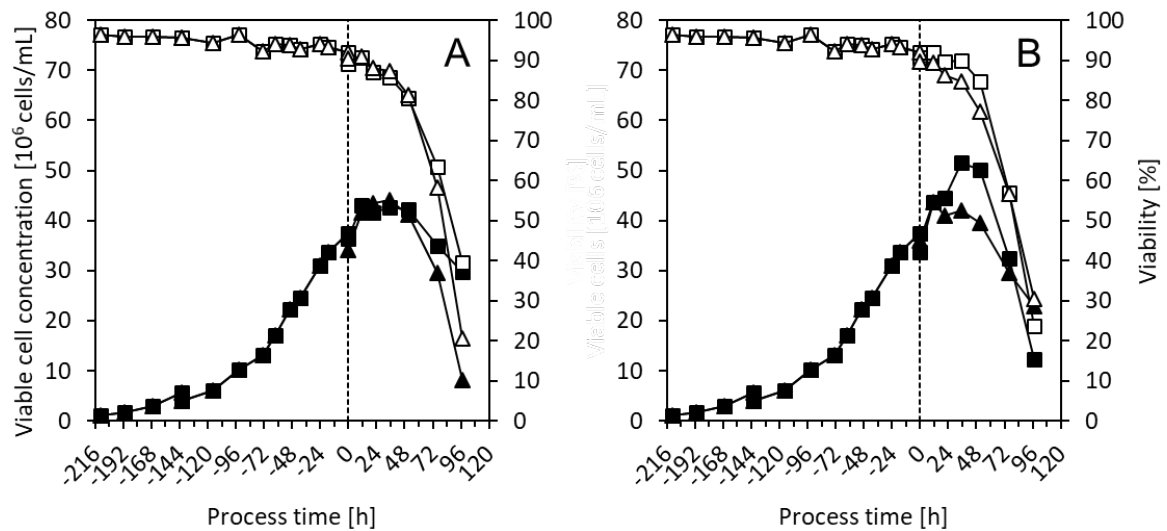


Figure 4.11. Growth kinetics of CR.pIX cells before and after infection with MVA-CR19 virus at HCD, applying a fed-batch (FB10) and a medium exchange (ME50) strategy after infection. CR.pIX cells were expanded in semi-perfusion and infected at  $37 \times 10^6$  cells/mL in 125 mL shake flasks (50 mL  $V_w$ ). Time of infection: 0 h (vertical dashed line). Viable cells concentrations (full symbols) and viability (empty symbols) are presented for A: fed-batch with concentrated medium (FB10) and B: 50% medium exchange at TOI (ME50). Infection was performed with two seed-virus banks: MC19a (squares) and MC19b (triangles) Figure adapted with permission from Vazquez-Ramirez et al. (2018) [200].

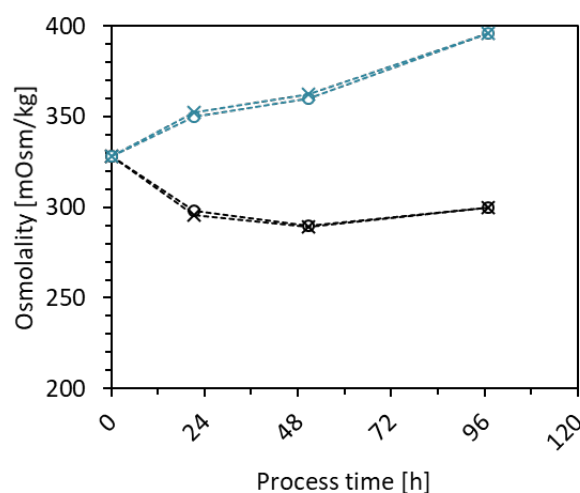


Figure 4.12. Osmolality profile observed during the propagation of the MVA-CR19 seed viruses MC19a and MC19b when applying a FB10 and a ME50 feeding strategy. FB10 (blue lines and symbols), ME50 (black lines and symbols), MC19a (empty circles) and MC19b (crosses). Time 0 represents the time of virus infection.



The application of the FB10 strategy led to a significant increase of the osmolality (Figure 4.12) up to 396 mOsm/kg at 96 hpi. Similar to observations in the experiment HBM1 (Figure 4.8), this large increase in osmolality can explain the difference in the cell growth after infection between the FB10 (Figure 4.11 A) and the ME50 strategy (Figure 4.11 B).

The FB10 strategy led to a maximum virus titer of  $1.0 \times 10^8$  pfu/mL at 35 hpi for both working banks (Figure 4.13 A, B), despite the subsequent addition of a 10-fold glucose-concentrated CD-U3 medium (0, 22 and 50 hpi) in FB to avoid glucose depletion [200]. This was reflected in the very low  $CSVY_{MVA}$  of 2.3 pfu/cell and  $P_{MVA}$  of  $2.4 \times 10^8$  pfu/(L×d) for both virus seeds (Table 4.7), which were around one log lower compared to the HCD perfusion cultivations HBM1 and HBM2 performed bioreactor (Table 4.6). Compared to infections at CCD (see Chapter 4.3), the  $CSVY_{MVA}$  and  $P_{MVA}$  using the FB10 strategy were almost 2  $\log_{10}$  lower (Table 4.4).

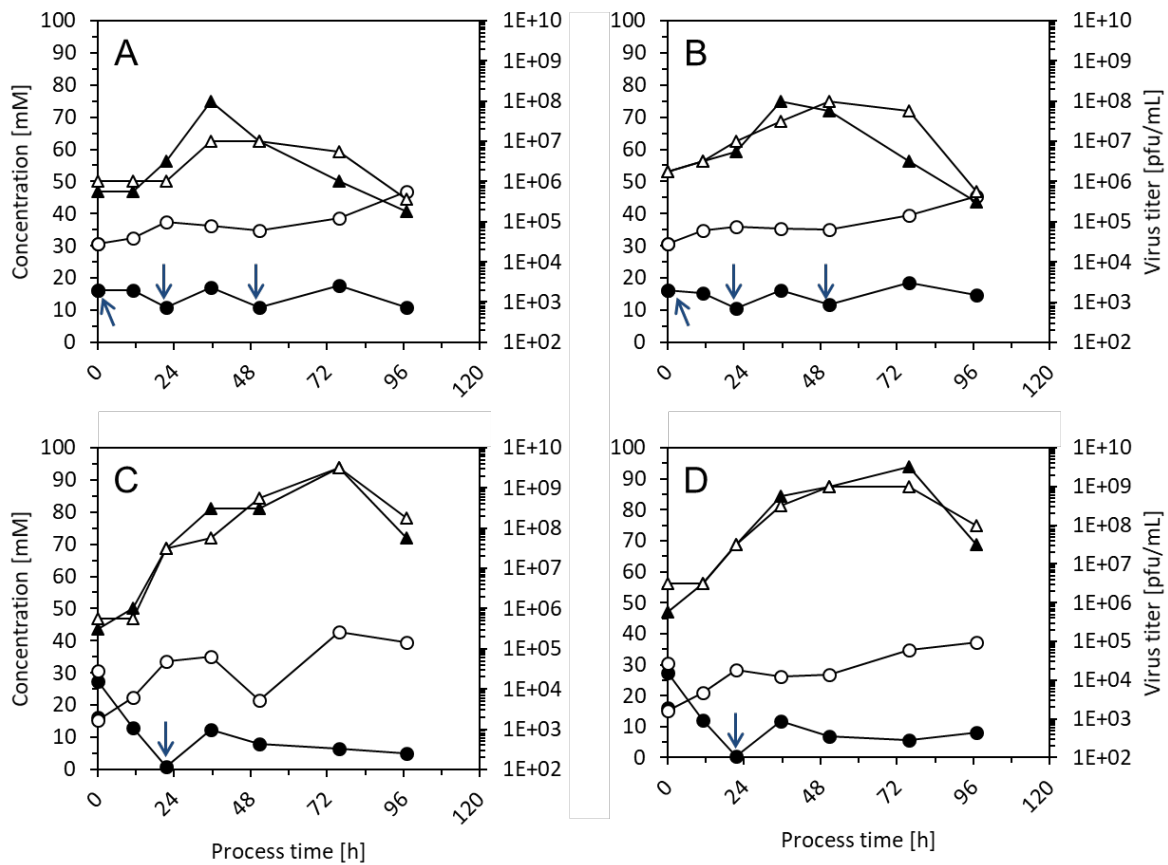


Figure 4.13. MVA-CR19 virus propagation and glucose/lactate concentrations in HCD cultures of CR.pIX cells applying a fed-batch (FB10) and a medium exchange (ME50) strategy. All cultivations were infected at  $37 \times 10^6$  cells/mL in 125 mL shake flasks (50 mL  $V_w$ ) with either seed virus MC19a or MC19B. A, B: Fed-batch with a 10-fold glucose- and glutamine-concentrated CD-U3 medium (FB10). C, D: 50% medium exchange at TOI (ME50). A, C: infections with the MC19a seed virus. B, D: infections with the MC19b seed virus. Glucose (filled circles) and lactate (empty circles) concentrations, virus titers of cell lysates (filled triangles) and in the supernatant (empty triangles). Time-points of bolus addition of a glucose-concentrated CD-U3 medium (blue arrows). Time 0 represents the time of virus infection. Figure adapted with permission from Vazquez-Ramirez et al. (2018) [200].

For the ME10 strategy, MVA-CR19 production improved considerably with a single 50% medium exchange at TOI followed by the addition of concentrated medium only at 21 hpi, when glucose was depleted (Figure 4.13 C, D). Despite a short-term glucose limitation, no negative effect in later virus propagation was observed and maximum virus titers of  $3.2 \times 10^9$  pfu/mL were obtained at around 72 hpi in both lysate and supernatant fractions, for both virus seeds [200] (Figure 4.13 C, D). “This demonstrated that 100% of the produced viruses can be harvested from supernatant at 72 hpi with no need of a cell-disrupting operation (e.g. freeze/thaw), as observed previously in CCD infections” [200]. With  $CSVY_{MVA}$  values of 62 and 72 pfu/cell and a  $P_{MVA}$  of  $6.0 \times 10^{10}$  pfu/(L×d) (Table 4.7), the results achieved were in the same range as for the HCD perfusion cultivations HBM1 and HBM2 performed bioreactor [200] (Table 4.6).

Table 4.7. Overview of MVA-CR19 virus production yields obtained with a fed-batch (FB10) and a medium exchange (ME50) strategy in HCD cultivations of CR.pIX cells in shake flasks. Adapted with permission from Vazquez-Ramirez et al. (2018) [200].

Experiment ID	Seed-virus	Harvest titer [pfu/mL]	$CSVY_{MVA}$ [pfu/cell] <sup>a</sup>	$P_{MVA}$ [pfu/(L×d)] <sup>b</sup>
FB10 *	MC19a	$1.0 \times 10^8$	2.3	$2.4 \times 10^8$
	MC19b	$1.0 \times 10^8$	2.3	$2.4 \times 10^8$
ME50 **	MC19a	$3.2 \times 10^9$	62	$6.0 \times 10^{10}$
	MC19b	$3.2 \times 10^9$	72	$6.0 \times 10^{10}$

\* Fed-batch with a 10-fold glucose- and glutamine-concentrated CD-U3 medium

\*\* Single medium exchange of 50% at TOI

<sup>a</sup> Cell-specific virus yield (for calculation refer to Chapter 3.5.5 Virus productivity estimations)

<sup>b</sup> Volumetric productivity (for calculation refer to Chapter 3.5.5 Virus productivity estimations)

“This suggested that the medium exchange at TOI rather than the exclusive glucose supply in FB with concentrated medium is required to improve MVA-CR19 virus propagation (especially from 0 to 24 hpi, Figure 4.13). Also, it has been reported that glutamine plays a minor role in energy supply for CR.pIX cells and that its absence might not influence the propagation of MVA in this cell line [274]. Therefore, the positive effect of a medium exchange at TOI on virus propagation might be also due to the dilution of inhibitory metabolites or signaling molecules rather than a better supply of substrates” [200].

---

### Strategies to maximize virus yields

This section consists of the results described in Chapter 3.3.3 of a previous publication by Vazquez-Ramirez et al. (2018) [200].

With the aim to maximize the virus yields, the combination of a medium exchange at TOI with adaptations in the medium supply and the virus harvest strategy (using normal CD-U3 medium) was investigated. The cellular material for the HCD cultures was generated from two 110 mL ( $V_w$ ) batch cultures (in two 250 mL shake flasks). In order to shorten the cell growth phase, the cells were inoculated at  $1.1 \times 10^6$  cells/mL and semi-perfusion was performed with a strict control of the time and the frequency of the medium exchange. Cell concentrations increased without any noticeable lag phase with a maximum specific growth rate of 0.023 1/h ( $t_2 = 30.1$  h), similar to other batch cultivations [29]. The culture was split into three 125 mL shake flasks after  $63 \times 10^6$  cells/mL were obtained to investigate the infection strategies described below.

To further reduce the risk of glucose limitation observed at 24 hpi with a 50% of medium exchange at TOI, a 100% medium exchange at TOI followed by three alternative feeding strategies was analyzed:

- I. Fed-batch (FB): a strategy similar to the VEF batch used by Pohlscheidt et al. (2008) [239] for the production of *Parapoxvirus ovis* in bovine kidney cells was carried out. A medium volume equal to the working volume at TOI (i.e. 20 mL) was added at time points 12, 24, 36 and 72 hpi (Figure 4.14). At 36 hpi, a working volume of 80 mL was reached (which is above the maximum working volume in the 125 mL shake flasks) and the cell suspension was transferred to a 250 mL shake flask to continue the experiment.
- II. Daily medium exchange (DME): 90% of the culture supernatant was exchanged every 24 h (Figure 4.14). This was achieved by centrifugation of the complete volume of the shake flask at  $200 \times g$ , 10 min, followed by harvest of 90% of the supernatant, and addition of fresh medium.  $V_w$  at TOI: 50 mL.
- III. Combination of fed-batch and daily medium exchange (F+D): medium was added in the fed-batch mode at 12 and 24 hpi. 90% of culture supernatant was exchanged at 36, 72 and 96 hpi (Figure 4.14). As before, the supernatants were collected as product harvest.

A schematic representation of those strategies is presented in Figure 4.14.

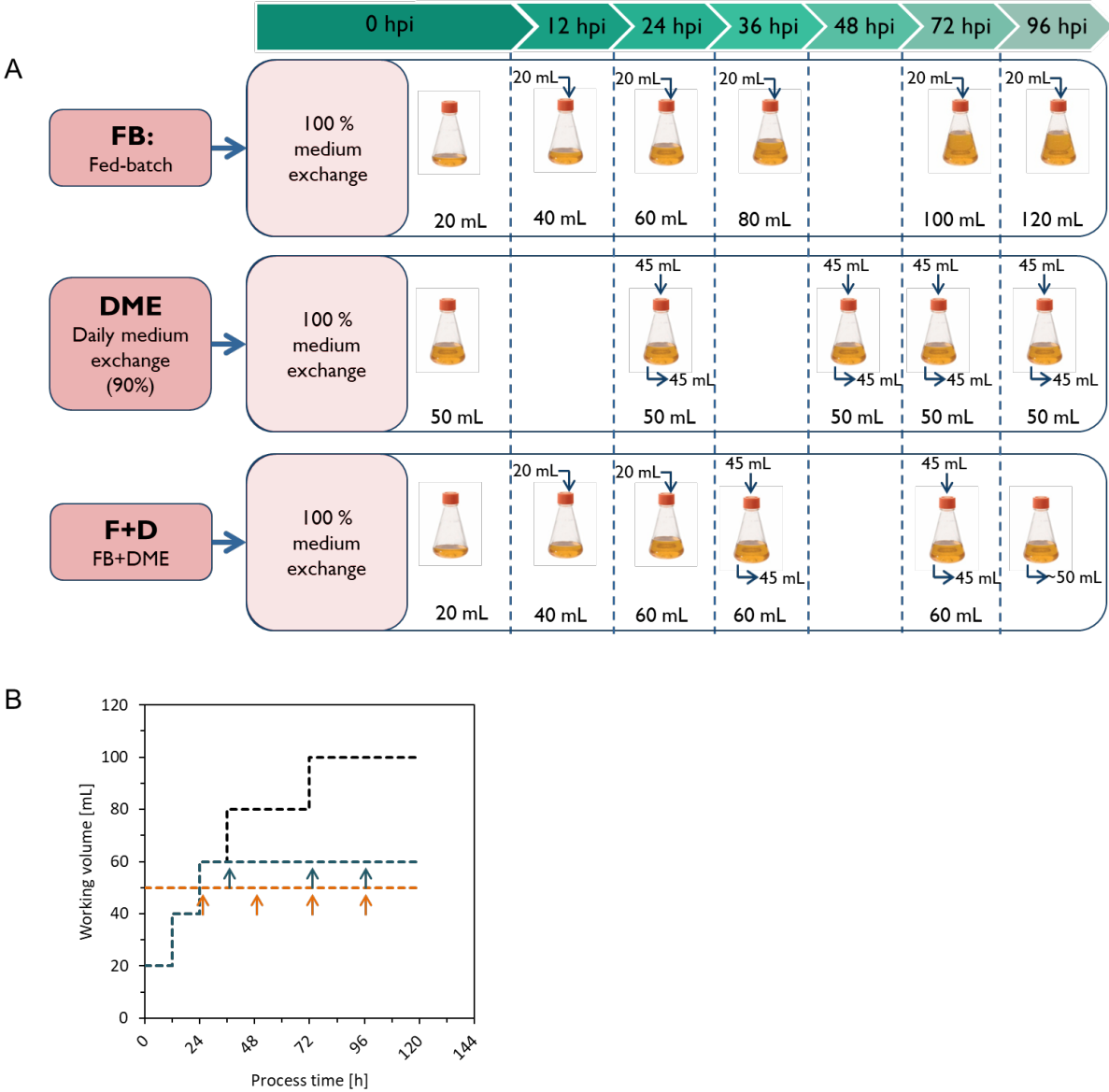


Figure 4.14. Schematic representation of further feeding strategies to improve MVA-CR19 virus propagation in CR.pIX cells infected at HCD in shake flasks. A: flowchart of the medium exchange and feeding regimes from infection time. B: change of working volume for the fed-batch (FB, black), daily medium exchange (DME, orange) and a fed-batch/daily medium exchange (F+D, blue) strategy. The arrows indicate the time-points of medium exchange.

Even a 100% medium exchange at TOI and 24 hpi could not completely prevent temporary depletions of glucose within the DME strategy (Figure 4.15 E, 24 and 48h hpi). Similarly, glucose limitations were observed at 24 and 72 hpi for the F+D (Figure 4.15 F) strategy. However, these short-term limitations did not compromise virus propagation: with virus titers higher than  $1.0 \times 10^8$  pfu/mL within the first 24 hpi (Figure 4.15 G–I) all experiments performed better than those with a 50% medium exchange (Figure 4.15 D).

Interestingly, the increase in volume for FB (Figure 4.15 D) and F+D (Figure 4.15 F) during the first 24 hpi did not result in a noticeable reduction of virus titers compared to the DME strategy (Figure 4.15 E). This positive effect of volume changes on virus titers, despite their expected reduction due to product dilution, was also documented previously for the VEF batch strategy [239].

At 36 hpi, the DME strategy showed a slight decrease in virus accumulation compared to both other strategies. This is possibly due to the removal of infectious particles (harvest of 90% supernatant) and a glucose limitation at 24 hpi. This contrasted with the FB and F+D strategies, where titers above  $1.0 \times 10^9$  pfu/mL were reached at 36 hpi. Nevertheless, a daily exchange of medium (DME, F+D strategy) extended the virus production phase, and allowed to achieve virus titers up to  $1.0 \times 10^{10}$  pfu/mL at 72 hpi. In contrast, the maximum titer was only  $3.7 \times 10^9$  pfu/mL for the FB at the same time point (Figure 4.15 G–I).

Product harvests (supernatant) obtained for the DME and F+D strategies showed consistently very similar virus titers to the lysates (except for harvests at 36 hpi in F+D) and even same titers at 72 hpi. Titters in this range were also obtained by Jordan et al. [32]. Accordingly, MVA-CR19 propagation in the CR.pIX cells does not require any disruption steps of the host cells to achieve very high product titers in HCD cultivations. The possibility to recover most of the viral particles directly from the supernatant reduces the complexity of the harvest process to a simpler clarification process via depth filtration or centrifugation.

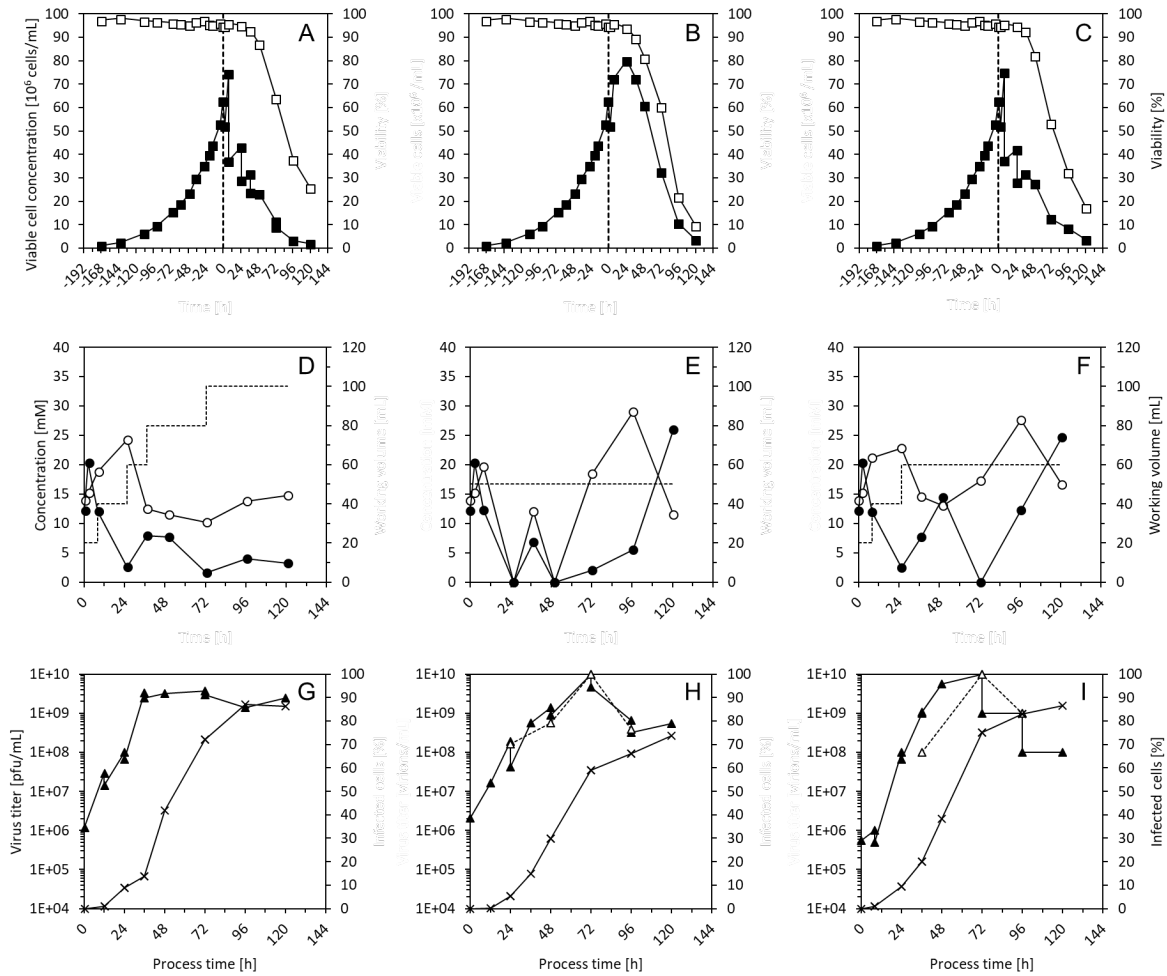


Figure 4.15. Cell growth kinetics, glucose/lactate concentration and MVA-CR19 virus propagation in HCD cultures of CR.pIX cells applying a fed-batch (FB), a daily medium exchange (DME) and a combined fed-batch/daily medium exchange (F+D) strategy. A, B, C: Viable cell concentrations (filled squares) and viability (empty squares). CR.pIX cells were expanded in semi-perfusion and infected at  $52.4 \times 10^6$  cells/mL in 125 mL shake flasks. Time of infection: 0 h (vertical dashed line). D, E, F: glucose (filled circles) and lactate (empty circles) concentrations, working volume (dashed line). G, H, I: virus titer in whole lysate (filled triangles) and supernatant/harvest (empty triangles), percentage of infected cells with respect to total cells (crosses). A, D, G: fed-batch (FB). B, E, H: daily medium exchange (DME). C, F, I: combined fed-batch/daily medium exchange (F+D). Figure adapted with permission from Vazquez-Ramirez et al. (2018) [200].

As another comparison between the different feeding strategies, the increase in the  $CSVY_{app}$ , in which only cells infected at 0 hpi were taken into account, and in  $P_{MVA}$  over the infection time are shown in Figure 4.16 A and B, respectively. Both FB-based strategies showed an earlier onset of virus release and maximum  $CSVY_{app}$  compared to the DME strategy. Furthermore, the maximum  $CSVY_{app}$  of the F+D strategy exceeded the yield of both other approaches by a factor of two or three. Regarding the  $P_{MVA}$ , the three feeding strategies showed comparable maximum values at 72 hpi (Figure 4.16 B). As expected, the difference became less evident for the  $CSVY_{MVA}$  (Table 4.8), which took into account cells produced even after TOI. However, FB-based strategies (FB and F+D) exhibited up to two times higher  $CSVY_{MVA}$  compared to DME (Table 4.8), which indicates an optimal balance between the

maintenance of healthy cells and the progress of virus replication. This observation is also supported by the higher percentage of infected cells obtained for the FB and F+D strategies (Figure 4.15 G–I).

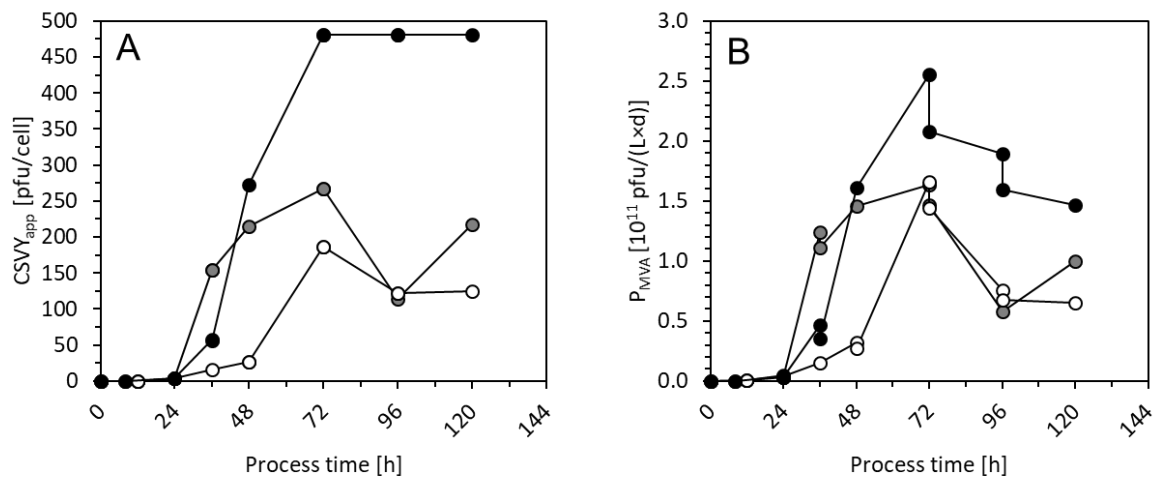


Figure 4.16. Time series of the MVA-CR19 virus production yields obtained with a fed-batch (FB), a daily medium exchange (DME) and a combined fed-batch/daily medium exchange (F+D) strategy in HCD cultivations of CR.pIX cells. All cultivations were carried out in 125 mL shake flasks A: apparent cell-specific yield (CSVY<sub>app</sub>). B: volumetric productivity ( $P_{MVA}$ ). FB (gray), DME (white) and F+D (black) strategies. Time of infection: 0 h. Figure adapted with permission from Vazquez-Ramirez et al. (2018) [200].

Since cells of all analyzed strategies originated from one single HCD-cultivation, for the calculation of  $P_{MVA}$ , the corresponding medium utilization of each strategy during the cell growth phase was calculated based on their working volume at TOI. This way, medium utilization until TOI was calculated 60% lower for FB and F+D strategies (working volume at TOI of 20 mL) compared to the DME (working volume at TOI of 50 mL). Accordingly, the F+D strategy provided the best  $P_{MVA}$ , since it provided the lowest medium consumption during the cell expansion phase and produced the highest amount of virus particles (Table 4.8). Overall, the F+D strategy optimally combined a low medium consumption with high virus yields. Another positive feature of substrate feeding in a fed-batch mode is that no virus is lost at early stages of infection, which helps to reach a higher fraction of infected cells and high titers at around 36 hpi (Figure 4.15 G–I) without reaching limiting glucose concentrations. At that time point, a first harvest should also be considered to collect a highly concentrated supernatant and to avoid the accumulation of by-products with a negative impact on virus replication (compare time course of virus titers in Figure 4.15 G and I). Furthermore, a transfer of the cell suspension to a new vessel was not required for the F+D strategy, which represents an advantage against the FB and the reported VEF batch [239] regarding the operation of large bioreactors.

Table 4.8. Overview of MVA-CR19 virus production yields obtained with a fed-batch (FB), a daily medium exchange (DME) and a combined fed-batch/daily medium exchange (F+D) strategy in HCD cultivations of CR.pIX cells in shake flasks. Adapted with permission from Vazquez-Ramirez et al. (2018) [200].

Feeding strategies	Harvest vol. <sup>a</sup> [mL]	Harvest titer [pfu/mL]	Max. cells [ $10^9$ ]	Pooled titer <sup>b</sup> [pfu/mL]	CSVY <sub>MVA</sub> [pfu/cell]	P <sub>MVA</sub> [pfu/(L×d)]
FB	100	$3.7 \times 10^9$	1.9	$3.7 \times 10^9$	200	$1.6 \times 10^{11}$
DME	H1: 45	$1.6 \times 10^8$	4.0	$3.8 \times 10^9$	130	$1.7 \times 10^{11}$
	H2: 45	$5.6 \times 10^8$				
	H3: 50	$1.0 \times 10^{10}$				
F+D	H1: 45	$1.0 \times 10^8$	1.9	$5.3 \times 10^9$	270	$2.6 \times 10^{11}$
	H2: 50	$1.0 \times 10^{10}$				

<sup>a</sup>H: harvest

<sup>b</sup> Corresponds to the theoretical titer of the pool of all harvests withdrawn during the virus propagation

\*All data correspond to values obtained at/up to 72 hpi (time of highest virus titer and productivity yields)

In accordance to the more than 10-fold increase in cell concentrations, all strategies resulted in product titers 10 times higher than the titers typically obtained at CCD. Accordingly, the tested HCD strategies showed CSVY<sub>MVA</sub> values comparable to the reference CCD cultivations (Table 4.4, Table 4.8), provably even with a slight increase. Similarly, the F+D strategy showed a P<sub>MVA</sub> up to four times higher than the CCD cultivations (Table 4.4, Table 4.8), however, still within the RSD of the virus titration method (see Chapter 3.5.5 of Materials and Methods).

For a further scale-up of either the DME or the F+D strategy, several limitations should be taken into account. For production scale, the medium exchange/product harvest cannot be done as immediate as performed with very low volumes and has to rely on the use of the ATF system and hollow fiber with an adequate membrane cut-off. However, an adaptation of strategies aiming for a dilution of possible inhibitors of infection, supply of nutrients and virus harvest during virus production phase can still be implemented in larger scales. An analysis on such adaptations is presented in the following Chapter 4.4.3.

#### 4.4.3 MVA-CR19 virus propagation applying a hybrid fed-batch/perfusion strategy

For the implementation of the F+D strategy in a bioreactor, CR.pIX cells were expanded to HCD in perfusion as defined previously in Chapter 4.2.1 using an ATF system. Additionally, the daily medium exchange performed in shake flasks during the virus propagation was substituted by a medium perfusion using an ATF system. The resulted operation mode was named as **hybrid FB/perfusion (HFP)**. A first cultivation, **HBM3**, was performed in a V<sub>w</sub> of 0.6 L using a 0.65 μm hollow fiber module L65U (Table 3.2) for cell expansion in perfusion and for the virus propagation phase.



Similar to the HBM2 run, the exponential cell growth in the HBM3 was maintained with a rate of 0.021 1/h ( $t_2 = 33.0$  h), and a viable cell concentration of  $52.9 \times 10^6$  cells/mL and a viability of 95% before infection were achieved. Two hours before infection, the perfusion rate was increased until a total medium exchange of  $1 V_R$  was achieved, as stated in Chapter 3.3.3 (see „medium supply during the virus propagation phase“) in Materials and Methods. After medium exchange, a viable cell concentration of  $49.9 \times 10^6$  cells/mL was measured and the volume of virus seed to achieve an MOI of 0.05 was calculated accordingly. A summary of performance parameters during the cell growth in perfusion is presented in Table 4.9.

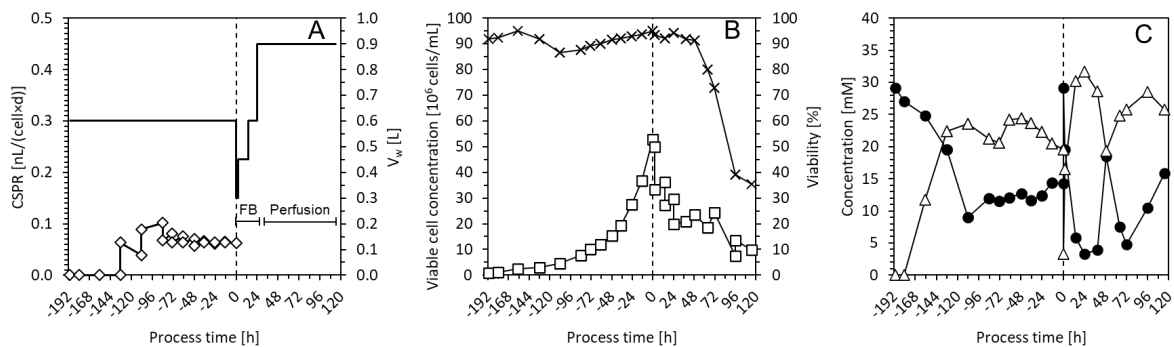


Figure 4.17. Feeding profile, cell growth kinetics and glucose/lactate concentration in a HCD culture of CR.pIX cells (HBM3), applying a hybrid FB/perfusion (HFP) strategy after infection with MVA-CR19 virus. A: cell-specific perfusion rate, CSPR, (empty diamonds) and working volume,  $V_w$ , (continuous line). The bioreactor was operated in perfusion mode at a  $V_w$  of 0.6 L until time of infection: 0 h (vertical dashed line). Then,  $1 V_R$  was exchanged with fresh medium using the ATF system. The bioreactor volume was then reduced to 0.3 L (by extracting 0.3 L of cell suspension) to allow for a volume expansion in the fed-batch phase (FB) after infection with MVA-CR19 virus. The FB phase continued until 24 hpi, when the medium supply was switched to perfusion mode. B: viable cell concentration (squares) and viability (crosses). CR.pIX cells were expanded in a 1 L perfusion bioreactor (0.6 L  $V_w$ ) to  $49.9 \times 10^6$  cells/mL and infected at an MOI of 0.05 after reducing the bioreactor volume to 0.3 L. C: glucose (filled circles) and lactate (triangles) concentrations. Time of infection: 0 h (vertical dashed line). Figure adapted with permission from Vazquez-Ramirez et al. (2019) [219].

At TOI, to perform the initial FB phase without exceeding the maximum  $V_w$  (1.0 L), one half of the volume was transferred to a second bioreactor for a parallel mock infection (data not shown). However, it was observed that a minimum  $V_w$  of 0.45 L would be required for operation of the bioreactor coupled to the ATF system. Therefore, infection was performed directly with 0.15 L of fresh virus-containing medium. Thus, the FB phase continued with the addition of 0.15 L at 12 hpi and 0.3 L at 24 hpi, reaching the planned maximum  $V_w$  of 0.9 L. The medium exchange, performed previously in small-scale shake flasks, was adapted to the bioreactor by starting perfusion at 24 hpi at a rate of  $1.8 V_R/d$  (1.62 L/d) to initiate the virus harvest. This way, similar to the small-scale experiments, first harvest (H1) of  $0.9 V_R$  (0.81 L) was collected at 36 hpi. At this time point, perfusion was adjusted to  $0.6 V_R/d$  (0.54 L/d) to complete a second harvest (H2) of  $0.9 V_R$  at 72 hpi. Perfusion was subsequently maintained at  $0.6 V_R/d$  until the end of the cultivation at 115 hpi.

As observed in Figure 4.18, virus harvest using the ATF system was suboptimal compared to the harvest achieved in shake flasks by simple centrifugation, despite the utilization of a 0.65  $\mu\text{m}$  hollow fiber module. Since the same membrane was used for the whole process, the low level of virus collection via the permeate line suggested a membrane fouling that could have been already present since the beginning of the virus propagation phase. Nevertheless, compared to the scale-down model (F+B) presented previously (Table 4.8), very comparable maximum virus titer and  $P_{MVA}$  were obtained, with a slight increase of 54% in  $CSVY_{MVA}$  (Table 4.10).

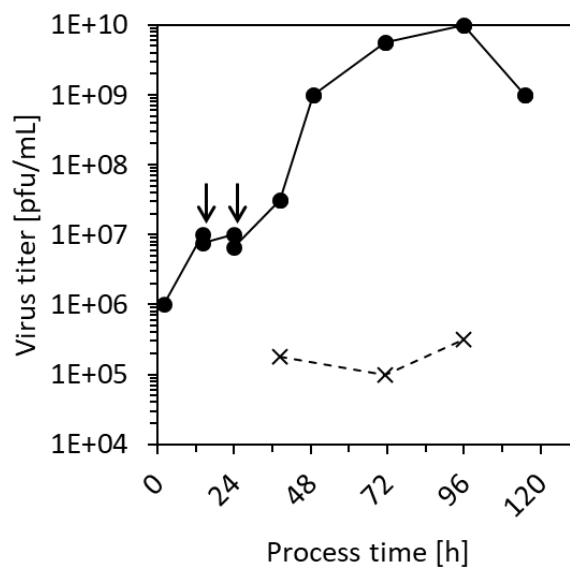


Figure 4.18. MVA-CR19 virus propagation at HCD in the HBM3 bioreactor, applying a hybrid FB/perfusion (HFP) strategy. Virus titers of cell lysates (filled circles) and in the permeate (crosses). Arrows: time points of CD-U3 medium addition. Time 0 represents the time of virus infection. Figure adapted with permission from Vazquez-Ramirez et al. (2019) [219].

With respect to the reference batch process at CCD (CSM2, Table 4.4), the application of a hybrid strategy in culture HBM3 resulted in a significantly higher product yield with a more than 10-fold increase in virus titer at time of harvest (harvest titer). Also, a 3-fold increase in both  $CSVY_{MVA}$  and  $P_{MVA}$  were obtained (Table 4.10).

In order to assess the suitability of a 0.65  $\mu\text{m}$  hollow fiber module for MVA-CR19 virus harvest in an ATF-based process, a fourth cultivation (**HBM4**) using two hollow fiber modules was carried out. The ATF system was operated with a 0.2  $\mu\text{m}$  hollow fiber module L20U (Table 3.2) for cell expansion and medium exchange before infection. Cell expansion in perfusion was controlled as defined previously in Chapter 4.2.1, with an additional on-line monitoring of cell concentration using a capacitance probe. During the FB phase, after infection, the ATF system continued pumping the cell suspension

(without perfusion) with the L20U hollow fiber. Then, at 26 hpi, a new 0.65  $\mu\text{m}$  hollow fiber module S65U (Table 3.2) was installed to start with the perfusion phase again at 36 hpi.

As observed in the HBM3 run, a very low  $V_w$  (3 L in HBM3) at TOI is needed in order to support the volume expansion derived from the FB phase of the HFP strategy. Since a minimum volume of 0.45 L is required for operation of the bioreactor coupled to the ATF system, the process was adjusted in order to perform cell infection at a comparable cell concentration without the need to discard half of the cell suspension. In this case, the cell expansion in perfusion was performed at a  $V_w$  of 0.6 L and the same target CSPR of 0.06 nL/(cell $\times$ d). Starting at a concentration of  $8 \times 10^6$  cells/mL, the cells were expanded in perfusion for around 48 h to a concentration  $26 \times 10^6$  cells/mL (Figure 4.19 B). Despite the difference in the starting cell concentration, the observed cell growth rate and average CSPR during cell propagation were in accordance to the previous runs (Table 4.9).

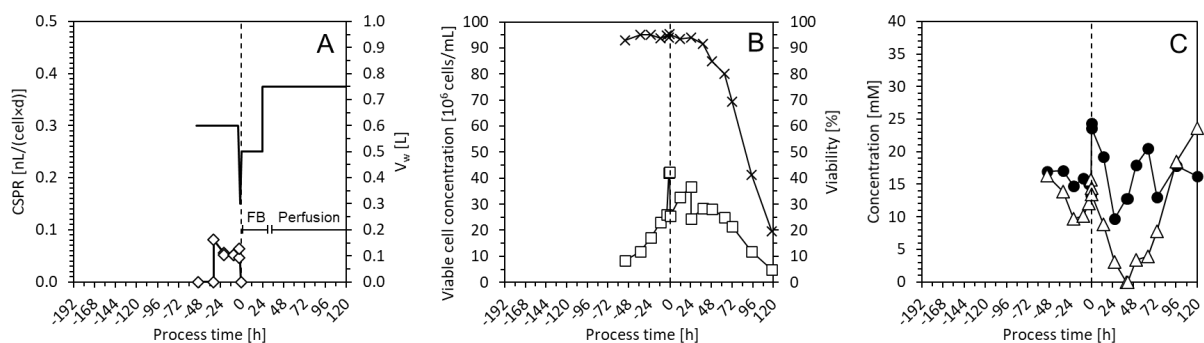


Figure 4.19. Feeding profile, cell growth kinetics and glucose/lactate concentration in a HCD culture of CR.pIX cells (HBM4), applying a hybrid FB/perfusion (HFP) strategy after infection with MVA-CR19 virus. A: cell-specific perfusion rate, CSPR, (empty diamonds) and working volume,  $V_w$ , (continuous line). The bioreactor was operated in perfusion mode at a  $V_w$  of 0.6 L for around 48 h, using a hollow fiber module L20U, until almost 4.4 h before infection (time of infection: 0 h, vertical dashed line). Then, the bioreactor volume was reduced to 0.3 L by stopping the feeding pump and collecting 0.3 L of cell-free permeate in the harvest bottle. 2 h before infection, perfusion was re-started and 1  $V_R$  was exchanged with fresh medium. Right after infection the FB phase was started and continued until 36 hpi, when the medium supply was switched to a perfusion mode using a new hollow fiber module (S65U). The perfusion phase continued until 120 hpi. B: viable cell concentration (squares) and viability (crosses). CR.pIX cells were expanded in a 1 L perfusion bioreactor (0.6 L  $V_w$ ) to  $26 \times 10^6$  cells/mL and infected at an MOI of 0.05 after concentrating the cell suspension to  $42.4 \times 10^6$  cells/mL. C: glucose (filled circles) and lactate (triangles) concentrations. Time of infection: 0 h (vertical dashed line). Figure adapted with permission from Vazquez-Ramirez et al. (2019) [219].

At the end of the growth phase in perfusion, the cell suspension was concentrated 2-fold (Figure 4.19 B) by stopping the feeding pump and setting the harvest pump at 0.21  $V_R$ /h (0.125 L/h) to reduce the  $V_w$  to 0.3 L (Figure 4.19 A). After collecting 0.3 L in the harvest bottle (around 2.4 h later), the feeding pump and the perfusion control were re-started and 1  $V_R$  was exchanged with fresh medium applying perfusion at 0.15 L/h for 2 h. At this point the cells reached a concentration of

## Results and Discussion

$42.4 \times 10^6$  cells/mL and MVA-CR19 virus was added at an MOI of 0.05 (process time = 0 in Figure 4.19). The FB phase was started right after by adding 0.2 L of fresh medium, increasing the  $V_w$  to 0.5 L. Next medium addition of 0.25 L was performed at 26 hpi to increase the  $V_w$  to 0.75 L (Figure 4.19 A) and the L20U hollow fiber was exchanged by a new S65U hollow fiber. Different to the HBM3 run, the perfusion phase was started at 36 hpi. The perfusion rate was maintained at a constant rate of 1 VR/d (0.75 L/d) until 120 hpi (Figure 4.19 A).

Table 4.9. Summary of process parameters and performance of HBM3 and HBM4 runs during the CR.pIX cell expansion in a perfusion in bioreactor. Adapted with permission from Vazquez-Ramirez et al. (2019) [219].

Experiment ID <sup>a</sup>	Working volume [mL]	Hollow fiber module	Seed cell concentration [ $10^6$ cells/mL]	$\mu_{\text{mean}}$ [1/h]	$\mu_{\text{max}}$ [1/h]	Actual average CSPR [nL/(cell×d)]	Duration [h] <sup>b</sup>
HBM3	600	0.65 $\mu\text{m}$	1.0	0.021 (n=12, SD=0.006)	0.029	0.068 (n=18, SD=0.013)	191
HBM4	600	0.20 $\mu\text{m}$	8.0	0.024 (n=4, SD=0.005)	0.031	0.057 (n=7, SD=0.011)	50

<sup>a</sup>H: high cell density, B: bioreactor, M: MVA-CR19

<sup>b</sup>Time from cell inoculation to infection

n: number of data points considered for the average calculations

As observed in previous cultivations at HCD, and in accordance to previous reports [32], practically 100% of the viruses appeared in the cultivation supernatant when maximum virus titer appeared, i.e. at 72 hpi (Figure 4.20). However, the change of the filtration membrane during the virus propagation phase enabled the harvest of almost all viruses present in the supernatant only during the first 26 h of harvest (i.e. from 26 to 48 hpi) (Figure 4.20). From 48 hpi forward, the virus concentration in the permeate line decreased considerably with respect to the virus in the bioreactor supernatant. Virus titer in the permeate line reached a titer of  $1 \times 10^6$  pfu/mL at 72 hpi, when the maximum virus titer of  $1 \times 10^{10}$  pfu/mL at 72 hpi was reached in bioreactor supernatant [219]. Further dilution of virus concentration to  $1 \times 10^5$  pfu/mL was observed up to 120 hpi, while titers in the bioreactor remained almost stable at the order of  $1 \times 10^9$  pfu/mL [219] (Figure 4.20). Similar to reactor HBM3, these observations suggested that a significant membrane fouling appeared at least after 24 h of perfusion, missing the most productive period of the virus propagation phase from 48 to 72 hpi [219] (Figure 4.20).

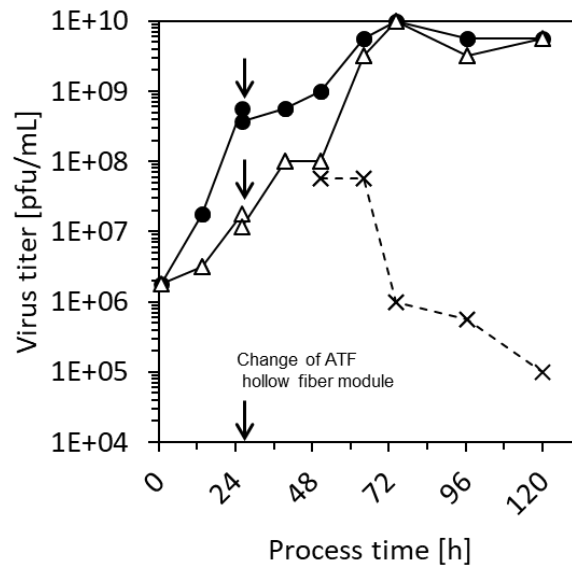


Figure 4.20. MVA-CR19 virus propagation at HCD in the HBM4 bioreactor, applying a hybrid FB/perfusion (HFP) strategy. Virus titers of cell lysates (filled circles), in the supernatant (triangles) and in the permeate (crosses). Arrows: time points of CD-U3 medium addition. At 26 hpi, the hollow fiber module used for cell expansion and medium exchange (L20U) replaced by a new hollow fiber module (S65U). The new S65U module was applied for virus harvest from 36 hpi onwards. Time 0 represents the time of virus infection. Figure adapted with permission from Vazquez-Ramirez et al. (2019) [219].

Nevertheless, the low virus titers obtained in the permeate did not affect the overall productivity, just as observed for the HBM3 run. Even when considering the low virus concentrations in the permeate as losses, virus productivity remained within the previously observed ranges. With a  $CSV_{MVA}$  of 352 pfu/cell and a  $P_{MVA}$  of  $2.8 \times 10^{11}$  pfu/(L×d) [219], the HBM4 run showed comparable productivity values with respect to HBM3 (Table 4.10), considering the RSD of the virus titration method (see Chapter 3.5.5 of Materials and Methods). Furthermore, the need of a continuous virus harvest from 26–36 hpi onwards, to avoid virus inactivation, suggested from results in the scale-down models (Figure 4.15 H, I), seemed not to play an important role in virus productivity. An observation that supports this hypothesis is the very low virus inactivation rate observed from the 72 hpi onwards (Figure 4.20), similar to previous bioreactor and shake flasks infections, suggesting a high stability of the virus at these cultivation conditions.

Table 4.10. Overview on production yields of MVA-CR19 virus in HCD cultivations of CR.pIX cells in a bioreactor, using a hybrid FB/perfusion (HFP) strategy. Adapted with permission from Vazquez-Ramirez et al. (2019) [219].

Experiment ID <sup>a</sup>	Working volume [mL]	Harvest titer [pfu/mL]	$t_T$ [d] <sup>b</sup>	Max. cells [ $10^9$ ]	$CSVY_{MVA}$ [pfu/cell] <sup>c</sup>	$P_{MVA}$ [pfu/(L×d)] <sup>d</sup>
HBM3	900	$1.0 \times 10^{10}$	10.9	21.9	410	$1.3 \times 10^{11}$
HBM4	750	$1.0 \times 10^{10}$	8.2	21.3	352	$2.8 \times 10^{11}$

<sup>a</sup>H: high cell density, B: bioreactor, M: MVA-CR19

<sup>b</sup>Total time from cell inoculation to maximum virus titer

<sup>c</sup>Cell-specific virus yield (for calculation refer to Chapter 3.5.5 Virus productivity estimations)

<sup>d</sup>Volumetric productivity (for calculation refer to Chapter 3.5.5 Virus productivity estimations)

The strategies applied for both HBM3 and HBM4 runs “simplify the production process because a single bioreactor can be used for cell expansion and virus propagation. In HBM3 run, one-half of the cell suspension (0.3 L) was removed before infection at  $50 \times 10^6$  cells/mL (Figure 4.17). This cell suspension could possibly be used to start a second bioreactor in parallel. In contrast, in the HBM4 run, cells were cultivated to  $25 \times 10^6$  cells/mL in 0.6 L and concentrated to  $50 \times 10^6$  cells/mL prior to infection (Figure 4.19). In both cases, the subsequent FB phase required the addition of almost three times the starting volume to avoid substrate limitations. This ratio was lower than the 1:4 reported by Pohlscheidt et al. (2008) [239] for the high-yield production of *Parapoxvirus ovis* at large scale, which—in addition—required transferring the cell suspension to a second larger bioreactor to perform the dilution steps. Since the initial FB phase of the HFP strategy seems to be a critical operation also for MVA-CR19 virus propagation, further studies should focus on the development of an optimized feed medium to enable a higher starting volume (preferably 60% of the maximum working volume) and a lower maximum dilution ratio (around 2:3) to simplify the hybrid strategy for implementation in large-scale bioreactors” [219].

#### 4.5 Propagation of influenza A virus in high cell density cultures

The HFP strategy developed for the propagation of MVA-CR19 virus was further investigated for the production of IAV at HCD. Several cultivations for the production of IAV in HCD perfusion cultures of CR cells showed that perfusion with virus retention can increase IAV titers while maintaining similar  $CSVY_{IAV}$  compared to the reference processes at CCD [42]. Nevertheless, a potential to further improve  $P_{IAV}$  either by means of medium or process development was also identified. Therefore, based on the improvements in the production yields of MVA-CR19 virus using the HFP strategy compared to the full perfusion cultures (i.e. HBM1 and HBM2), it was investigated whether a similar outcome can be expected for IAV.

---

In the next chapter, a cultivation of CR.pIX cells in a bioreactor operated completely in perfusion mode is described. Later the application of the HFP strategy for IAV propagation and a comparison with the full perfusion culture and a reference CCD processes is described.

#### 4.5.1 Influenza A virus propagation applying perfusion

A process operated completely in perfusion mode (i.e. both cell expansion and virus propagation) based on Genzel et al. (2014) [42] was performed as a reference HCD process for the production of IAV and taken as benchmark for process optimization. This cultivation, identified as **HBI1**, was performed at a  $V_w$  of 0.8 L in a 1 L perfusion bioreactor (with a L500 hollow fiber module, 500 kDa cut-off) and inoculated at a cell concentration of  $1.3 \times 10^6$  cells/mL. The target CSPR was set at  $0.062 \text{ nL}/(\text{cell} \times \text{d})$ , based on the actual glucose concentration in CD-U3 medium (39.6 mM), the theoretical glucose consumption rate ( $8.54 \times 10^{-11} \text{ mmol}/(\text{cell} \times \text{h})$ ) and an expected glucose concentration in the bioreactor of 6 mM. As for all other perfusion runs, the perfusion rate  $Q$  was re-adjusted every 12 or 24 h as described in Chapter 3.3.3. The CR.pIX cells were cultivated up to  $23.7 \times 10^6$  cells/mL as described previously in Chapter 4.2.1. The applied perfusion regime differed to the method reported by Genzel et al. (2014) [42] in that it aimed at the minimization of medium spending by adjusting the perfusion rate to the actual cell requirement (i.e. based on a constant and low CSPR).

The HBI1 run was used to define the perfusion strategy for CR.pIX cells. Therefore, a detailed discussion on the cell growth phase is described in Chapter 4.2.1. Figure 4.21 presents an overview of the cell growth kinetics along the complete IAV production process (before and after infection with IAV).

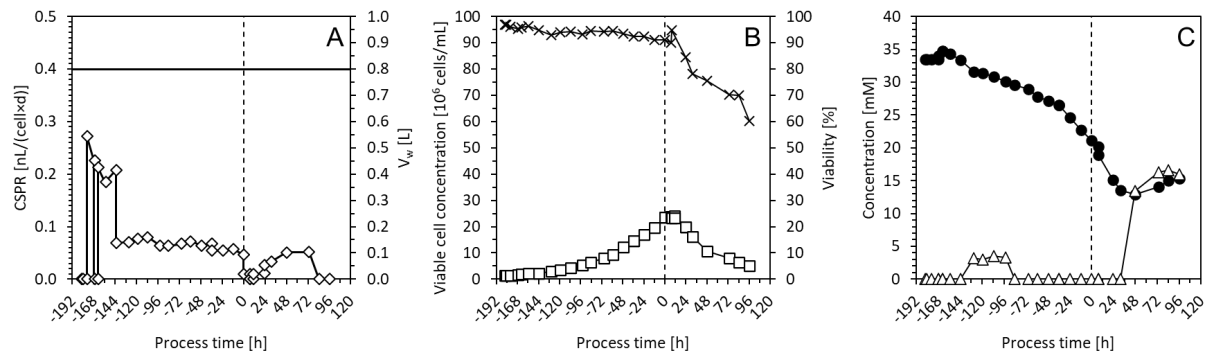


Figure 4.21. Feeding profile, cell growth kinetics and glucose/lactate concentration in a HCD perfusion culture of CR.pIX cells (HBI1), before and after infection with IAV. A: cell-specific perfusion rate, CSPR, (empty diamonds) and working volume,  $V_w$ , (continuous line). The bioreactor was operated in perfusion mode at a  $V_w$  of 0.8 L for around 176 h using a hollow fiber module L500 (500 kDa). At time of infection (0 h, vertical dashed line), perfusion was stopped and IAV and trypsin were added. The reactor was maintained in batch mode until around 4 hpi, when perfusion was resumed. The perfusion regime continued until 96 hpi, when the cultivation was stopped. B: viable cell concentration (squares) and viability (crosses). CR.pIX cells were expanded to  $23.7 \times 10^6$  cells/mL and infected at an MOI of  $1 \times 10^{-3}$ . C: glucose (filled circles) and lactate (triangles) concentrations. Time of infection: 0 h (vertical dashed line).

For the HBI1 run, no medium exchange prior to infection with IAV was performed, given the high glucose concentration (21.1 mM) and the lactate concentration below the limit of detection reached at TOI (Figure 4.21, C), which indicated a suitable condition for virus infection. Right before infection, the perfusion was stopped and IAV plus trypsin were added at the described concentrations (see Chapter 3.4.2). The perfusion was re-started 4 hpi (cultivation in batch mode after infection is required to allow viruses to enter into the cells [42]) based on calculations described in Chapter 3.3.3 (see “Medium supply during the virus propagation phase”).

During the initial batch phase, the glucose concentration decreased to around 15 mM and lactate concentration increased to around 13 mM, which were in an acceptable range. After re-starting perfusion, the CSPR was maintained between 0.011 and 0.051 nL/(cell×d), which was lower than the target CSPR of 0.062 nL/(cell×d) (Figure 4.21, A). Despite the lower CSPR, no glucose depletion or high lactate accumulation were observed (Figure 4.21, C). Additionally, the viable cell concentration and viability showed the known characteristic depletion profiles after virus infection [29, 42] (Figure 4.21, B).

The virus production yields obtained in the HBI1 run are reported in the next chapter and compared with a cultivation operated with the HFP strategy.



## 4.5.2 Influenza A virus propagation applying the hybrid fed-batch/perfusion strategy

In Chapter 4.4.3 it was shown that the HFP strategy was a competitive alternative to a full perfusion process (i.e. applying perfusion for both cell expansion and virus propagation) to increase productivity of MVA-CR19 at HCD. For IAV, it was reported that a room for optimization of HCD perfusion processes might exist, in order to maintain either the  $CSVY_{IAV}$  or the  $P_{IAV}$  values in the corresponding typical CCD processes [42, 43]. Therefore, it was next investigated whether the HFP strategy could have the potential to alleviate the known drawbacks of the current HCD perfusion approaches and deliver IAV productivity comparable to the reference CCD process.

The intended cultivation, identified as **HBI2**, was performed at a  $V_w$  of 0.6 L in a 1 L perfusion bioreactor (with a S500 hollow fiber module, 500 kDa cut-off) and inoculated at a CR.pIX cell concentration of  $1.1 \times 10^6$  cells/mL. The cells were expanded in perfusion mode up to  $26.9 \times 10^6$  cells/mL, applying a perfusion control linked to pH control, which was based on the lactate accumulation (resulting from glucose consumption). A detailed description of this on-line perfusion control is presented in Chapter 4.6.1.

Around 4 h before infection, the cell suspension was concentrated almost 2-fold (Figure 4.22 A) by stopping the feeding pump and setting the harvest pump at  $0.25 V_R/h$  (0.15 L/h) to reduce the  $V_w$  to 0.3 L. After having collected 0.3 L in the harvest bottle (around 2 h before infection), the feeding pump and the perfusion control were re-started and  $1 V_R$  (0.3 L) was exchanged with fresh medium applying perfusion at 0.15 L/h for 2 h. At this point the cells reached a concentration of  $47.4 \times 10^6$  cells/mL. The ATF hollow fiber module was then replaced by a new L65U module (0.65  $\mu\text{m}$ ) that was later applied for the perfusion phase of the HFP strategy. Since the ATF system was only re-started with new module at 26 hpi, no oscillations in the bioreactor volume were experienced at this point and the stirrer was well submerged at a  $V_w$  of 0.3 L, assuring proper mixing.

Differences in the virus propagation dynamics were considered beforehand for the optimal application of the HFP strategy. It is reported that a first increase in virus titers in the cultivation's supernatant can be observed from 4 to 12 hpi and that maximum virus titer can be achieved as early as 12 hpi [286]. Initial analysis on the propagation of IAV in small-scale HCD cultures of CR.pIX cells showed that maximum virus titers could be observed from 15 to 24 hpi. Therefore, IAV and trypsin were added at the described concentrations (see Chapter 3.4.2) and a total of 0.1 mL medium were added first from 0 to 10 hpi. Finally from 10 to 12 hpi, a total of 0.41 mL of medium were added to reach a final  $V_w$  of 0.81 L. Then bioreactor remained in batch mode until 24 hpi, when perfusion phase was started at a rate of  $1 V_R/d$  (0.81 L/d), using the new L65U module (Figure 4.22 A).

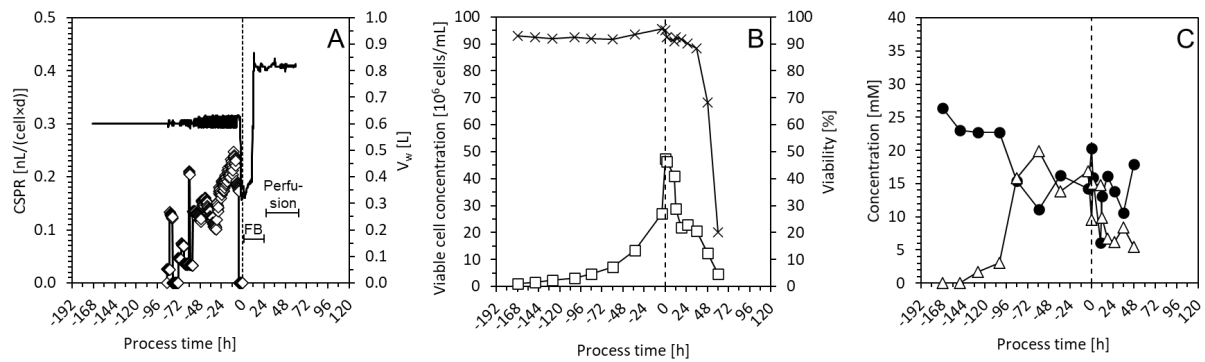


Figure 4.22. Feeding profile, cell growth kinetics and glucose/lactate concentration in a HCD culture of CR.pIX cells (HBI2), applying a hybrid FB/perfusion (HFP) strategy after infection with IAV. A: cell-specific perfusion rate, CSPR, (empty diamonds) and working volume,  $V_w$ , (continuous line). The bioreactor was operated in perfusion at a  $V_w$  of 0.6 L for around 85 h, using a hollow fiber module S500 (500 kDa), until 4 h before infection (time of infection: 0 h, vertical dashed line). Then, the bioreactor volume was reduced to 0.3 L by stopping the feeding pump and collecting 0.3 L of cell-free permeate in the harvest bottle. 2 h before infection, perfusion was re-started and 1  $V_R$  was exchanged with fresh medium. Right before infection, the ATF hollow fiber module was replaced by an L65U (0.65  $\mu$ m). Right after infection the FB phase was started and continued until 24 hpi, when the medium supply was switched to a perfusion mode using the new hollow fiber module L65U. The perfusion phase continued until 60 hpi. B: viable cell concentration (squares) and viability (crosses). CR.pIX cells were expanded in a 1 L perfusion bioreactor (0.6 L  $V_w$ ) to  $26.9 \times 10^6$  cells/mL and infected at an MOI of  $1 \times 10^{-3}$  after concentrating the cell suspension to  $47.4 \times 10^6$  cells/mL. C: glucose (filled circles) and lactate (triangles) concentrations. Time of infection: 0 h (vertical dashed line). Figure adapted with permission from Vazquez-Ramirez et al. (2019) [219].

A maximum HA titer for the HBI2 reactor of  $3.27 \log_{10}$  (HAU/100  $\mu$ L) could be observed at least until 60 hpi, in contrast to the maximum of  $2.41 \log_{10}$  (HAU/100  $\mu$ L) obtained until 96 hpi for the reference reactor CBI1 infected at  $4.0 \times 10^6$  cells/mL (Figure 4.23 A). This represents an almost 10-fold increase in the HA virus titer, in accordance to the around 10 times higher cell concentration in the HBI2 reactor of  $47.4 \times 10^6$  cells/mL at TOI (Figure 4.22 B). A similar increase was obtained for the maximum concentration of infectious virions (TCID<sub>50</sub>). In this regard, maximum TCID<sub>50</sub> titers of  $7.60 \times 10^7$  virions/mL and  $4.30 \times 10^8$  virions/mL were obtained for CBI1 (at 19 hpi) and HBI2 (at 48 hpi), respectively (Figure 4.23 B). Compared to the HBI1 reactor, which was fully operated in perfusion and yielded a maximum HA titer of  $2.60 \log_{10}$  (HAU/100  $\mu$ L) at 48 hpi, HBI2 showed a slight increase in virus titer. Considering a standard deviation of the HA titration method of  $\pm 0.081 \log_{10}$  (HAU/100  $\mu$ L), this can also be regarded as a significant difference.

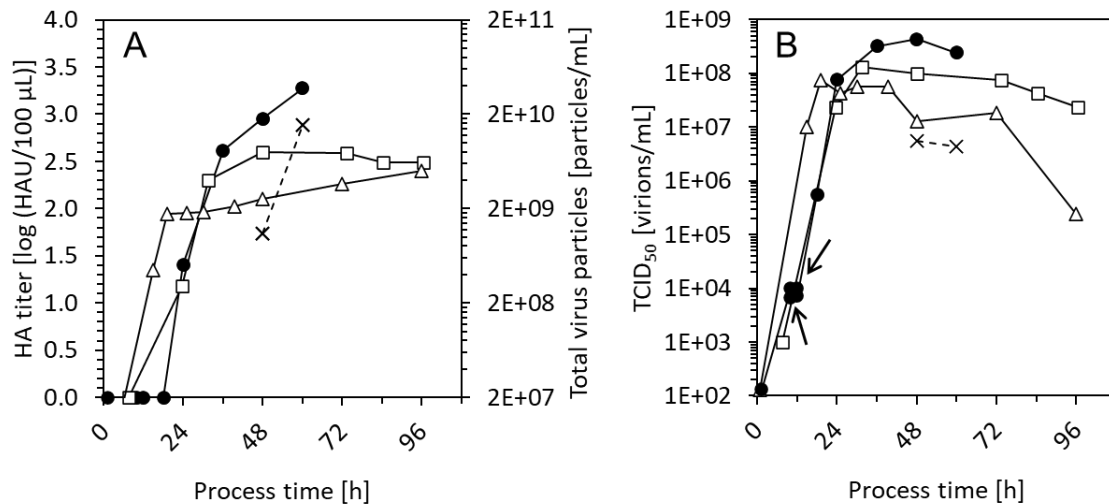


Figure 4.23. Comparison of the propagation of IAV in HCD and CCD cultures of CR.pIX cells. One run at HCD perfusion (HBI1), one run applying the hybrid FB/perfusion strategy (HBI2) and one run at conventional cell density (CBI1) are presented. HBI1 (squares), HBI2 (bioreactor supernatant: filled circles, permeate: crosses), and CBI1 (triangles). A: HA titers and total virus titers. B: TCID<sub>50</sub> titers. Arrows: time points of CD-U3 medium addition. Total IAV particles (TIP) were calculated with equation 6 (see Chapter 3.5.4). Figure adapted with permission from Vazquez-Ramirez et al. (2019) [219].

As expected, a difference in the virus propagation dynamics was observed for HCD (HBI1 and HBI2) and CCD (CBI1) cultures. This was clearly reflected in the difference of time points of their maximum virus titers and could have been caused by the difference in the cell concentrations at TOI and in the operation conditions, more specifically the medium feeding strategies applied in the HCD cultures.

The delay in the onset of the virus titer increase and the obvious dilution of the final product due to the medium feeding didn't influence negatively the productivity of the HBI2 reactor, with respect to the reference CBI1 and the HBI1 cultivations (Table 4.11). The  $P_{IAV}$  of  $5.43 \times 10^{11}$  particles/(L×d) (obtained from the maximum HA titer) for the HBI2 reactor was comparable to the one observed for CBI1 ( $6.53 \times 10^{11}$  particles/(L×d)) and higher than the one observed for the HBI1 cultivation ( $1.81 \times 10^{11}$  particles/(L×d)) (Table 4.11). This suggested an optimal medium utilization during influenza propagation at HCD very likely due to the application of the HFP feeding strategy during virus propagation. Similarly, with a  $CSVY_{IAV} = 1300$  particles/cell (obtained from the maximum HA titer) very comparable to the CBI1 (Table 4.11), no cell density effect was detected for the HBI2 cultivation. In summary, from both productivity parameters, the HCD production of influenza with the HFP strategy was comparable to the CCD process, demonstrating the suitability of the HFP feeding strategy for the optimal propagation of IAV at HCD. This result opens the potential to apply this strategy for the production of viruses, other than the MVA virus with different infection dynamics. Similar to MVA-CR19 virus production, only a low amount of product was collected in the permeate line and, therefore, was neglected for the calculations of  $CSVY_{IAV}$  and  $P_{IAV}$ .

Table 4.11. Overview of parameters and production yields of IAV in HCD cultivations of CR.pIX cells in bioreactors. Adapted with permission from Vazquez-Ramirez et al. (2019) [219].

Experiment ID <sup>a</sup>	Cultivation system	Hollow fiber module	Harvest volume [mL]	Harvest titer [particles/mL]	t <sub>T</sub> [d] <sup>b</sup>	Max. cells [10 <sup>9</sup> ]	CSVY <sub>IAV</sub> [particles/cell] <sup>c</sup>	P <sub>IAV</sub> [particles/(L×d)] <sup>d</sup>
HB11 (Perfusion)	STR	500 kDa	800	8.05 × 10 <sup>9</sup>	9.6	19.0	340	1.81 × 10 <sup>11</sup>
HB12 (HFP)	STR	0.65 μm	810	3.80 × 10 <sup>10</sup>	9.5	23.7	1300	5.43 × 10 <sup>11</sup>
CB11 (Batch)	STR	NA	800	5.23 × 10 <sup>9</sup>	8.0	3.1	1344	6.53 × 10 <sup>11</sup>

<sup>a</sup> H: high cell density, C: conventional cell density, B: bioreactor, I: IAV

<sup>b</sup> Total time from cell inoculation to maximum virus titer

<sup>c</sup> Cell-specific virus yield (for calculation refer to Chapter 3.5.5 Virus productivity estimations)

<sup>d</sup> Volumetric productivity (for calculation refer to Chapter 3.5.5 Virus productivity estimations)

## 4.6 Implementation of on-line tools for perfusion process control and virus production monitoring at high cell density

### 4.6.1 On-line pH-based perfusion control

As described in Chapter 4.5.2, an option for pH-based perfusion control was evaluated for the cell growth phase of the HB12 run. Therefore, it was assumed that glucose consumption rate of cells is more or less constant over cultivation time and the resulting lactate release leads to medium acidification [219]. Assuming that the produced CO<sub>2</sub> would be buffered by the sodium bicarbonate contained in the medium, perfusion could be started when pH is below a certain set-point. Therefore, after inoculation, pH control was turned off and pH was allowed to decrease to the optimal cultivation pH of 7.2. Once the set-point was reached (110 h before infection), pH control was started using a 0.1 M NaOH solution. From 85.5 h to 60 h before infection, pH-based perfusion control was started using the CD-U3 medium (basal pH of 7.7 ± 0.1) and a pH set-point of 7.2. As observed in Figure 4.24 A, the pH was controlled properly at a value of 7.2, applying a CSPR close to the expected 0.06 nL/(cell×d). However, after observing a glucose decrease from 15.9 to 11.1 mM, the control set-point was increased to a pH of 7.35. This led to an increase of the average CSPR to 0.15 nL/(cell×d) and an increase in glucose concentration from 11.1 to 16.2 mM. Consequently, the pH set-point was re-adjusted to 7.3, leading to a stabilization of the glucose concentration between 14.2 and 16.2 mM with an average CSPR of 0.2 nL/(cell×d). At this point, the target concentration of 25 × 10<sup>6</sup> cells/ml was reached and cell growth phase was ended.

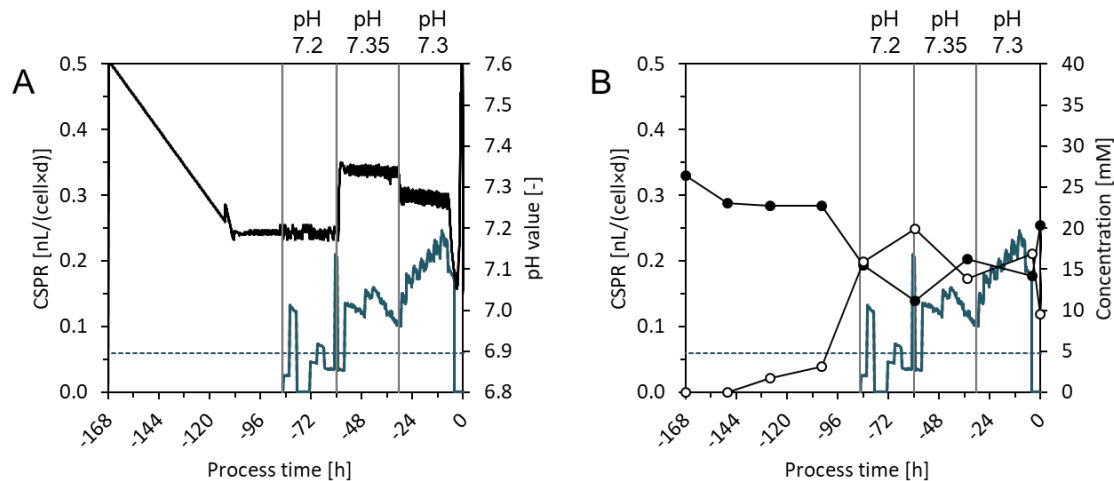


Figure 4.24. pH-based perfusion control during expansion of CR.pIX cells in cultivation HBI2 using CD-U3 medium. A: cell-specific perfusion rates (CSPR, green line) for different pH set-points (black line) of 7.2, 7.35 and 7.3. B: glucose (filled circles) and lactate (empty circles) concentrations at different CSPR values resulting from the three pH set-points of 7.2, 7.35 and 7.3. Dotted line: expected CSPR of 0.06 nL/(cell×d).

The pH-based perfusion control applied in the HBI2 run “led to a  $\mu_{\max} = 0.025$  1/h and an overall  $\mu_{\text{mean}} = 0.019$  1/h, which was in accordance with previous HCD bioreactor cultivations” [219] (Table 4.12, HBI2). Neither “glucose limitation nor a significant lactate accumulation were observed” [219] (Figure 4.24 B) compared to the cell concentration-based perfusion strategies (see Figure 4.9, Figure 4.17, Figure 4.19 and Figure 4.21). The high average CSPR of 0.119 nL/(cell×d) (Table 4.12, Figure 4.24 A) obtained in the cell growth phase led to an increase in medium consumption (16.7  $V_R$ ) compared to the reference HBI1 process (3.9  $V_R$ ).

Table 4.12. Summary of process parameters and performance during the propagation of CR.pIX cells used for the propagation of influenza A virus (IAV) in a bioreactor. Adapted with permission from Vazquez-Ramirez et al. (2019) [219].

Experiment ID <sup>a</sup>	Working volume [mL]	Hollow fiber module	Seed cell concentration [ $10^6$ cells/mL]	$\mu_{\text{mean}}$ [1/h]	$\mu_{\text{max}}$ [1/h]	Actual average CSPR [nL/(cell×d)]	Duration [h] <sup>b</sup>
HBI1 (Perfusion)	800	500 kDa	1.0	0.017 (n=18, SD=0.011)	0.055	0.072 (n=24, SD=0.010)	183
HBI2 (HFP)	600	0.65 $\mu\text{m}$	1.0	0.019 (n=7, SD=0.004)	0.025	0.119 (n=20, SD=0.061) <sup>c</sup>	168
CBI1 (Batch)	800	NA <sup>d</sup>	0.8	0.020 (n=6, SD=0.009)	0.033	NA	82

<sup>a</sup> H: high cell density, C: conventional cell density, B: bioreactor, I: IAV

<sup>b</sup> Time from cell inoculation to infection

<sup>c</sup> No constant CSPR was targeted and varied strongly depending on the pH-based perfusion control

<sup>d</sup> Since the cultivation was performed in batch mode, and ATF perfusion system was not needed

n: number of data points considered for the average calculations

Despite the high medium consumption rates, this perfusion control enabled to maintain glucose concentrations above 10 mM (Figure 4.24 B) and allowed for cell viabilities above 92% (Figure 4.22

B). “Different to the HIPCOP strategy proposed by Hiller et al. (2017) [41], which operates at glucose limitation and a lactate consumption regime for CHO cell cultivations, this strategy allowed for a perfusion control without reaching low glucose concentrations that might negatively affect the growth of CR.pIX cells. Additionally, since the perfusion rates depend on the pH control of the cultivation, reducing the pH set point could further minimize medium use” [219].

The on-line pH-based method for perfusion control here presented, was likewise described by Nikolay et al. (2020) [264], using data set supplied by the present author.

#### 4.6.2 On-line capacitance-based monitoring of cell concentration

The on-line biomass sensor used for HBM2 cultivation enabled a very good estimation of the VCV compared to off-line ViCell-based measurements. The method was not only applicable to the cell growth phase but also the MVA-CR19 virus and IAV propagation phase up to late stages of infection [219] (Figure 4.25 A). “This demonstrated the robustness of on-line capacitance measurements for VCVs corresponding to cell concentrations up to  $40 \times 10^6$  cells/mL, and expanded measurement to stages where virus-induced cell damage and apoptosis is widely spread among the infected cell population” [219].

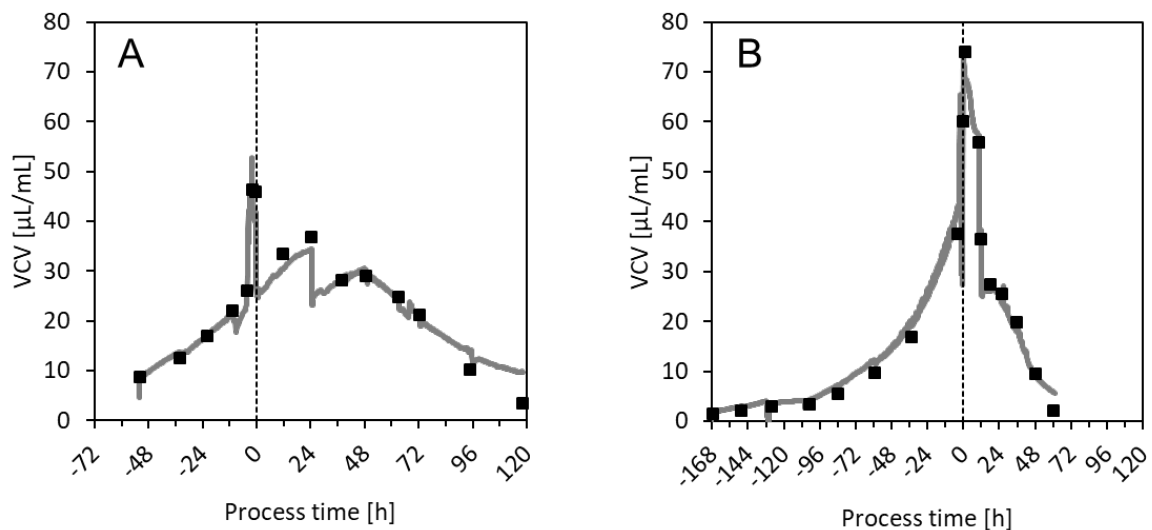


Figure 4.25. On-line monitoring of total viable cell volume per culture volume (VCV) with a capacitance probe for HBM2 (A) and HBI2 (B). On-line permittivity values were used to estimate the VCV ( $\mu\text{L/mL}$ ) (gray line) as described in Chapter 3.5. Off-line VCV values were determined from the viable cell numbers and cell diameter classes as described before (Chapter 3.5). Time of infection: 0 h (vertical dashed line). Figure adapted with permission from Vazquez-Ramirez et al. (2019) [219].

Similar to the HBM2 run for MVA-CR19 virus production, the implemented on-line biomass sensor data fitted the reference off-line VCV measurements up to late stages of the IAV propagation in the HBI2 run (Figure 4.25 B). Although the same correlation factor ( $VCV/\varepsilon = 1.2$ ) seemed to be suitable for on-line monitoring of both HBM2 and HBI2 runs, batch-to-batch variations might be expected and adjustments of this value might be needed when a larger number of experiments are carried out. Moreover, variations in the correlation factor could be anticipated when using different cells lines, media and cultivation systems. In case that this on-line tool is implemented for the automated control of the perfusion rate (e.g. via a fixed a CSPR value), an accurate  $VCV/\varepsilon$  factor becomes more critical and adjustments during the perfusion will likely have to be performed. Indeed, this last aspect was observed recently for the production of Zika virus in HCD cultures fully operated in perfusion mode, where the perfusion was controlled using the permittivity readouts to assure a constant CSPR [240]. Similarly, for the specific case of the HFP strategy, the acceptable on-line VCV determination observed for HBM2 and HBI2 (during the cell growth and the virus propagation phase) can be used for a control of the CSPR during the cell expansion in perfusion and the cell concentration-specific medium addition for the FB regime during the propagation phase of MVA-CR19 virus and IAV.

#### 4.6.3 On-line monitoring of cellular dielectric properties during virus propagation

As described before, the dielectric properties of the cells can change when intracellular metabolite concentration or the cell's membrane composition are altered [258-260], as occurs when permissive cells are infected and the virus propagation takes place [266]. In this regard, a reproducible progression of the characteristic frequency ( $f_c$ ) was observed during the propagation phase of both MVA-CR19 virus (Figure 4.26 A) and IAV (Figure 4.26 B and C). In both cases  $f_c$  showed oscillations during virus propagation before increasing strongly when accumulation of infectious viruses particles stopped and cell viability decreased drastically (Figure 4.26 A to C). For MVA-CR19 this effect was observed between 0 and 72 hpi at HCD (Figure 4.26 A), whereas for IAV it occurred between 0 and 36 hpi at HCD (Figure 4.26 B) and between 0 and 28 hpi at conventional cell density (Figure 4.26 C). This oscillatory pattern was not observed for a reference mock-infected cultivation (Figure 4.26 D) and only a moderate increase of  $f_c$  happened from 60 hpi, as result of cell death due to medium depletion.

For all three infected cultivations (HBM1, HBI2 and CBI0), each  $f_c$  characteristic cycle observed may fit with periodic intracellular and cells' membrane changes occurring due to virus propagation. More specifically, allocation of viral proteins at the membrane of infected cells may first slowly produce an increase in the  $f_c$  needed to polarize the cells. Then  $f_c$  decreases to its initial basal value when viral particles are released to the medium and infected cells either recover their membrane composition

(although not integrity) or get fragmented by the viral burst. This correlation may repeat regularly until massive cell death/apoptosis occurs. At this point cells' dielectric properties are altered at such a level that the system requires every time a higher  $f_c$  to polarize remaining “viable” cells. These results are in accordance to previous studies where characteristic phases of virus propagation were found to correlate strongly with consistent variations in the  $f_c$  [265] (non-envelope viruses), the intracellular conductivity ( $\sigma_i$ ) and the membrane capacitance ( $C_m$ ) [266] (enveloped viruses).

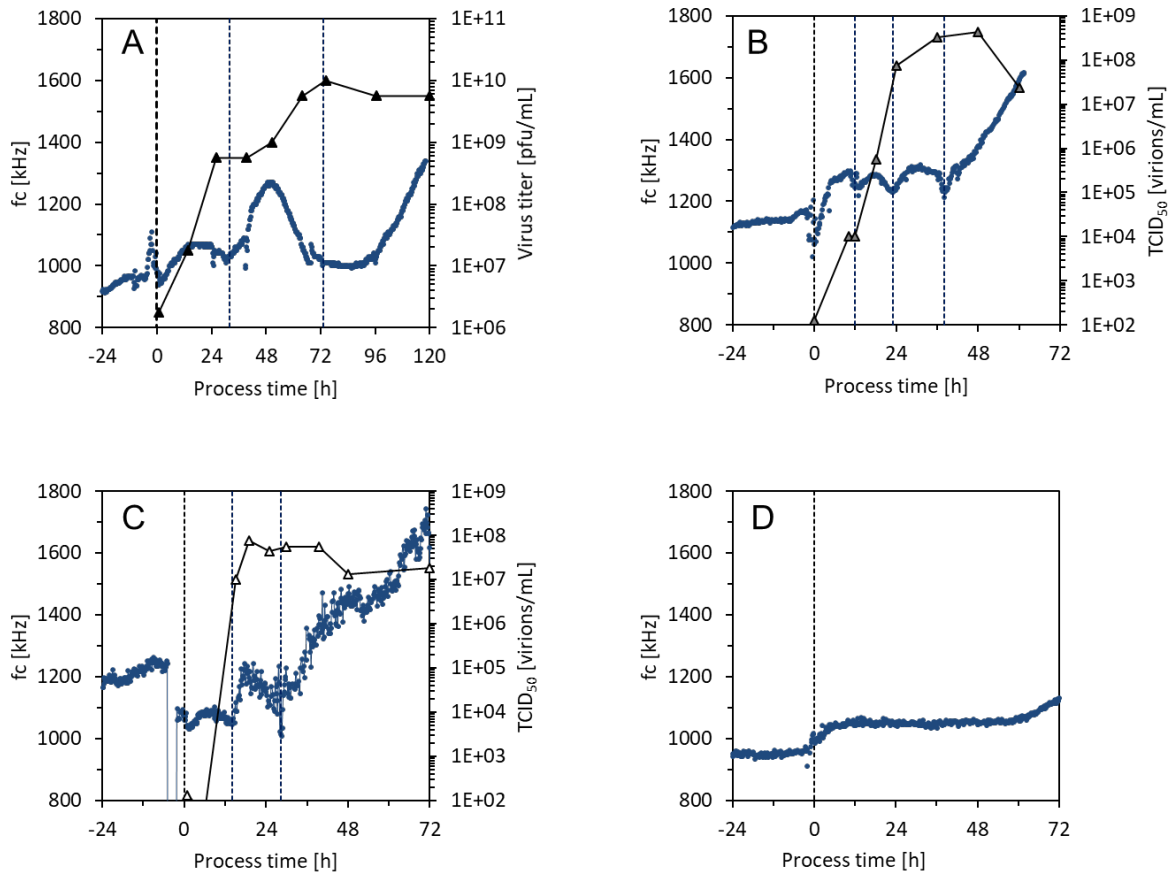


Figure 4.26. Progress of the characteristic frequency ( $f_c$ ) in CR.pIX cells cultivations during MVA-CR19 and IAV propagation. A: HBM1, B: HBI2, C: CBI0 and D: CBI0-Mock. Infectious virus concentration (triangles), characteristic frequency  $f_c$  (blue). Time of infection: 0 h (vertical dashed line).

Due to the complexity of virus propagation dynamics, additional analysis, such as imaging flow cytometry, may contribute to confirm the correlation between  $f_c$  (and other cell dielectric properties) with the virus propagation cycles. Additionally, experiments to analyze the impact of different MOI values on the variability of the  $f_c$  profiles could provide supportive information to demonstrate the consistency of these observations.



---

## 5 Conclusions

### 5.1 Cultivation of CR.pIX cells at high cell density in perfusion

Although CD-U3 medium was originally not developed for perfusion processes [27], it proved to support HCD cultivations in semi- and full perfusion mode with consistent cell growth rates and minimal medium consumption. For example, “a first HCD cultivation using CR.pIX cells in a bioreactor using an ATF-based perfusion system resulted in similar specific cell growth rates to those previously reported for the same cell line in CCD [29], and the parental cell line CR [42]” [200]. A target CSPR of 0.062 nL/(cell×d), which was defined based on the specific cell growth rate and glucose consumption rate, properly supported HCD cultivations. Applying this strategy, cell proliferation up to  $50 \times 10^6$  cells/mL with an average specific growth rate of 0.019 1/h and minimum medium consumption were achieved. Further cultivations in shake flasks applying a semi-perfusion mode with a fixed CSPR of 0.060 nL/(cell×d) allowed for cell densities up to  $83 \times 10^6$  cells/mL. According to the theoretical  $k_L a$  of the shake flasks, cell concentrations exceeding  $100 \times 10^6$  cells/mL seem feasible in these cultivation system. Under these conditions, CR.pIX cells achieved specific growth rates of 0.023 1/h ( $t_2 = 30$  h).

This CSPR-based perfusion strategy allowed for a moderate medium consumption in bioreactor ( $6.15 V_R$  for HBM3 and  $1.98 V_R$  for HBM4) when cultivating CR.pIX cells at around  $50 \times 10^6$  cells/mL. Despite the low medium utilization, the average specific cell growth rates for both HBM3 and HBM4 cultivations were comparable to the growth rate observed in shake flask cultivations (0.023 1/h). Under this sustained growth rate, it took only around 8 d to reach a minimum viable cell concentration of  $50 \times 10^6$  cells/mL. In comparison, “Petiot et al. (2011) [233] reported a medium utilization of around  $3.5 V_R$  to expand HEK293 cells within 9 d from 0.25 to  $15 \times 10^6$  cells/mL (before infection with IAV). Genzel et al. (2014) [42] reported a medium consumption of  $11.3 V_R$  to propagate CR cells to  $50 \times 10^6$  cells/mL before infection with IAV. Therefore, the results here represent a significant reduction in medium consumption before virus infection, which is an important contribution towards lower COG in large-scale production” [219].

## 5.2 Propagation of MVA-CR19 virus at high cell density

HCD experiments in small scale shake flasks “suggested that maximum virus yields depend on a high viability of cells at TOI, and could be increased if conditioned medium was replaced at TOI. A partial medium replacement may dilute inhibitory metabolites and replenish nutrients that have been depleted during the cell proliferation phase” [200]. Based on that, an optimal infection and virus propagation strategy may comprise “a complete medium exchange, followed by fed-batch intervals. Such a strategy is a good option especially for viruses with replication cycles that are longer than the time needed to deplete the available glucose given in the initial medium exchange. Once this first critical initial infection stage is overcome, a (semi-) continuous medium exchange could be applied to collect infectious virus material and to avoid the accumulation of toxic by-products” [200]. Here, the application of these options at HCD allowed for a 10-fold increase in MVA-CR19 virus titer, and comparable  $CSVY_{MVA}$  and  $P_{MVA}$ , with respect to the reference CCD cultivations [200]. Overall, the study in shake flasks helped to demonstrate that replication of MVA-CR19 is not inhibited by high cell concentrations, and that small-scale cultivations in shake flasks can be employed for maximizing yields of viruses produced in cell culture.

The adaptation of the small-scale strategy to bioreactors coupled to an ATF perfusion system (cultivations HBM3 and HBM4) suggested the establishment of a HFP strategy. As mentioned in a previous publication by Vazquez-Ramirez et al. (2019) [219], “this strategy resulted in a 10- to 100-fold increase in virus titers compared to the current standard production platform in CEF cells [33, 34]. With respect to cultivations performed at conventional cell densities using CR.pIX cells [26, 118, 274], EB14 cells [202], and EB66 cells [31], up to 10-fold higher titers were obtained”. The  $CSVY_{MVA}$  values obtained with the HFP strategy (410 and 352 pfu/cell) were also competitive, compared to the reported values for CEF cells (500 pfu/cell) [11], DF-1 cells (100–200 pfu/cell) [111], CR.pIX cells (50–200 pfu/cell) [26, 29] and EB66 cells (25–50 pfu/cell) [31], for non-intensified processes at lower cell densities [219]. Compared to adherent CEF and the DF-1 cells that are currently used in industry, CR.pIX cell cultivations operated in HCD (e.g. using the HFP strategy) represent a very promising alternative regarding scale-up and productivity. Namely, the production of large amounts of vaccines would require a smaller number of batches, produced in HCD suspension cultures in bioreactors with a considerably smaller footprint compared to the cultivation systems for adherent cells.

Compared to the current suspension cell-based processes for MVA virus production, the application of the HFP strategy at HCD looks also beneficial. As reported previously in Vazquez-Ramirez et al. (2019) [219], “batch production of MVA virus with CR.pIX cells [29, 118] and EB66 cells [31] requires more or less the same time and the same media volumes”. Accordingly, volumetric productivities of around  $2.0 \times 10^{10}$  pfu/(L×d) are obtained, whereas values around one log higher (1.3

---

and  $2.8 \times 10^{11}$  pfu/(L×d)) were obtained with the HFP strategy. In order to assess these differences, it is important to consider the large error ( $\pm 0.4$  log) in the infectivity assay used for the quantification of MVA-CR19 virus (Chapter 3.5.3) and the limited number of cultivations performed with the HFP strategy. In this regard, additional confirmation experiments should be performed and the improvement of the virus quantification method should be carried on to reduce the detection error. Based on the current results presented here, applying the HFP strategy “would allow for 100,000 doses per liter of cell-free supernatant, considering that single doses of  $1 \times 10^8$  pfu per individual are currently used in clinical studies involving recombinant MVA-based vaccines [22]” [219].

“Due to its application as a viral vector, maintaining the infectivity of MVA virus is a critical quality attribute. It is promising that titers were found to remain stable from 72 to 120 hpi (Figure 4.18 and Figure 4.20). This suggested a low virus inactivation rate for the specific cultivation conditions chosen. While continuous virus harvesting failed for the chosen ATF system, the use of other cell retention devices including acoustic filter and settlers might be evaluated again for large-scale production to avoid potential product entrapment within the ATF hollow fiber module” [219]. In this regard, a follow-up project to the present work has demonstrated the use of an acoustic filter and an inclined settler as an alternative to the ATF-based processes for the continuous MVA virus harvest in processes fully operated in perfusion mode [287]. Also, recently a commercial alternative, the Virus Harvest Unit (VHU<sup>®</sup>, Artemis Biosystems) was applied for continuous harvesting of lentivirus, overcoming the limitations of the available ATF hollow fiber modules.

“One major property of the MVA-CR19 virus, its capacity to propagate in single cell suspension cultures, may additionally help to facilitate the recovery of infectious particles directly from the culture supernatant without the need of cell disruption [32]” [219]. From both shake flask (Figure 4.13 C and D) and bioreactor cultivations (Figure 4.20) it was demonstrated that “the maximum titers at 72 hpi accounted entirely for virus in the supernatant with most of the cells showing a viability  $> 70\%$ . Hence, a clarification step at this point with a carefully chosen cell retention system would suffice to recover the MVA-CR19 virus from the bioreactor. Based on the very high performance of the HFP strategy during cultivation and the simplification of the clarification/harvest step, it is possible that high costs related to the implementation of „complex“ perfusion processes (purchase of dedicated equipment and training of staff) can be more than compensated even at industrial scale” [219].

### 5.3 Propagation of influenza A virus at high cell density

The HFP strategy showed also a big potential for maintaining a high  $CSVY_{IAV}$  and  $P_{IAV}$  at HCD cultures. Regarding the  $CSVY_{IAV}$ , the 1300 particles/cell were within the ranges observed here and in other publications at CCD for the same CR.pIX cells [26]. This also applies to HCD processes (in perfusion mode) for the parental suspension cell line AGE1.CR [42]. Although the  $P_{IAV}$  using the HFP strategy (HBI2) was very comparable to that obtained in full perfusion (HBI1) and in the reference CCD culture (CBI1), i.e. in the order of  $10^{11}$  particles/(L×d) (Table 4.11), a reduction of the medium utilization can be reached when applying a low CSPR perfusion process for cell expansion. This can be achieved, on the one side, by applying accurate on-line tools for VCV or cell concentration measurements such as the capacitance probe or, on the other side, through medium optimization. In any of both cases, the complexity of processes and COG should be closely evaluated and efforts to minimize both aspects should be considered.

With regard to the full perfusion run HBI1,  $CSVY_{IAV}$  seemed lower compared to the HBI2 and the CBI1 runs. This might be a result of the different feeding strategies applied. However, based on the low number of experimental runs and the large error of infectivity assays used for virus quantification, the collection of additional data on both HFP and HCD perfusion cultivations will help to confirm this observations. Additionally, aspects such as the actual virus harvest through the cell retention system (possibly in a discontinuous way as suggested by Tapia et al. (2014) [235]) and/or the use of alternative cultivation systems should be explored. In that sense, the VHU<sup>®</sup> perfusion system might be a suitable option, since it's application has been demonstrated for the continuous harvest of lentivirus, a virus with a similar size to IAV. Moreover, recent follow-up projects to the present work have also suggested that both the bioreactor type (i.e. STR or orbital shaken bioreactor) [236] and the perfusion system (i.e. ATF or acoustic settler) [288] can influence the IAV productivity in HCD cultivations of CR.pIX cells fully operated in perfusion mode. In a similar way, it seems worth to explore alternative bioreactor types (e.g. shaken bioreactor) and perfusion systems (e.g. inclined settlers, acoustic settlers) that could potentiate the capacity of the HFP strategy to maintain high production yields, based on the results here presented using a STR and an ATF perfusion system.

---

## 5.4 Using on-line tools for perfusion process control and virus production monitoring at high cell density

Applying a pH-based perfusion control during the cell growth phase (Chapter 4.6.1), a similar specific cell growth rate was achieved compared to the earlier proposed CSPR-based strategy. Maximum specific cell growth rate of  $\mu_{\max} = 0.025$  1/h and an average  $\mu_{\text{mean}} = 0.019$  were obtained, which agreed with the values obtained using the CSPR-based strategy. Additionally, glucose limitation and significant lactate accumulation were avoided. With this strategy, however, medium was used at an average CSPR of 0.119 nL/(cell×d) (Table 4.12, Figure 4.24), which led to a significant “increase in medium consumption (16.7  $V_R$ ) compared to the reference perfusion process (3.9  $V_R$ )” [219]. Since the perfusion rates depended on the pH control of the cultivation, the pH set point could be reduced to a minimum value where the cultivation system can still control the perfusion rate without nutrient limitations. This will further allow for a minimization of the medium feeding rates.

Additional process monitoring was possible using dielectric spectroscopy. Specially, on-line VCV estimations correlated well with off-line measurements up to late stages of MVA-CR19 and IAV propagation phase. This opens the possibility to apply accurate feeding strategies not only during the cell growth phase (perfusion) but also during the virus propagation phase. This way, the cultivation strategy (feeding profiles, perfusion profile, supplement addition) during virus propagation phase can be defined based on the VCV and the infection dynamics of each virus type.

Important information can also be obtained from other dielectric properties, such as the characteristic frequency ( $f_c$ ). This parameter may help to define a characteristic fingerprint of the propagation dynamics of each virus, assuming that the observed oscillation frequencies are defined by the progress of infection of each virus type. A potential application of this on-line monitoring can be anticipated for fully continuous virus production, where any variation in the steady state of the system can generate disturbances in the  $f_c$  fingerprint of the process. This can ultimately be used for corrective measurements to keep the process in the control limits without the need to perform intensive off-line analytics (e.g. direct virus titration).

## 5.5 Final remarks

Process intensification using HCD cultures can contribute to the supply of large amounts of viral vaccines. HCD cultures could be implemented on existing facilities for conventional batch production, to increase manufacturing capacities and support vaccine supply, e.g. in emerging and developing countries where vaccines are most urgently needed. A promising solution to reach competitive production yields at HCD is the application of the HFP strategy, which was described here for the production of MVA-CR19 virus and IAV in small STRs. The application of the HFP strategy resulted in a “7- to 20-fold increase in virus titers without compromising cell-specific yields and volumetric productivities that often hinder the establishment of intensified processes” [219]. The potential of this approach was demonstrated with the titers of  $10^{10}$  pfu/mL obtained for MVA-CR19 virus and could be an alternative to the current technology that relies on cultivation of primary CEF and the DF-1 adherent cells as substrates for MVA virus production.

Although the HCD options presented here rely on the use of an ATF perfusion system for cell expansion and/or virus propagation, their process principles can also be explored using less complex and low-cost perfusion systems, such as cell settlers. In addition, the constant operational intervention that perfusion and vaccine production processes normally require can be minimized applying the PAT tools presented here. In summary, the present work, using two different viruses (MVA-CR19 and IAV), may be instructive for modernization of current conventional approaches in viral vaccine production.

---

## List of figures

Figure 2.1. Schematic structure of influenza A virus (IAV). .....	15
Figure 2.2. Replication cycle of influenza A virus (IAV). .....	17
Figure 2.3. Schematic structure of an infectious intracellular mature vaccinia virion (IMV). .....	21
Figure 2.4. Replication cycle of vaccinia virus (VACV). .....	23
Figure 2.5. Biphasic process for the production of MVA virus in suspension cultures of CR.pIX and EB66 cells. ....	26
Figure 2.6. Schematic representation of a perfusion process. ....	29
Figure 2.7. Schematic representation of the perfusion-based HCD production of recombinant proteins and viruses. ....	32
Figure 2.8. Schematic illustration of the $\beta$ -dispersion spectrum of the observed permittivity. ....	41
Figure 3.1. Schematic process diagram (A) and example photograph (B) of the ATF-based perfusion bioreactor layout for the cultivation of CR.pIX cells at HCD. ....	48
Figure 4.1. Dissolved oxygen concentration (DO) in a 0.8 L Biostat <sup>®</sup> B Plus bioreactor at different oxygen flow rates. ....	58
Figure 4.2. Pure oxygen flow rates along the cultivation of CR cells (DPM3 run). ....	60
Figure 4.3. Oxygen supply rate per cell and hour at different concentrations of CR cells (DPM3 run). ....	61
Figure 4.4. CR.pIX cell kinetics applying a CSPR-based manual perfusion control in a 0.8 L bioreactor. ....	64
Figure 4.5. Medium spent applying a CSPR-based manual perfusion control in a 0.8 L bioreactor. ...	64
Figure 4.6. Cultivation of CR.pIX cells to high cell densities applying semi-perfusion in 250 mL shake flasks (110 mL $V_w$ ). ....	66

## List of figures

---

Figure 4.7. MVA-CR19 virus propagation in CR.pIX cells infected at CCD ( $2.0 \times 10^6$ cells/mL) in shake flasks .....	67
Figure 4.8. Cell growth kinetics, glucose/lactate concentration and osmolality in a HCD perfusion culture of CR.pIX cells (HBM1), before and after infection with MVA-CR19 virus.....	69
Figure 4.9. Cell growth kinetics, glucose/lactate concentration and osmolality in a HCD perfusion culture of CR.pIX cells (HBM2), before and after infection with MVA-CR19 virus.....	70
Figure 4.10. Comparison of the propagation of MVA-CR19 virus in HCD perfusion and CCD cultures of CR.pIX cells. ....	72
Figure 4.11. Growth kinetics of CR.pIX cells before and after infection with MVA-CR19 virus at HCD, applying a fed-batch (FB10) and a medium exchange (ME50) strategy after infection.....	74
Figure 4.12. Osmolality profile observed during the propagation of the MVA-CR19 seed viruses MC19a and MC19b when applying a FB10 and a ME50 feeding strategy.....	74
Figure 4.13. MVA-CR19 virus propagation and glucose/lactate concentrations in HCD cultures of CR.pIX cells applying a fed-batch (FB10) and a medium exchange (ME50) strategy. ....	75
Figure 4.14. Schematic representation of further feeding strategies to improve MVA-CR19 virus propagation in CR.pIX cells infected at HCD in shake flasks. ....	78
Figure 4.15. Cell growth kinetics, glucose/lactate concentration and MVA-CR19 virus propagation in HCD cultures of CR.pIX cells applying a fed-batch (FB), a daily medium exchange (DME) and a combined fed-batch/daily medium exchange (F+D) strategy. ....	80
Figure 4.16. Time series of the MVA-CR19 virus production yields obtained with a fed-batch (FB), a daily medium exchange (DME) and a combined fed-batch/daily medium exchange (F+D) strategy in HCD cultivations of CR.pIX cells.....	81
Figure 4.17. Feeding profile, cell growth kinetics and glucose/lactate concentration in a HCD culture of CR.pIX cells (HBM3), applying a hybrid FB/perfusion (HFP) strategy after infection with MVA-CR19 virus.....	83
Figure 4.18. MVA-CR19 virus propagation at HCD in the HBM3 bioreactor, applying a hybrid FB/perfusion (HFP) strategy.....	84
Figure 4.19. Feeding profile, cell growth kinetics and glucose/lactate concentration in a HCD culture of CR.pIX cells (HBM4), applying a hybrid FB/perfusion (HFP) strategy after infection with MVA-	



---

CR19 virus. A: cell-specific perfusion rate, CSPR, (empty diamonds) and working volume, $V_w$ , (continuous line). .....	85
Figure 4.20. MVA-CR19 virus propagation at HCD in the HBM4 bioreactor, applying a hybrid FB/perfusion (HFP) strategy.....	87
Figure 4.21. Feeding profile, cell growth kinetics and glucose/lactate concentration in a HCD perfusion culture of CR.pIX cells (HBI1), before and after infection with IAV.....	90
Figure 4.22. Feeding profile, cell growth kinetics and glucose/lactate concentration in a HCD culture of CR.pIX cells (HBI2), applying a hybrid FB/perfusion (HFP) strategy after infection with IAV.....	92
Figure 4.23. Comparison of the propagation of IAV in HCD and CCD cultures of CR.pIX cells. ....	93
Figure 4.24. pH-based perfusion control during expansion of CR.pIX cells in cultivation HBI2 using CD-U3 medium. ....	95
Figure 4.25. On-line monitoring of total viable cell volume per culture volume (VCV) with a capacitance probe for HBM2 (A) and HBI2 (B). ....	96
Figure 4.26. Progress of the characteristic frequency ( $f_c$ ) in CR.pIX cells cultivations during MVA-CR19 and IAV propagation. ....	98

## List of tables

Table 2.1. History of vaccine development. ....	5
Table 2.2. Summary of main types of vaccines licensed for use in humans. ....	7
Table 2.3. Commercially available influenza vaccines produced in cell culture. ....	19
Table 2.4. Overview on viruses produced in HCD cultures reported in literature. ....	33
Table 3.1 Parameters for the measurement of the bioreactor $k_{La}$ for the cultivation of CR.pIX cells. ....	45
Table 3.2. Summary of characteristics and operational properties of the hollow fibers used for all ATF experiments.....	47
Table 3.3. Dilution steps for the measurement of cell concentration using the cell counter Vi-CELL™ XR.....	51
Table 3.4. Standard deviations derived from the method validation for the measurement of metabolite concentrations using the BioProfile 100 Plus Nova analyzer.....	52
Table 4.1. $k_{La}$ values at different oxygen flow rates for a Biostat® B Plus benchtop bioreactor at 0.8 L working volume and under operation conditions defined in Table 3.1. ....	59
Table 4.2. Summary of $k_{La}$ values for BIOSTAT® bioreactors with different nominal volumes and settings.....	59
Table 4.3. Empirical parameters for the estimation of $k_{La}$ in 125 mL and 250 mL baffled disposable shake flasks at 37 °C and a filling level of 40%.....	65
Table 4.4 Overview of different cultivation runs for MVA production in CR.pIX suspension cells at conventional cell densities (CCD). ....	68
Table 4.5. Summary of process parameters and performance of HBM1 and HBM2 runs during the CR.pIX cell expansion in a perfusion in bioreactor. ....	71
Table 4.6. Overview of MVA-CR19 virus production yields obtained in HCD perfusion cultivations of CR.pIX cells in bioreactor (HBM1 and HBM2). ....	73

---

Table 4.7. Overview of MVA-CR19 virus production yields obtained with a fed-batch (FB10) and a medium exchange (ME50) strategy in HCD cultivations of CR.pIX cells in shake flasks.....	76
Table 4.8. Overview of MVA-CR19 virus production yields obtained with a fed-batch (FB), a daily medium exchange (DME) and a combined fed-batch/daily medium exchange (F+D) strategy in HCD cultivations of CR.pIX cells in shake flasks.....	82
Table 4.9. Summary of process parameters and performance of HBM3 and HBM4 runs during the CR.pIX cell expansion in a perfusion in bioreactor. ....	86
Table 4.10. Overview on production yields of MVA-CR19 virus in HCD cultivations of CR.pIX cells in a bioreactor, using a hybrid FB/perfusion (HFP) strategy.....	88
Table 4.11. Overview of parameters and production yields of IAV in HCD cultivations of CR.pIX cells in bioreactors.....	94
Table 4.12. Summary of process parameters and performance during the propagation of CR.pIX cells used for the propagation of influenza.....	95

## References

- [1] Plotkin SL, Plotkin SA. A short history of vaccination. In: Plotkin SA, editor. *Vaccines*. 6th ed. St. Louis, Missouri: Elsevier Saunders; 2013.
- [2] Ozawa S, Clark S, Portnoy A, Grewal S, Stack ML, Sinha A, et al. Estimated economic impact of vaccinations in 73 low- and middle-income countries, 2001-2020. *Bull World Health Organ*. 2017;95:629-38.
- [3] Milian E, Kamen AA. Current and emerging cell culture manufacturing technologies for influenza vaccines. *Biomed Res Int*. 2015;2015:1-11.
- [4] Stohr K, Bucher D, Colgate T, Wood J. Influenza virus surveillance, vaccine strain selection, and manufacture. *Methods Mol Biol*. 2012;865:147-62.
- [5] Wong SS, Webby RJ. Traditional and new influenza vaccines. *Clin Microbiol Rev*. 2013;26:476-92.
- [6] Dormitzer PR, Tsai TF, Del Giudice G. New technologies for influenza vaccines. *Hum Vaccin Immunother*. 2012;8:45-58.
- [7] Hilleringmann M, Jobst B, Baudner BC. Influenza Cell-Culture Vaccine Production. *Molecular Vaccines 2014*; 823-37.
- [8] Hardy CT, Young SA, Webster RG, Naeve CW, Owens RJ. Egg fluids and cells of the chorioallantoic membrane of embryonated chicken eggs can select different variants of influenza A (H3N2) viruses. *Virology*. 1995;211:302-6.
- [9] Robertson JS, Bootman JS, Newman R, Oxford JS, Daniels RS, Webster RG, et al. Structural changes in the haemagglutinin which accompany egg adaptation of an influenza A(H1N1) virus. *Virology*. 1987;160:31-7.
- [10] Reisinger KS, Block SL, Izu A, Groth N, Holmes SJ. Subunit influenza vaccines produced from cell culture or in embryonated chicken eggs: comparison of safety, reactogenicity, and immunogenicity. *J Infect Dis*. 2009;200:849-57.
- [11] Carroll MW, Moss B. Host range and cytopathogenicity of the highly attenuated MVA strain of vaccinia virus: propagation and generation of recombinant viruses in a nonhuman mammalian cell line. *Virology*. 1997;238:198-211.

- 
- [12] Drexler I, Heller K, Wahren B, Erfle V, Sutter G. Highly attenuated modified vaccinia virus Ankara replicates in baby hamster kidney cells, a potential host for virus propagation, but not in various human transformed and primary cells. *J Gen Virol*. 1998;79:347-52.
- [13] Sutter G, Moss B. Nonreplicating vaccinia vector efficiently expresses recombinant genes. *Proc Natl Acad Sci U S A*. 1992;89:10847-51.
- [14] von Krempelhuber A, Vollmar J, Pokorny R, Rapp P, Wulff N, Petzold B, et al. A randomized, double-blind, dose-finding Phase II study to evaluate immunogenicity and safety of the third generation smallpox vaccine candidate IMVAMUNE. *Vaccine*. 2010;28:1209-16.
- [15] Gilbert SC. Clinical development of Modified Vaccinia virus Ankara vaccines. *Vaccine*. 2013;31:4241-6.
- [16] Iyer SS, Amara RR. DNA/MVA Vaccines for HIV/AIDS. *Vaccines (Basel)*. 2014;2:160-78.
- [17] Haagmans BL, van den Brand JM, Raj VS, Volz A, Wohlsein P, Smits SL, et al. An orthopoxvirus-based vaccine reduces virus excretion after MERS-CoV infection in dromedary camels. *Science*. 2016;351:77-81.
- [18] Brault AC, Domi A, McDonald EM, Talmi-Frank D, McCurley N, Basu R, et al. A Zika Vaccine Targeting NS1 Protein Protects Immunocompetent Adult Mice in a Lethal Challenge Model. *Sci Rep*. 2017;7:1-11.
- [19] Domi A, Feldmann F, Basu R, McCurley N, Shifflett K, Emanuel J, et al. A Single Dose of Modified Vaccinia Ankara expressing Ebola Virus Like Particles Protects Nonhuman Primates from Lethal Ebola Virus Challenge. *Sci Rep*. 2018;8:1-9.
- [20] Bisht H, Roberts A, Vogel L, Bukreyev A, Collins PL, Murphy BR, et al. Severe acute respiratory syndrome coronavirus spike protein expressed by attenuated vaccinia virus protectively immunizes mice. *Proc Natl Acad Sci U S A*. 2004;101:6641-6.
- [21] Hess RD, Weber F, Watson K, Schmitt S. Regulatory, biosafety and safety challenges for novel cells as substrates for human vaccines. *Vaccine*. 2012;30:2715-27.
- [22] Gomez CE, Perdiguero B, Garcia-Arriaza J, Esteban M. Clinical applications of attenuated MVA poxvirus strain. *Expert Rev Vaccines*. 2013;12:1395-416.
- [23] Altenburg AF, Kreijtz JH, de Vries RD, Song F, Fux R, Rimmelzwaan GF, et al. Modified vaccinia virus ankara (MVA) as production platform for vaccines against influenza and other viral respiratory diseases. *Viruses*. 2014;6:2735-61.
- [24] Jordan I, Sandig V. Cell line for propagation of highly attenuated alphaviruses. In: Organization WIP, editor. C12N 7/00 (2006.01) ed2008.

## References

---

- [25] Jordan I, Lohr V, Genzel Y, Reichl U, Sandig V. Elements in the Development of a Production Process for Modified Vaccinia Virus Ankara. *Microorganisms*. 2013;1:100-21.
- [26] Lohr V, Rath A, Genzel Y, Jordan I, Sandig V, Reichl U. New avian suspension cell lines provide production of influenza virus and MVA in serum-free media: studies on growth, metabolism and virus propagation. *Vaccine*. 2009;27:4975-82.
- [27] Jordan I, Northoff S, Thiele M, Hartmann S, Horn D, Howing K, et al. A chemically defined production process for highly attenuated poxviruses. *Biologicals*. 2011;39:50-8.
- [28] Lohr V, Genzel Y, Jordan I, Katinger D, Mahr S, Sandig V, et al. Live attenuated influenza viruses produced in a suspension process with avian AGE1.CR.pIX cells. *Bmc Biotechnol*. 2012;12:79.
- [29] Lohr V. Characterization of the avian designer cells AGE1.CR and AGE1.CR.pIX considering growth, metabolism and production of influenza virus and Modified Vaccinia Virus Ankara (MVA). Magdeburg, Germany: Otto von Guericke University Magdeburg; 2014.
- [30] Harrison SC, Alberts B, Ehrenfeld E, Enquist L, Fineberg H, McKnight SL, et al. Discovery of antivirals against smallpox. *Proc Natl Acad Sci U S A*. 2004;101:11178-92.
- [31] Leon A, David AL, Madeline B, Guianvarc'h L, Dureau E, Champion-Arnaud P, et al. The EB66(R) cell line as a valuable cell substrate for MVA-based vaccines production. *Vaccine*. 2016;34:5878-85.
- [32] Jordan I, Horn D, John K, Sandig V. A genotype of modified vaccinia Ankara (MVA) that facilitates replication in suspension cultures in chemically defined medium. *Viruses*. 2013;5:321-39.
- [33] Meiser A, Boulanger D, Sutter G, Krijnse Locker J. Comparison of virus production in chicken embryo fibroblasts infected with the WR, IHD-J and MVA strains of vaccinia virus: IHD-J is most efficient in trans-Golgi network wrapping and extracellular enveloped virus release. *J Gen Virol*. 2003;84:1383-92.
- [34] Gilbert PA, Comanita L, Barrett J, Peters A, Szabat M, McFadden G, et al. Current Status for High Titre Poxvirus Stock Preparation in CEF Under Serum-Free Medium Conditions: Implication for Vaccine Development. *Cytotechnology*. 2005;48:79-88.
- [35] Chotteau V. Perfusion Processes. *Cell Eng*. 2015;9:407-43.
- [36] Pollock J, Ho SV, Farid SS. Fed-batch and perfusion culture processes: economic, environmental, and operational feasibility under uncertainty. *Biotechnology and bioengineering*. 2013;110:206-19.
- [37] Yang WC, Lu J, Kwiatkowski C, Yuan H, Kshirsagar R, Ryll T, et al. Perfusion seed cultures improve biopharmaceutical fed-batch production capacity and product quality. *Biotechnology progress*. 2014;30:616-25.

- 
- [38] Yang WC, Minkler DF, Kshirsagar R, Ryll T, Huang YM. Concentrated fed-batch cell culture increases manufacturing capacity without additional volumetric capacity. *J Biotechnol.* 2016;217:1-11.
- [39] Chon JH, Zarbis-Papastoitsis G. Advances in the production and downstream processing of antibodies. *N Biotechnol.* 2011;28:458-63.
- [40] Pohlscheidt M, Jacobs M, Wolf S, Thiele J, Jockwer A, Gabelsberger J, et al. Optimizing capacity utilization by large scale 3000 L perfusion in seed train bioreactors. *Biotechnology progress.* 2013;29:222-9.
- [41] Hiller GW, Ovalle AM, Gagnon MP, Curran ML, Wang W. Cell-controlled hybrid perfusion fed-batch CHO cell process provides significant productivity improvement over conventional fed-batch cultures. *Biotechnology and bioengineering.* 2017;114:1438-47.
- [42] Genzel Y, Vogel T, Buck J, Behrendt I, Ramirez DV, Schiedner G, et al. High cell density cultivations by alternating tangential flow (ATF) perfusion for influenza A virus production using suspension cells. *Vaccine.* 2014;32:2770-81.
- [43] Petiot E, Jacob D, Lanthier S, Lohr V, Ansorge S, Kamen AA. Metabolic and kinetic analyses of influenza production in perfusion HEK293 cell culture. *Bmc Biotechnol.* 2011;11:84.
- [44] Vogel T. *Influenza Impfstoffherstellung in Hohlfasermodulen.* Esslingen, Germany: HS Esslingen; 2012.
- [45] Clem AS. Fundamentals of vaccine immunology. *J Glob Infect Dis.* 2011;3:73-8.
- [46] Fitz RH. Zabdiel Boylston, inoculator and the epidemic of smallpox in Boston in 1721. *Bull Johns Hopkins Hosp.* 1911;22:315-27.
- [47] Pead P, Jesty B. *Dorset's Vaccination Pioneer.* Timefile Books Chichester, England. 2009.
- [48] Baxby D. Edward Jenner's inquiry after 200 years. *BMJ.* 1999;318:390.
- [49] Sherman IW. *The Power of Plagues.* ASM Press Washington, DC. 2006.
- [50] Langer WL. Immunization against smallpox before Jenner. *Sci Am.* 1976 234:112-7.
- [51] Plotkin SA. Vaccines: the fourth century. *Clin Vaccine Immunol.* 2009;16:1709-19.
- [52] Guy B, Briand O, Lang J, Saville M, Jackson N. Development of the Sanofi Pasteur tetravalent dengue vaccine: One more step forward. *Vaccine.* 2015;33:7100-11.
- [53] Ulmer JB, Valley U, Rappuoli R. Vaccine manufacturing: challenges and solutions. *Nature biotechnology.* 2006;24:1377-83.

## References

---

- [54] Woodruff AM, Goodpasture EW. The Susceptibility of the Chorio-Allantoic Membrane of Chick Embryos to Infection with the Fowl-Pox Virus. *Am J Pathol.* 1931;7:209-225.
- [55] Salk JE, Francis T, Jr. Immunization against influenza. *Ann Intern Med.* 1946;25:443-52.
- [56] Salk JE, Pearson HE, et al. Immunization against influenza with observations during an epidemic of influenza A one year after vaccination. *Am J Hyg.* 1945;42:307-22.
- [57] Centers for Disease Control and Prevention. 2019.
- [58] Wolff MW, Reichl U. Downstream Processing: From Egg to Cell Culture-Derived Influenza Virus Particles. *Chem Eng Technol.* 2008;31:846-57.
- [59] Maassab HF, Francis T, Jr., Davenport FM, Hennessy AV, Minuse E, Anderson G. Laboratory and clinical characteristics of attenuated strains of influenza virus. *Bull World Health Organ.* 1969;41:589-94.
- [60] Clements ML, Betts RF, Tierney EL, Murphy BR. Resistance of adults to challenge with influenza A wild-type virus after receiving live or inactivated virus vaccine. *Journal of clinical microbiology.* 1986;23:73-6.
- [61] Maassab HF. Adaptation and growth characteristics of influenza virus at 25 degrees c. *Nature.* 1967;213:612-4.
- [62] Partridge J, Kieny MP. Global production capacity of seasonal influenza vaccine in 2011. *Vaccine.* 2013;31:728-31.
- [63] McLean KA, Goldin S, Nannei C, Sparrow E, Torelli G. The 2015 global production capacity of seasonal and pandemic influenza vaccine. *Vaccine.* 2016;34:5410-3.
- [64] Blyden BE, Watler PK. New approaches to improved vaccine manufacturing in embryonated eggs. *BioPharm Int. Suppl.* 2010 Jan 2;2010;4-9.
- [65] Pujar NS, Sagar SL, Lee AL. History of Vaccine Process Development. *Vaccine Development and Manufacturing: John Wiley & Sons, Inc.;* 2014;1-24.
- [66] Parker L, Wharton SA, Martin SR, Cross K, Lin Y, Liu Y, et al. Effects of egg-adaptation on receptor-binding and antigenic properties of recent influenza A (H3N2) vaccine viruses. *J Gen Virol.* 2016;97:1333-44.
- [67] Yang L, Cheng Y, Zhao X, Wei H, Tan M, Li X, et al. Mutations associated with egg adaptation of influenza A(H1N1)pdm09 virus in laboratory based surveillance in China, 2009–2016. *Biosafety and Health.* 2019;1:41-5.
- [68] Tosh PK, Jacobson RM, Poland GA. Influenza vaccines: from surveillance through production to protection. *Mayo Clinic proceedings Mayo Clinic.* 2010;85:257-73.



- 
- [69] Yang HJ. Safety of influenza vaccination in children with allergic diseases. *Clin Exp Vaccine Res.* 2015;4:137-44.
- [70] Enders JF, Weller TH, Robbins FC. Cultivation of the Lansing Strain of Poliomyelitis Virus in Cultures of Various Human Embryonic Tissues. *Science.* 1949;109:85-7.
- [71] Barrett PN, Mundt W, Kistner O, Howard MK. Vero cell platform in vaccine production: moving towards cell culture-based viral vaccines. *Expert Rev Vaccines.* 2009;8:607-18.
- [72] Butel JS. Simian virus 40, poliovirus vaccines, and human cancer: research progress versus media and public interests. *Bull World Health Organ.* 2000;78:195-8.
- [73] Fang Q, Yang L, Zhu W, Liu L, Wang H, Yu W, et al. Host range, growth property, and virulence of the smallpox vaccine: vaccinia virus Tian Tan strain. *Virology.* 2005;335:242-51.
- [74] Maas R, van Zoelen D, Oei H, Claassen I. Replacement of primary chicken embryonic fibroblasts (CEF) by the DF-1 cell line for detection of avian leucosis viruses. *Biologicals.* 2006;34:177-81.
- [75] Aunins JG. Viral vaccine production in cell culture. *Encyclopedia of cell technology.* 2000.
- [76] Hayflick L, Moorhead PS. The serial cultivation of human diploid cell strains. *Exp Cell Res.* 1961;25:585-621.
- [77] Pagano JS, Boettiger M, Bonnevier JO, Gard S. The Response and the Lack of Spread in Swedish School Children Given an Attenuated Poliovirus Vaccine Prepared in a Human Diploid Cell Strain. *Am J Hyg.* 1964;79:74-85.
- [78] Jacobs JP, Jones CM, Baille JP. Characteristics of a human diploid cell designated MRC-5. *Nature.* 1970;227:168-70.
- [79] Hayflick L. A brief history of cell substrates used for the preparation of human biologicals. *Dev Biol (Basel).* 2001;106:5-4.
- [80] Koprowski H. After Pasteur: History of New Rabies Vaccines. In: Plotkin SA, editor. *History of Vaccine Development.* New York, NY: Springer New York; 2011;103-7.
- [81] Ma B, He LF, Zhang YL, Chen M, Wang LL, Yang HW, et al. Characteristics and viral propagation properties of a new human diploid cell line, Walvax-2, and its suitability as a candidate cell substrate for vaccine production. *Hum Vaccin Immunother.* 2015;11:998-1009.
- [82] Christman SA, Kong BW, Landry MM, Kim H, Foster DN. Modulation of p53 expression and its role in the conversion to a fully immortalized chicken embryo fibroblast line. *FEBS Lett.* 2005;579:6705-15.

## References

---

- [83] Ozturk SS. Cell Culture Technology - An Overview. In: Ozturk SS, Hu WS, editors. Cell culture technology for pharmaceutical and cell-based therapies. Boca Raton, FL: CRC Press, Taylor & Francis Group 2006;1-13.
- [84] Bakker WA, Thomassen YE, van't Oever AG, Westdijk J, van Oijen MG, Sundermann LC, et al. Inactivated polio vaccine development for technology transfer using attenuated Sabin poliovirus strains to shift from Salk-IPV to Sabin-IPV. *Vaccine*. 2011;29:7188-96.
- [85] Thomassen YE, van 't Oever AG, Vinke M, Spiekstra A, Wijffels RH, van der Pol LA, et al. Scale-down of the inactivated polio vaccine production process. *Biotechnology and bioengineering*. 2013;110:1354-65.
- [86] Thomassen YE, Rubingh O, Wijffels RH, van der Pol LA, Bakker WA. Improved poliovirus D-antigen yields by application of different Vero cell cultivation methods. *Vaccine*. 2014;32:2782-8.
- [87] Tiwari M, Parida M, Santhosh SR, Khan M, Dash PK, Rao PV. Assessment of immunogenic potential of Vero adapted formalin inactivated vaccine derived from novel ECSA genotype of Chikungunya virus. *Vaccine*. 2009;27:2513-22.
- [88] Rourou S, van der Ark A, van der Velden T, Kallel H. A microcarrier cell culture process for propagating rabies virus in Vero cells grown in a stirred bioreactor under fully animal component free conditions. *Vaccine*. 2007;25:3879-89.
- [89] Butler M, Burgener A, Patrick M, Berry M, Moffatt D, Huzel N, et al. Application of a serum-free medium for the growth of Vero cells and the production of reovirus. *Biotechnology progress*. 2000;16:854-8.
- [90] Rourou S, van der Ark A, Majoul S, Trabelsi K, van der Velden T, Kallel H. A novel animal-component-free medium for rabies virus production in Vero cells grown on Cytodex 1 microcarriers in a stirred bioreactor. *Applied microbiology and biotechnology*. 2009;85:53-63.
- [91] Rourou S, van der Ark A, van der Velden T, Kallel H. Development of an animal-component free medium for vero cells culture. *Biotechnology progress*. 2009;25:1752-61.
- [92] Toriniwa H, Komiya T. Long-term stability of Vero cell-derived inactivated Japanese encephalitis vaccine prepared using serum-free medium. *Vaccine*. 2008;26:3680-9.
- [93] Paillet C, Forno G, Kratje R, Etcheverrigaray M. Suspension-Vero cell cultures as a platform for viral vaccine production. *Vaccine*. 2009;27:6464-7.
- [94] Zanin MP, Webster DE, Martin JL, Wesselingh SL. Japanese encephalitis vaccines: moving away from the mouse brain. *Expert Rev Vaccines*. 2003;2:407-16.
- [95] Genzel Y, Fischer M, Reichl U. Serum-free influenza virus production avoiding washing steps and medium exchange in large-scale microcarrier culture. *Vaccine*. 2006;24:3261-72.

- 
- [96] Genzel Y, Olmer RM, Schafer B, Reichl U. Wave microcarrier cultivation of MDCK cells for influenza virus production in serum containing and serum-free media. *Vaccine*. 2006;24:6074-87.
- [97] Genzel Y, Reichl U. Vaccine Production. In: Pörtner R, editor. *Animal Cell Biotechnology*. Totowa, NJ: Humana Press; 2007;457-73.
- [98] Doroshenko A, Halperin SA. Trivalent MDCK cell culture-derived influenza vaccine Optaflu (Novartis Vaccines). *Expert Rev Vaccines*. 2009;8:679-88.
- [99] Genzel Y, Reichl U. Continuous cell lines as a production system for influenza vaccines. *Expert Rev Vaccines*. 2009;8:1681-92.
- [100] Oxford JS, Manuguerra C, Kistner O, Linde A, Kunze M, Lange W, et al. A new European perspective of influenza pandemic planning with a particular focus on the role of mammalian cell culture vaccines. *Vaccine*. 2005;23:5440-9.
- [101] Brown SW, Mehtali M. The Avian EB66(R) Cell Line, Application to Vaccines, and Therapeutic Protein Production. *PDA journal of pharmaceutical science and technology / PDA*. 2010;64:419-25.
- [102] Guehenneux F, Pain B. Avian cell lines for the production of useful substances. 2003.
- [103] Biswas A, Hutchins R. Embryonic stem cells. *Stem Cells Dev*. 2007;16:213-22.
- [104] Kraus B, von Fircks S, Feigl S, Koch SM, Fleischanderl D, Terler K, et al. Avian cell line - Technology for large scale vaccine production. *BMC proceedings*. 2011;5(8):P52.
- [105] Meyer HP, Schmidhalter D. *Industrial Scale Suspension Culture of Living Cells*: Wiley; 2014.
- [106] Giard DJ, Aaronson SA, Todaro GJ, Arnstein P, Kersey JH, Dosik H, et al. In vitro cultivation of human tumors: establishment of cell lines derived from a series of solid tumors. *J Natl Cancer Inst*. 1973;51:1417-23.
- [107] Shabram P, Kolman JL. Evaluation of a549 as a new vaccine cell substrate: digging deeper with massively parallel sequencing. *PDA journal of pharmaceutical science and technology / PDA*. 2014;68:639-50.
- [108] Ogura H, Fujiwara T. Establishment and characterization of a virus-free chick cell line. *Acta Med Okayama*. 1987;41:141-3.
- [109] Coussens PM, Smith KA, Weber PS, Colvin CJ. Immortalized chick embryo cell line adapted to serum-free growth conditions and capable of replicating human and reassortant H5N1 influenza strains for vaccine production. *Vaccine*. 2011;29:8661-8.

## References

---

- [110] Granicher G, Coronel J, Pralow A, Marichal-Gallardo P, Wolff M, Rapp E, et al. Efficient influenza A virus production in high cell density using the novel porcine suspension cell line PBG.PK2.1. *Vaccine*. 2019;37:7019-28.
- [111] Garber DA, O'Mara LA, Zhao J, Gangadhara S, An I, Feinberg MB. Expanding the repertoire of Modified Vaccinia Ankara-based vaccine vectors via genetic complementation strategies. *Plos One*. 2009;4:e5445.
- [112] Perez P, M QM, Lazaro-Frias A, Jimenez de Oya N, Blazquez AB, Escribano-Romero E, et al. A Vaccine Based on a Modified Vaccinia Virus Ankara Vector Expressing Zika Virus Structural Proteins Controls Zika Virus Replication in Mice. *Sci Rep*. 2018;8:17385.
- [113] Petricciani J, Sheets R. An overview of animal cell substrates for biological products. *Biologicals*. 2008;36:359-62.
- [114] Grachev V, Magrath D, Griffiths E, Petricciani JC, Chiu YY, Dobbelaer R, et al. WHO requirements for the use of animal cells as in vitro substrates for the production of biologicals - (requirements for biological substances no. 50) (Reprinted from WHO Technical Report Series, No.878, 1998). *Biologicals*. 1998;26:175-93.
- [115] Wierenga DE, Cogan J, Petricciani JC. Administration of tumor cell chromatin to immunosuppressed and non-immunosuppressed non-human primates. *Biologicals*. 1995;23:221-4.
- [116] Fallaux FJ, Bout A, van der Velde I, van den Wollenberg DJ, Hehir KM, Keegan J, et al. New helper cells and matched early region 1-deleted adenovirus vectors prevent generation of replication-competent adenoviruses. *Hum Gene Ther*. 1998;9:1909-17.
- [117] Altaras NE, Aunins JG, Evans RK, Kamen A, Konz JO, Wolf JJ. Production and formulation of adenovirus vectors. *Adv Biochem Eng Biotechnol*. 2005;99:193-260.
- [118] Jordan I, Vos A, Beilfuss S, Neubert A, Breul S, Sandig V. An avian cell line designed for production of highly attenuated viruses. *Vaccine*. 2009;27:748-56.
- [119] Olivier S, Jacoby M, Brillon C, Bouletreau S, Mollet T, Nerriere O, et al. EB66 cell line, a duck embryonic stem cell-derived substrate for the industrial production of therapeutic monoclonal antibodies with enhanced ADCC activity. *Mabs-Austin*. 2010;2:405-15.
- [120] Tintrup H. CAP-Technology: Production of biopharmaceuticals in human amniocytes. *Abstr Pap Am Chem S*. 2011;241.
- [121] Graham FL, Smiley J, Russell WC, Nairn R. Characteristics of a human cell line transformed by DNA from human adenovirus type 5. *J Gen Virol*. 1977;36:59-74.

- 
- [122] Farson D, Tao L, Ko D, Li Q, Brignetti D, Segawa K, et al. Development of novel E1-complementary cells for adenoviral production free of replication-competent adenovirus. *Mol Ther*. 2006;14:305-11.
- [123] Lewis JA, Brown EL, Duncan PA. Approaches to the release of a master cell bank of PER.C6 cells; a novel cell substrate for the manufacture of human vaccines. *Dev Biol (Basel)*. 2006;123:165-76; discussion 83-97.
- [124] Ledwith BJ, Lanning CL, Gumprecht LA, Anderson CA, Coleman JB, Gatto NT, et al. Tumorigenicity assessments of Per.C6 cells and of an Ad5-vectored HIV-1 vaccine produced on this continuous cell line. *Dev Biol (Basel)*. 2006;123:251-63; discussion 65-6.
- [125] Schiedner G, Hertel S, Bialek C, Kewes H, Waschutza G, Volpers C. Efficient and reproducible generation of high-expressing, stable human cell lines without need for antibiotic selection. *Bmc Biotechnol*. 2008;8:13.
- [126] Kovesdi I, Hedley SJ. Adenoviral producer cells. *Viruses*. 2010;2:1681-703.
- [127] Schiedner G, Hertel S, Kochanek S. Efficient transformation of primary human amniocytes by E1 functions of Ad5: generation of new cell lines for adenoviral vector production. *Hum Gene Ther*. 2000;11:2105-16.
- [128] Hadicke O, Lohr V, Genzel Y, Reichl U, Klamt S. Evaluating differences of metabolic performances: statistical methods and their application to animal cell cultivations. *Biotechnology and bioengineering*. 2013;110:2633-42.
- [129] Petiot E, Proust A, Traversier A, Durous L, Dappozze F, Gras M, et al. Influenza viruses production: Evaluation of a novel avian cell line DuckCelt(R)-T17. *Vaccine*. 2018;36:3101-11.
- [130] Lamb RA, Krug RM. Orthomyxoviridae: the viruses and their replication. In: Fields BN, Knipe DM, Howley PM, editors. *Fields' virology*. 4th ed. Philadelphia, PA: Wolters Kluwer Health/Lippincott Williams & Wilkins; 2001;1487-531.
- [131] Krammer F, Smith GJD, Fouchier RAM, Peiris M, Kedzierska K, Doherty PC, et al. Influenza. *Nat Rev Dis Primers*. 2018;4:3.
- [132] Palese P, Shaw ML. Orthomyxoviridae: the viruses and their replication. In: Fields BN, Knipe DM, Howley PM, editors. *Fields' virology*. 5th ed. Philadelphia, PA: Wolters Kluwer Health/Lippincott Williams & Wilkins; 2007;1647-89.
- [133] Wright PF, Webster RG. Orthomyxoviruses. In: Fields BN, Knipe DM, Howley PM, editors. *Fields' virology*. 4th ed. Philadelphia, PA: Wolters Kluwer Health/Lippincott Williams & Wilkins; 2001;1533-74.

## References

---

- [134] Tong S, Li Y, Rivailier P, Conrardy C, Castillo DA, Chen LM, et al. A distinct lineage of influenza A virus from bats. *Proc Natl Acad Sci U S A*. 2012;109:4269-74.
- [135] Ma W, Garcia-Sastre A, Schwemmler M. Expected and Unexpected Features of the Newly Discovered Bat Influenza A-like Viruses. *PLoS Pathog*. 2015;11:1-6.
- [136] Crawford PC, Dubovi EJ, Castleman WL, Stephenson I, Gibbs EP, Chen L, et al. Transmission of equine influenza virus to dogs. *Science*. 2005;310:482-5.
- [137] Subbarao K, Joseph T. Scientific barriers to developing vaccines against avian influenza viruses. *Nat Rev Immunol*. 2007;7:267-78.
- [138] Skehel JJ, Wiley DC. Receptor binding and membrane fusion in virus entry: the influenza hemagglutinin. *Annu Rev Biochem*. 2000;69:531-69.
- [139] Perdue ML, Garcia M, Senne D, Fraire M. Virulence-associated sequence duplication at the hemagglutinin cleavage site of avian influenza viruses. *Virus Res*. 1997;49:173-86.
- [140] Klenk HD, Garten W. Host cell proteases controlling virus pathogenicity. *Trends Microbiol*. 1994;2:39-43.
- [141] Leyssen P, De Clercq E, Neyts J. Molecular strategies to inhibit the replication of RNA viruses. *Antiviral research*. 2008;78:9-25.
- [142] Cheung TK, Poon LL. Biology of influenza A virus. *Annals of the New York Academy of Sciences*. 2007;1102:1-25.
- [143] Schnitzler SU, Schnitzler P. An update on swine-origin influenza virus A/H1N1: a review. *Virus Genes*. 2009;39:279-92.
- [144] Nunes-Correia I, Ramalho-Santos J, Nir S, Pedroso de Lima MC. Interactions of influenza virus with cultured cells: detailed kinetic modeling of binding and endocytosis. *Biochemistry*. 1999;38:1095-101.
- [145] Potter C. Influenza. *Principles and Practice of Clinical Virology*. 2004:271 - 97.
- [146] Mora R, Rodriguez-Boulan E, Palese P, Garcia-Sastre A. Apical budding of a recombinant influenza A virus expressing a hemagglutinin protein with a basolateral localization signal. *J Virol*. 2002;76:3544-53.
- [147] Hornickova Z. Different progress of MDCK cell death after infection by two different influenza virus isolates. *Cell Biochem Funct*. 1997;15:87-93.
- [148] Mohler L, Flockerzi D, Sann H, Reichl U. Mathematical model of influenza A virus production in large-scale microcarrier culture. *Biotechnology and bioengineering*. 2005;90:46-58.

- 
- [149] Rimmelzwaan GF, Baars M, Claas EC, Osterhaus AD. Comparison of RNA hybridization, hemagglutination assay, titration of infectious virus and immunofluorescence as methods for monitoring influenza virus replication in vitro. *J Virol Methods*. 1998;74:57-66.
- [150] Schulze-Horsel J, Schulze M, Agalaridis G, Genzel Y, Reichl U. Infection dynamics and virus-induced apoptosis in cell culture-based influenza vaccine production-Flow cytometry and mathematical modeling. *Vaccine*. 2009;27:2712-22.
- [151] Beauchemin CA, Handel A. A review of mathematical models of influenza A infections within a host or cell culture: lessons learned and challenges ahead. *BMC public health*. 2011;11 Suppl 1:S7.
- [152] Neumann G, Noda T, Kawaoka Y. Emergence and pandemic potential of swine-origin H1N1 influenza virus. *Nature*. 2009;459:931-9.
- [153] Gerdil C. The annual production cycle for influenza vaccine. *Vaccine*. 2003;21:1776-9.
- [154] Hickling J, D'Hondt E. A review of production technologies for influenza virus vaccines, and their suitability for deployment in developing countries for influenza pandemic preparedness. *World Health Organization Initiative for Vaccine Research*. 2006;1-34.
- [155] Orenstein WA, Schaffner W. Lessons learned: role of influenza vaccine production, distribution, supply, and demand--what it means for the provider. *The American journal of medicine*. 2008;121:S22-7.
- [156] Maassab HF. Biologic and immunologic characteristics of cold-adapted influenza virus. *Journal of immunology*. 1969;102:728-32.
- [157] Nachbagauer R, Feser J, Naficy A, Bernstein DI, Guptill J, Walter EB, et al. A chimeric hemagglutinin-based universal influenza virus vaccine approach induces broad and long-lasting immunity in a randomized, placebo-controlled phase I trial. *Nat Med*. 2021;27:106-14.
- [158] Ambrose CS, Luke C, Coelingh K. Current status of live attenuated influenza vaccine in the United States for seasonal and pandemic influenza. *Influenza Other Respir Viruses*. 2008;2:193-202.
- [159] Palker T, Kiseleva I, Johnston K, Su Q, Toner T, Szymkowiak C, et al. Protective efficacy of intranasal cold-adapted influenza A/New Caledonia/20/99 (H1N1) vaccines comprised of egg- or cell culture-derived reassortants. *Virus Res*. 2004;105:183-94.
- [160] Rudenko L, Desheva J, Korovkin S, Mironov A, Rekstin A, Grigorieva E, et al. Safety and immunogenicity of live attenuated influenza reassortant H5 vaccine (phase I-II clinical trials). *Influenza Other Respir Viruses*. 2008;2:203-9.
- [161] Tree JA, Richardson C, Fooks AR, Clegg JC, Looby D. Comparison of large-scale mammalian cell culture systems with egg culture for the production of influenza virus A vaccine strains. *Vaccine*. 2001;19:3444-50.

## References

---

- [162] Ng SK. Current cell-based influenza vaccine production technology as pandemic contingency. *Hum Vaccin Immunother*. 2012;8:267-71.
- [163] Extance A. Cell-based flu vaccines ready for US prime time. *Nat Rev Drug Discov*. 2011;10:246.
- [164] Patriarca PA. Use of cell lines for the production of influenza virus vaccines: an appraisal of technical, manufacturing, and regulatory considerations. World Health Organization. 2007; Updated 14 Apr 2007.
- [165] Greenberg DP, Robertson CA, Noss MJ, Blatter MM, Biedenkopf R, Decker MD. Safety and immunogenicity of a quadrivalent inactivated influenza vaccine compared to licensed trivalent inactivated influenza vaccines in adults. *Vaccine*. 2013;31:770-6.
- [166] Perez Rubio A, Eiros JM. Cell culture-derived flu vaccine: Present and future. *Hum Vaccin Immunother*. 2018;14:1874-82.
- [167] Manini I, Domnich A, Amicizia D, Rossi S, Pozzi T, Gasparini R, et al. Flucelvax (Optaflu) for seasonal influenza. *Expert Rev Vaccines*. 2015;14:789-804.
- [168] Clark TW, Pareek M, Hoschler K, Dillon H, Nicholson KG, Groth N, et al. Trial of 2009 influenza A (H1N1) monovalent MF59-adjuvanted vaccine. *N Engl J Med*. 2009;361:2424-35.
- [169] Cox MM, Izikson R, Post P, Dunkle L. Safety, efficacy, and immunogenicity of Flublok in the prevention of seasonal influenza in adults. *Ther Adv Vaccines*. 2015;3:97-108.
- [170] Bangham CR, Kirkwood TB. Defective interfering particles and virus evolution. *Trends Microbiol*. 1993;1:260-4.
- [171] Fenner F. Smallpox Eradication: The Vindication of Jenner's Prophecy. *History of Vaccine Development*. 2011:27-32.
- [172] Mayr A, Hochstein-Mintzel V, Stickl H. Abstammung, Eigenschaften und Verwendung des attenuierten Vaccinia-Stammes MVA. *Infection*. 1975;3:6-14.
- [173] Mayr A, Munz E. [Changes in the vaccinia virus through continuing passages in chick embryo fibroblast cultures]. *Zentralbl Bakteriolog Orig*. 1964;195:24-35.
- [174] Meisinger-Henschel C, Schmidt M, Lukassen S, Linke B, Krause L, Konietzny S, et al. Genomic sequence of chorioallantois vaccinia virus Ankara, the ancestor of modified vaccinia virus Ankara. *J Gen Virol*. 2007;88:3249-59.
- [175] Meyer H, Sutter G, Mayr A. Mapping of deletions in the genome of the highly attenuated vaccinia virus MVA and their influence on virulence. *J Gen Virol*. 1991;72 ( Pt 5):1031-8.



- 
- [176] Sutter G, Wyatt LS, Foley PL, Bennink JR, Moss B. A recombinant vector derived from the host range-restricted and highly attenuated MVA strain of vaccinia virus stimulates protective immunity in mice to influenza virus. *Vaccine*. 1994;12:1032-40.
- [177] Drillien R, Spehner D, Hanau D. Modified vaccinia virus Ankara induces moderate activation of human dendritic cells. *J Gen Virol*. 2004;85:2167-75.
- [178] Liu L, Chavan R, Feinberg MB. Dendritic cells are preferentially targeted among hematolymphocytes by Modified Vaccinia Virus Ankara and play a key role in the induction of virus-specific T cell responses in vivo. *Bmc Immunol*. 2008;9:15.
- [179] Cottingham MG, Carroll MW. Recombinant MVA vaccines: dispelling the myths. *Vaccine*. 2013;31:4247-51.
- [180] Kremer M, Volz A, Kreijtz JH, Fux R, Lehmann MH, Sutter G. Easy and efficient protocols for working with recombinant vaccinia virus MVA. *Methods Mol Biol*. 2012;890:59-92.
- [181] Smith GL, Moss B. Infectious poxvirus vectors have capacity for at least 25 000 base pairs of foreign DNA. *Gene*. 1983;25:21-8.
- [182] Moss B. Poxviridae: The viruses and their replication. In: Knipe DM HP, editor. *Fields virology*. Philadelphia: Lippincott Williams & Wilkins; 2007;2905-46.
- [183] Moss B. Poxvirus DNA replication. *Cold Spring Harb Perspect Biol*. 2013;5.
- [184] Smith GL, Vanderplassen A, Law M. The formation and function of extracellular enveloped vaccinia virus. *J Gen Virol*. 2002;83:2915-31.
- [185] McFadden G. Poxvirus tropism. *Nat Rev Microbiol*. 2005;3:201-13.
- [186] Kates J, Beeson J. Ribonucleic acid synthesis in vaccinia virus. I. The mechanism of synthesis and release of RNA in vaccinia cores. *J Mol Biol*. 1970;50:1-18.
- [187] Jefferts ER, Holowczak JA. RNA synthesis in vaccinia-infected L cells: inhibition of ribosome formation and maturation. *Virology*. 1971;46:730-44.
- [188] Radosevic K, Rodriguez A, Lemckert A, Goudsmit J. Heterologous prime-boost vaccinations for poverty-related diseases: advantages and future prospects. *Expert Rev Vaccines*. 2009;8:577-92.
- [189] Nascimento IP, Leite LC. Recombinant vaccines and the development of new vaccine strategies. *Braz J Med Biol Res*. 2012;45:1102-11.
- [190] Robert-Guroff M. Replicating and non-replicating viral vectors for vaccine development. *Curr Opin Biotechnol*. 2007;18:546-56.

## References

---

- [191] Coutant F, Frenkiel MP, Despres P, Charneau P. Protective antiviral immunity conferred by a nonintegrative lentiviral vector-based vaccine. *Plos One*. 2008;3:e3973.
- [192] Gilbert SC, Moorthy VS, Andrews L, Pathan AA, McConkey SJ, Vuola JM, et al. Synergistic DNA-MVA prime-boost vaccination regimes for malaria and tuberculosis. *Vaccine*. 2006;24:4554-61.
- [193] Cebere I, Dorrell L, McShane H, Simmons A, McCormack S, Schmidt C, et al. Phase I clinical trial safety of DNA- and modified virus Ankara-vectored human immunodeficiency virus type 1 (HIV-1) vaccines administered alone and in a prime-boost regime to healthy HIV-1-uninfected volunteers. *Vaccine*. 2006;24:417-25.
- [194] Webster DP, Dunachie S, Vuola JM, Berthoud T, Keating S, Laidlaw SM, et al. Enhanced T cell-mediated protection against malaria in human challenges by using the recombinant poxviruses FP9 and modified vaccinia virus Ankara. *Proc Natl Acad Sci U S A*. 2005;102:4836-41.
- [195] Stickl H, Hochstein-Mintzel V, Mayr A, Huber HC, Schafer H, Holzner A. MVA vaccination against smallpox: clinical tests with an attenuated live vaccinia virus strain (MVA) (author's transl). *Dtsch Med Wochenschr*. 1974;99:2386-92.
- [196] Mayr A. Smallpox vaccination and bioterrorism with pox viruses. *Comp Immunol Microbiol Infect Dis*. 2003;26:423-30.
- [197] Boukhebz H, Bellon N, Limacher JM, Inchauspe G. Therapeutic vaccination to treat chronic infectious diseases: current clinical developments using MVA-based vaccines. *Hum Vaccin Immunother*. 2012;8:1746-57.
- [198] Gomez CE, Najera JL, Krupa M, Perdiguero B, Esteban M. MVA and NYVAC as vaccines against emergent infectious diseases and cancer. *Curr Gene Ther*. 2011;11:189-217.
- [199] Gomez CE, Perdiguero B, Garcia-Arriaza J, Esteban M. Poxvirus vectors as HIV/AIDS vaccines in humans. *Hum Vaccin Immunother*. 2012;8:1192-207.
- [200] Vazquez-Ramirez D, Genzel Y, Jordan I, Sandig V, Reichl U. High-cell-density cultivations to increase MVA virus production. *Vaccine*. 2018;36:3124-33.
- [201] Coulibaly S, Bruhl P, Mayrhofer J, Schmid K, Gerencer M, Falkner FG. The nonreplicating smallpox candidate vaccines defective vaccinia Lister (dVVL) and modified vaccinia Ankara (MVA) elicit robust long-term protection. *Virology*. 2005;341:91-101.
- [202] Guehenneux F, Pain B. Production of poxviruses with adherent or non adherent avian cell lines. WO 2005/007840 A1. 2005.
- [203] Jordan I, Sandig V. Highly efficient, chemically defined and fully scalable biphasic production of vaccine viruses. *BMC proceedings*. 2011;5 Suppl 8:O1.

- [204] Griffiths JB, Looby D, Racher AJ. Maximisation of perfusion systems and process comparison with batch-type cultures. Maximisation of perfusion cultures. *Cytotechnology*. 1992;9:3-9.
- [205] Tapia F, Vazquez-Ramirez D, Genzel Y, Reichl U. Bioreactors for high cell density and continuous multi-stage cultivations: options for process intensification in cell culture-based viral vaccine production. *Applied microbiology and biotechnology*. 2016;100:2121-32.
- [206] Ozturk SS. Optimization and Scale-up of High Density Cell Culture Bioreactors. In: Galindo E, Ramirez OT, editors. *Advances in Bioprocess Engineering*. Springer ed. Netherlands 1994;133-9.
- [207] Ozturk SS. Engineering challenges in high density cell culture systems. *Cytotechnology*. 1996;22:3-16.
- [208] Clincke MF, Molleryd C, Zhang Y, Lindskog E, Walsh K, Chotteau V. Very high density of CHO cells in perfusion by ATF or TFF in WAVE bioreactor. Part I. Effect of the cell density on the process. *Biotechnology progress*. 2013;29:754-67.
- [209] Czermak P, Pörtner R, Brix A. *Special Engineering Aspects. Cell and Tissue Reaction Engineering*. Berlin, Heidelberg: Springer Berlin Heidelberg; 2009;83-172.
- [210] Abu-Absi S, Xu S, Graham H, Dalal N, Boyer M, Dave K. Cell culture process operations for recombinant protein production. *Adv Biochem Eng Biotechnol*. 2014;139:35-68.
- [211] Pörtner R. Bioreactors for Mammalian Cells. In: Al-Rubeai M, editor. *Cell Eng*. Cham: Springer International Publishing; 2015;89-135.
- [212] Kompala DS, Ozturk SS. Optimization of high cell density perfusion bioreactors. In: Ozturk SS, Hu WS, editors. *Cell culture technology for pharmaceutical and cell-based therapies*. Boca Raton, FL: CRC Press, Taylor & Francis Group 2006;387-416.
- [213] Kompala DS, Ozturk SS. Optimization of high cell density perfusion bioreactors. In: Ozturk SS, Hu WS, editors. *Cell Culture Technology for Pharmaceutical and Cell-Based Therapies*: Taylor & Francis: New York; 2006.
- [214] Chuppa S, Tsai YS, Yoon S, Shackelford S, Rozales C, Bhat R, et al. Fermentor temperature as a tool for control of high-density perfusion cultures of mammalian cells. *Biotechnology and bioengineering*. 1997;55:328-38.
- [215] Castilho L, Moraes A, Augusto E, Butler M. *Animal cell technology : from biopharmaceuticals to gene therapy*. New York ; Abingdon England: Taylor & Francis Group; 2008.
- [216] Konstantinov K, Goudar C, Ng M, Meneses R, Thrift J, Chuppa S, et al. The "push-to-low" approach for optimization of high-density perfusion cultures of animal cells. *Adv Biochem Eng Biotechnol*. 2006;101:75-98.

## References

---

- [217] Deschênes JS, Desbiens A, Perrier M, Kamen A. Use of cell bleed in a high cell density perfusion culture and multivariable control of biomass and metabolite concentrations. *Asia-Pacific Journal of Chemical Engineering*. 2006;1:82-91.
- [218] Hiller GW, Clark DS, Blanch HW. Cell retention-chemostat studies of hybridoma cells-analysis of hybridoma growth and metabolism in continuous suspension culture in serum-free medium. *Biotechnology and bioengineering*. 1993;42:185-95.
- [219] Vazquez-Ramirez D, Jordan I, Sandig V, Genzel Y, Reichl U. High titer MVA and influenza A virus production using a hybrid fed-batch/perfusion strategy with an ATF system. *Applied microbiology and biotechnology*. 2019;103:3025-35.
- [220] Wang SB, Godfrey S, Radoniqi F, Lin H, Coffman J. Larger Pore Size Hollow Fiber Membranes as a Solution to the Product Retention Issue in Filtration-Based Perfusion Bioreactors. *Biotechnol J*. 2019;14:e1800137.
- [221] de la Broise D, Noiseux M, Massie B, Lemieux R. Hybridoma perfusion systems: a comparison study. *Biotechnology and bioengineering*. 1992;40:25-32.
- [222] Zhang Y, Stobbe P, Silvander CO, Chotteau V. Very high cell density perfusion of CHO cells anchored in a non-woven matrix-based bioreactor. *Journal of biotechnology*. 2015.
- [223] Padawer I, Ling WL, Bai Y. Case Study: an accelerated 8-day monoclonal antibody production process based on high seeding densities. *Biotechnology progress*. 2013;29:829-32.
- [224] Aunins JG. Viral Vaccine Production in Cell Culture. *Encyclopedia of Cell Technology*: John Wiley & Sons, Inc.; 2003.
- [225] Lindsay DA, Betenbaugh MJ. Quantification of Cell-Culture Factors Affecting Recombinant Protein Yields in Baculovirus-Infected Insect Cells. *Biotechnology and bioengineering*. 1992;39:614-8.
- [226] Maranga L, Brazao TF, Carrondo MJT. Virus-like particle production at low multiplicities of infection with the baculovirus insect cell system. *Biotechnology and bioengineering*. 2003;84:245-53.
- [227] Cortin V, Thibault J, Jacob D, Garnier A. High-titer adenovirus vector production in 293S cell perfusion culture. *Biotechnology progress*. 2004;20:858-63.
- [228] Yuk IH, Olsen MM, Geyer S, Forestell SP. Perfusion cultures of human tumor cells: a scalable production platform for oncolytic adenoviral vectors. *Biotechnology and bioengineering*. 2004;86:637-42.
- [229] Henry O, Dormond E, Perrier M, Kamen A. Insights into adenoviral vector production kinetics in acoustic filter-based perfusion cultures. *Biotechnology and bioengineering*. 2004;86:765-74.

- 
- [230] Galvez J, Lecina M, Sola C, Cairo JJ, Godia F. Optimization of HEK-293S cell cultures for the production of adenoviral vectors in bioreactors using on-line OUR measurements. *J Biotechnol.* 2012;157:214-22.
- [231] Van Herk H, Luitjens A. Method for the production of ad26 adenoviral vectors. Google Patents; 2011.
- [232] Bock A, Schulze-Horsel J, Schwarzer J, Rapp E, Genzel Y, Reichl U. High-density microcarrier cell cultures for influenza virus production. *Biotechnology progress.* 2011;27:241-50.
- [233] Petiot E, Jacob D, Lanthier S, Lohr V, Ansorge S, Kamen AA. Metabolic and Kinetic analyses of influenza production in perfusion HEK293 cell culture. *Bmc Biotechnol.* 2011;11:84.
- [234] Sun B, Yu X, Kong W, Sun S, Yang P, Zhu C, et al. Production of influenza H1N1 vaccine from MDCK cells using a novel disposable packed-bed bioreactor. *Applied microbiology and biotechnology.* 2013;97:1063-70.
- [235] Tapia F, Vogel T, Genzel Y, Behrendt I, Hirschel M, Gangemi JD, et al. Production of high-titer human influenza A virus with adherent and suspension MDCK cells cultured in a single-use hollow fiber bioreactor. *Vaccine.* 2014;32:1003-11.
- [236] Coronel J, Behrendt I, Burgin T, Anderlei T, Sandig V, Reichl U, et al. Influenza A virus production in a single-use orbital shaken bioreactor with ATF or TFF perfusion systems. *Vaccine.* 2019;37:7011-8.
- [237] Bissinger T, Fritsch J, Mihut A, Wu Y, Liu X, Genzel Y, et al. Semi-perfusion cultures of suspension MDCK cells enable high cell concentrations and efficient influenza A virus production. *Vaccine.* 2019;37:7003-10.
- [238] Ghani K, Garnier A, Coelho H, Transfiguracion J, Trudel P, Kamen A. Retroviral vector production using suspension-adapted 293GPG cells in a 3L acoustic filter-based perfusion bioreactor. *Biotechnology and bioengineering.* 2006;95:653-60.
- [239] Pohlscheidt M, Langer U, Minuth T, Bodeker B, Apeler H, Horlein HD, et al. Development and optimisation of a procedure for the production of Parapoxvirus ovis by large-scale microcarrier cell culture in a non-animal, non-human and non-plant-derived medium. *Vaccine.* 2008;26:1552-65.
- [240] Nikolay A, Leon A, Schwamborn K, Genzel Y, Reichl U. Process intensification of EB66(R) cell cultivations leads to high-yield yellow fever and Zika virus production. *Applied microbiology and biotechnology.* 2018;102:8725-37.
- [241] Dowd JE, Jubb A, Kwok KE, Piret JM. Optimization and control of perfusion cultures using a viable cell probe and cell specific perfusion rates. *Cytotechnology.* 2003;42:35-45.

## References

---

- [242] Nadeau I, Kamen A. Production of adenovirus vector for gene therapy. *Biotechnol Adv.* 2003;20:475-89.
- [243] Henry O, Perrier M, Kamen A. Metabolic flux analysis of HEK-293 cells in perfusion cultures for the production of adenoviral vectors. *Metab Eng.* 2005;7:467-76.
- [244] Sanders BP, Edo-Matas D, Custers JH, Koldijk MH, Klaren V, Turk M, et al. PER.C6((R)) cells as a serum-free suspension cell platform for the production of high titer poliovirus: a potential low cost of goods option for world supply of inactivated poliovirus vaccine. *Vaccine.* 2013;31:850-6.
- [245] Mercier SM, Diepenbroek B, Martens D, Wijffels RH, Streefland M. Characterization of apoptosis in PER.C6 batch and perfusion cultures. *Biotechnology and bioengineering.* 2014;112:569–78.
- [246] Vellinga J, Smith JP, Lipiec A, Majhen D, Lemckert A, van Ooij M, et al. Challenges in manufacturing adenoviral vectors for global vaccine product deployment. *Hum Gene Ther.* 2014;25:318-27.
- [247] Van Herk H, Luitjens A. Method for the production of ad26 adenoviral vectors. 2011.
- [248] Nienow AW, Scott WH, Hewitt CJ, Thomas CR, Lewis G, Amanullah A, et al. Scale-down studies for assessing the impact of different stress parameters on growth and product quality during animal cell culture. *Chemical Engineering Research and Design.* 2013;91:2265-74.
- [249] Wang S, Godfrey S, Ravikrishnan J, Lin H, Vogel J, Coffman J. Shear contributions to cell culture performance and product recovery in ATF and TFF perfusion systems. *J Biotechnol.* 2017;246:52-60.
- [250] Karst DJ, Serra E, Villiger TK, Soos M, Morbidelli M. Characterization and comparison of ATF and TFF in stirred bioreactors for continuous mammalian cell culture processes. *Biochemical Engineering Journal.* 2016;110:17-26.
- [251] Henry O, Dormond E, Perrier M, Kamen A. Insights into adenoviral vector production kinetics in acoustic filter-based perfusion cultures. *Biotechnology and bioengineering.* 2004;86:765-74.
- [252] Roya S, Mehrad MF. The Applicable Approach to Increase the Animal viral Vaccine Production by Rolling Method in Iran. 15th Congress of the Federation of Asian Veterinary Associations, Fava-Oie Joint Symposium on Emerging Diseases, Proceedings. 2008:115-7.
- [253] Josefsberg JO, Buckland B. Vaccine process technology. *Biotechnology and bioengineering.* 2012;109:1443-60.
- [254] Streefland M, Martens DE, Beuvery EC, Wijffels RH. Process analytical technology (PAT) tools for the cultivation step in biopharmaceutical production. *Eng Life Sci.* 2013;13:212-23.

- 
- [255] Casablanco A, Gámez X, Lecina M, Solà C, Cairó JJ, Gòdia F. Comparison of control strategies for fed-batch culture of hybridoma cells based on on-line monitoring of oxygen uptake rate, optical cell density and glucose concentration. *Journal of Chemical Technology & Biotechnology*. 2013;88:1680-9.
- [256] Konstantinov K, Chuppa S, Sajan E, Tsai Y, Yoon S, Golini F. Real-time biomass-concentration monitoring in animal-cell cultures. *Trends in biotechnology*. 1994;12:324-33.
- [257] Kamen AA, Bedard C, Tom R, Perret S, Jardin B. On-line monitoring of respiration in recombinant-baculovirus infected and uninfected insect cell bioreactor cultures. *Biotechnology and bioengineering*. 1996;50:36-48.
- [258] Foster KR, Schwan HP. Dielectric properties of tissues and biological materials: a critical review. *Crit Rev Biomed Eng*. 1989;17:25-104.
- [259] Ansorge S, Esteban G, Schmid G. Multifrequency permittivity measurements enable on-line monitoring of changes in intracellular conductivity due to nutrient limitations during batch cultivations of CHO cells. *Biotechnology progress*. 2010;26:272-83.
- [260] Ansorge S, Esteban G, Schmid G. On-line monitoring of infected Sf-9 insect cell cultures by scanning permittivity measurements and comparison with off-line biovolume measurements. *Cytotechnology*. 2007;55:115-24.
- [261] Cannizzaro C, Gugerli R, Marison I, von Stockar U. On-line biomass monitoring of CHO perfusion culture with scanning dielectric spectroscopy. *Biotechnology and bioengineering*. 2003;84:597-610.
- [262] Mercier SM, Rouel PM, Lebrun P, Diepenbroek B, Wijffels RH, Streefland M. Process analytical technology tools for perfusion cell culture. *Eng Life Sci*. 2016;16:25-35.
- [263] Parta L, Zalai D, Borbely S, Putics A. Application of dielectric spectroscopy for monitoring high cell density in monoclonal antibody producing CHO cell cultivations. *Bioprocess Biosyst Eng*. 2014;37:311-23.
- [264] Nikolay A, Bissinger T, Granicher G, Wu Y, Genzel Y, Reichl U. Perfusion Control for High Cell Density Cultivation and Viral Vaccine Production. *Methods Mol Biol*. 2020;2095:141-68.
- [265] Ansorge S, Lanthier S, Transfiguracion J, Henry O, Kamen A. Monitoring lentiviral vector production kinetics using online permittivity measurements. *Biochemical Engineering Journal*. 2011;54:16-25.
- [266] Petiot E, Ansorge S, Rosa-Calatrava M, Kamen A. Critical phases of viral production processes monitored by capacitance. *J Biotechnol*. 2017;242:19-29.

## References

---

- [267] Esmonde-White KA, Cuellar M, Uerpmann C, Lenain B, Lewis IR. Raman spectroscopy as a process analytical technology for pharmaceutical manufacturing and bioprocessing. *Anal Bioanal Chem.* 2017;409:637-49.
- [268] Streefland M, van de Waterbeemd B, Happe H, van der Pol LA, Beuvery EC, Tramper J, et al. PAT for vaccines: the first stage of PAT implementation for development of a well-defined whole-cell vaccine against whooping cough disease. *Vaccine.* 2007;25:2994-3000.
- [269] Whelan J, Craven S, Glennon B. In situ Raman spectroscopy for simultaneous monitoring of multiple process parameters in mammalian cell culture bioreactors. *Biotechnology progress.* 2012;28:1355-62.
- [270] Bhatia H, Mehdizadeh H, Drapeau D, Yoon S. In-line monitoring of amino acids in mammalian cell cultures using raman spectroscopy and multivariate chemometrics models. *Eng Life Sci.* 2018;18:55-61.
- [271] Desai S, Mishra SV, Joshi A, Sarkar D, Hole A, Mishra R, et al. Raman spectroscopy-based detection of RNA viruses in saliva: A preliminary report. *J Biophotonics.* 2020;13:e202000189.
- [272] Rodriguez-Casado A, Molina M, Carmona P. Core protein-nucleic acid interactions in hepatitis C virus as revealed by Raman and circular dichroism spectroscopy. *Appl Spectrosc.* 2007;61:1219-24.
- [273] Pezzotti G, Zhu W, Adachi T, Horiguchi S, Marin E, Boschetto F, et al. Metabolic machinery encrypted in the Raman spectrum of influenza A virus-inoculated mammalian cells. *J Cell Physiol.* 2020;235:5146-70.
- [274] Lohr V, Hadicke O, Genzel Y, Jordan I, Bunttemeyer H, Klamt S, et al. The avian cell line AGE1.CR.pIX characterized by metabolic flux analysis. *Bmc Biotechnol.* 2014;14:72.
- [275] Rehberg M, Ritter JB, Genzel Y, Flockerzi D, Reichl U. The relation between growth phases, cell volume changes and metabolism of adherent cells during cultivation. *J Biotechnol.* 2013;164:489-99.
- [276] Reed LJ, Muench H. A Simple Method of Estimating Fifty Per Cent Endpoints<sup>12</sup>. *American Journal of Epidemiology.* 1938;27:493-7.
- [277] Kalbfuss B, Knochlein A, Krober T, Reichl U. Monitoring influenza virus content in vaccine production: precise assays for the quantitation of hemagglutination and neuraminidase activity. *Biologicals.* 2008;36:145-61.
- [278] Genzel Y, Reichl U. Vaccine production - state of the art and future needs in upstream processing. In: Pörtner R, editor. *Animal Cell Biotechnology: Methods and Protocols* Totowa, New Jersey: HUMANA Press Inc.; 2007;457-73.



- 
- [279] Genzel Y, Rödig J, Rapp E, Reichl U. Vaccine production: upstream processing with adherent or suspension cell lines. In: Pörtner R, editor. *Animal Cell Biotechnology: Methods and Protocols*. Clifton, N.J.: Humana Press Inc.; 2014;371-93.
- [280] Garcia-Ochoa F, Gomez E. Bioreactor scale-up and oxygen transfer rate in microbial processes: an overview. *Biotechnol Adv*. 2009;27:153-76.
- [281] Czermak P, Weber C, Nehring D. A ceramic microsparging aeration system for cell culture reactors. *Publication Series of IBPT –University of Applied Sciences Giessen-Friedberg*. 2005;1.
- [282] Nehring D, Czermak P, Vorlop J, Lubben H. Experimental study of a ceramic microsparging aeration system in a pilot-scale animal cell culture. *Biotechnology progress*. 2004;20:1710-7.
- [283] Bliem RF. *Bioreactor systems and effects*: Springer-Verlag; 1991.
- [284] Van't Riet K. Review of Measuring Methods and Results in Nonviscous Gas-Liquid Mass Transfer in Stirred Vessels. *Industrial & Engineering Chemistry Process Design and Development*. 1979;18:357-64.
- [285] Schiefelbein S, Frohlich A, John GT, Beutler F, Wittmann C, Becker J. Oxygen supply in disposable shake-flasks: prediction of oxygen transfer rate, oxygen saturation and maximum cell concentration during aerobic growth. *Biotechnol Lett*. 2013;35:1223-30.
- [286] Frensing T, Kupke SY, Bachmann M, Fritzsche S, Gallo-Ramirez LE, Reichl U. Influenza virus intracellular replication dynamics, release kinetics, and particle morphology during propagation in MDCK cells. *Applied microbiology and biotechnology*. 2016;100:7181-92.
- [287] Granicher G, Tapia F, Behrendt I, Jordan I, Genzel Y, Reichl U. Production of Modified Vaccinia Ankara Virus by Intensified Cell Cultures: A Comparison of Platform Technologies for Viral Vector Production. *Biotechnol J*. 2020:e2000024.
- [288] Granicher G, Coronel J, Trampler F, Jordan I, Genzel Y, Reichl U. Performance of an acoustic settler versus a hollow fiber-based ATF technology for influenza virus production in perfusion. *Applied microbiology and biotechnology*. 2020;104:4877-88.

## List of contributions

### Publications

---

**Vazquez-Ramirez D\***, Jordan I, Sandig V, Genzel Y, Reichl U. High titer MVA and influenza A virus production using a hybrid fed-batch/perfusion strategy with an ATF system. Applied microbiology and biotechnology. 2019; 103:3025-35

*\*First author*

**Vazquez-Ramirez D\***, Genzel Y, Jordan I, Sandig V, Reichl U. High-cell-density cultivations to increase MVA virus production. Vaccine. 2018; 36:3124-33

*\*First author*

Tapia F\*, **Vazquez-Ramirez D\***, Genzel Y, Reichl U. Bioreactors for high cell density and continuous multi-stage cultivations: options for process intensification in cell culture-based viral vaccine production. Applied microbiology and biotechnology. 2016; 100:2121-32

*\*Both authors contributed equally. Vazquez-Ramirez contributed with sections for high cell density cultivations*

**Vazquez-Ramirez D\***, Genzel Y, Jordan I, Sandig V, Reichl U. Bewertung von Kultivierungsstrategien für die Produktion des modifizierten Vacciniavirus Ankara (MVA) in Hochzelldichte. Sonderausgabe des ProcessNet und 31. DECHEMA-Jahrestagung der Biotechnologen, Chem. Ing. Tech. 2014;86:1500

*\*First author*

Genzel Y, Vogel T, Buck J, Behrendt I, **Ramirez DV\***, Schiedner G, et al. High cell density cultivations by alternating tangential flow (ATF) perfusion for influenza A virus production using suspension cells. Vaccine. 2014; 32:2770-81

*\*Author contributed with measurements of bioreactor  $k_La$  and calculations of theoretical maximum cell concentrations*

### Congress presentations

---

25<sup>th</sup> ESACT Meeting      **Poster:** „On-line monitoring of MVA and influenza virus replication at high cell-densities“. Lausanne, Switzerland, 14<sup>th</sup> - 17<sup>th</sup> May, 2017

Vaccine Technology VI      **Poster:** „Intensification of MVA and influenza virus production through high-cell-density cultivation approaches“. Albufeira, Portugal, 12<sup>th</sup> - 17<sup>th</sup> June, 2016

Cell Culture Engineering XV      **Short oral presentation and poster:** „Process optimization for semi-continuous virus production at high cell densities“. La Quinta, Palm Springs, USA, 8<sup>th</sup> - 13<sup>th</sup> May, 2016

---

4 <sup>th</sup> BioProScale Symposium Berlin	<b>Poster:</b> „On-line monitoring tools in batch and (semi-) perfusion cultivations for vaccine production”. Berlin, Germany, 6 <sup>th</sup> - 8 <sup>th</sup> April, 2016
24 <sup>th</sup> ESACT Meeting	<b>Poster:</b> „Process intensification beyond the cell density effect: stable cell-specific MVA virus production at 60×10 <sup>6</sup> cells/mL“. Barcelona, Spain, 31 <sup>st</sup> May - 3 <sup>rd</sup> June, 2015
DECHEMA-Himmelfahrts-tagung 2015	<b>Oral presentation:</b> „Down-scaled process development for the production of viral vaccines at high cell-densities“. Hamburg, Germany, 11 <sup>th</sup> - 13 <sup>th</sup> May, 2015
Vaccine Technology V	<b>Poster:</b> „Assessment of cultivation strategies for the production of Modified Vaccinia Ankara (MVA) at high cell-densities”. Playa del Carmen, Mexico, 8 <sup>th</sup> - 12 <sup>th</sup> June, 2014
23 <sup>th</sup> ESACT Meeting	<b>Poster:</b> „Development of a flow cytometry-based assay for the quantification of infectious influenza virions “. Lille, France, 23 <sup>rd</sup> - 26 <sup>th</sup> June, 2013

### Course contributions

---

Second Hybrid Modeling Summer School 2015. Organizer, in collaboration with Dr. Moritz von Stosch, Newcastle University. Max Planck Institute for Dynamics of Complex Technical Systems Magdeburg Magdeburg, Germany, 7<sup>th</sup> - 9<sup>th</sup> September, 2016

Biannual Pupils Practical Course (Schülerpraktikum) “Verfahrenstechnik und Technische Kybernetik”. Tutor for theoretical and practical course “Virus Production in cell culture”. Max Planck Institute for Dynamics of Complex Technical Systems Magdeburg, Germany, 2013-2016

### Supervised projects

---

#### Master Thesis

Lemke, V. “Suspension cell-based influenza virus production at high-cell-density”. Otto-von-Guericke-Universität Magdeburg, 2015

#### Internship

Suarez Heredia, C. R. “Towards a high-cell density perfusion culture system with Tangential Flow Filtration (TFF) for viral vaccine production”. The University of Manchester, 2015

#### Besondere Lernleistung (High school final report)

Ganzer, A. “Untersuchung von Suspensionszellen für die Nutzung in der Influenza Virus Herstellung”. Ratsgymnasium Wolfsburg, 2014

# Appendices

## Appendix 1. List of hollow fiber modules

Module <sup>a</sup>	Brand	Model	Membrane material <sup>b</sup>	Pore size	EL [cm] <sup>c</sup>	Area [cm <sup>2</sup> ]	f <sub>n</sub> <sup>d</sup>	d <sub>i</sub> [mm] <sup>e</sup>
L500	GE	UFP-500-E-4X2MA	PS	500 kDa	66.7	850	50	1.00
L65U	GE	CFP-6-D-4X2MA	PS	0.65 μm	66.0	950	75	0.75
L65U	Spectrum	S04-E65U-07-N	PES	0.65 μm	41.5	1075	110	0.75
L20U	Spectrum	S06-P20U-10-S	PES	0.20 μm	65.0	1500	75	1.00
S500	Spectrum	T06-E500-10-S	mPES	500 kDa	65.0	245	12	1.00
S50U	Spectrum	T04-P50U-10-N	PES	0.50 μm	41.5	180	14	1.00
S65U	Spectrum	T04-E65U-07-N	PES	0.65 μm	41.5	195	20	0.75

<sup>a</sup> Internal code. Surface: S (small), L (large); pore size: 65U (0.65 μm), 50U (0.50 μm), 20U (0.2 μm), 500 (500 kDa)

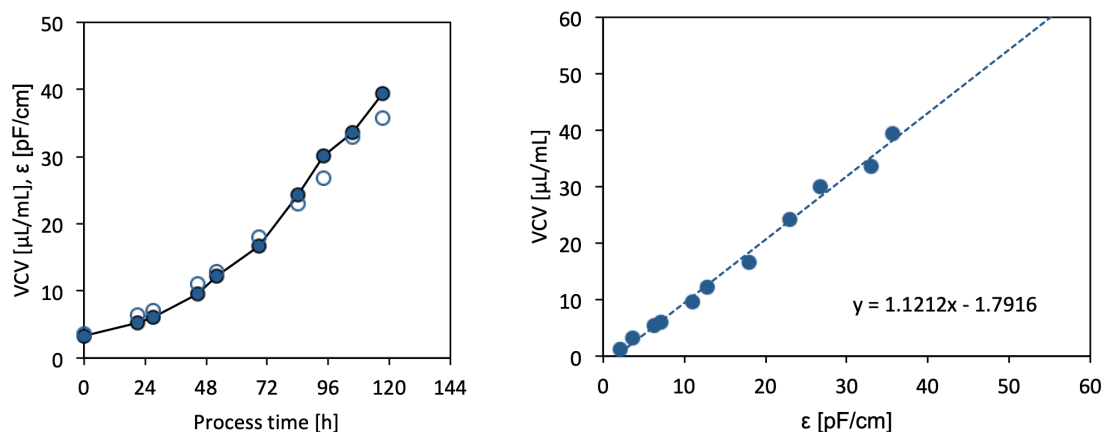
<sup>b</sup> PS: polysulfone, PES: polyethersulfone, mPES: modified polyethersulfone

<sup>c</sup> Effective length

<sup>d</sup> Number of fibers in the HF module

<sup>e</sup> Internal diameter

## Appendix 2. Calibration curve of the capacitance probe



Full symbols: Offline (Vicell). Empty symbols: Online (Incyte)